FRIEDRICH-SCHILLER-
UNIVERSITÄT
JENA

Polymer-based hybrid nanoparticles for bioapplications

Dissertation

Zur Erlangung des akademischen Grades doctor rerum naturalium

(Dr. rer. nat.)

Vorgelegt dem Rat der Chemisch-Geowissenschaftlichen Fakultät

der Friedrich-Schiller-Universität Jena

von M.Sc. Pelin Sungur,

geb. am 25.09.1989 in Altındağ, Ankara / Türkei

Gutachter: 1. Prof. Dr. Ulrich S. Schubert (Universität Jena)

2. Prof. Dr. Felix Schacher (Universität Jena)

Tag der öffentlichen Verteidigung: 27.11.2019

To my family & myself

Contents

List of abbreviations

acetyl-CoA ……	Acetyl-coenzyme A
AROP ……	Anionic ring-opening polymerization
ATP ……	Adenosine triphosphate
ATRP ……	Atom transfer radical polymerization
BDMA ……	Benzyldimethylamine
BF-TEM ……	Bright-field transmission electron microscopy
CAC ……	Citric acid cycle
CaP ……	Calcium phosphate
CCD ……	Charge coupled device
CMC ……	Critical micelle concentration
CROP ……	Cationic ring-opening polymerization
Cryo-EM ……	Cryo electron microscopy
Cryo-TEM ……	Cryo transmission electron microscopy
DDSA ……	Dodecenylsuccinic anhydride
DLS ……	Dynamic light scattering
DMP-30 ……	*Tris*(dimethylaminomethyl) phenol
DNA ……	Deoxyribonucleic acid
EDX ……	Energy dispersive X-ray
EELS ……	Electron energy loss spectroscopy
FBS ……	Fetal bovine serum
FTIR ……	Fourier-transform infrared spectroscopy
GA ……	Glutaraldehyde
GLUT ……	Glucose transporters
HAADF ……	High-angle annular dark-field
HEK-293 ……	Human embryonic kidney cells
HT-29 ……	Human colon cancer
LCST ……	Lower critical solution temperature
LPS ……	Lipopolysaccharide
LR ……	London resin
*Ni*PAm ……	*N*-Isopropylacrylamide
NMA ……	Nadic methyl anhydride

NMP ……	Nitroxide-mediated polymerization
OM ……	Optical microscopy
PDI ……	Polydispersity index
PDMAEMA ……	Poly[2-(*N*,*N*-dimethylamino)ethyl methacrylate]
PEG ……	Poly(ethylene glycol)
PEHG ……	Poly(ethyl hexyl glycidyl ether)
PEI ……	Poly(ethylene imine)
PEtOx ……	Poly(2-ethyl-2-oxazoline)
PLL ……	Poly-L-(lysine)
RAFT ……	Reversible addition fragmentation chain transfer
RNA ……	Ribonucleic acid
S. aureus ……	*Staphylococcus aureus*
STEM ……	Scanning transmission electron microscopy
TEM ……	Transmission electron microscopy
UA ……	Uranyl acetate
UV-VIS ……	Ultraviolet-visible spectroscopy

1. Introduction

The treatment of diseases is one of the major global challenges. With increasing understanding of the biochemical and biophysical processes associated with infection or mutation of cells in life-threatening diseases, medicine and pharmacy have succeeded in discovering and developing more effective pharmaceutical materials for treatments. One milestone in the development of efficient therapeutics is the introduction of the "magic bullet" concept by Paul Ehrlich in 1908,[1] when he proposed to facilitate a drug with two functional units; the first one directed to bind the component to the target, a so-called haptophore, and the toxophore, which kills the target. In 1975, Helmut Ringsdorf introduced the concept to conjugate an active drug to an appropriate polymeric carrier with the aim to modulate the drug uptake by cells.[2] This concept enabled to facilitate a macromolecule with a number of different functions. According to Ringsdorf's model, polymer drug conjugates can comprise components designed for imaging, targeting and drug loading.

The utilization of polymers and polymer nanoparticle systems to implement this paradigm represents a very versatile approach, as modern synthesis techniques of polymer systems enable the controlled fabrication of polymer architectures,[3] including the synthesis of polymer protein conjugates, polymer-small drug conjugates, dendrimers, polymer nanoparticles and others.[4] Furthermore, the drug conjugation and facilitating the polymers with individual functional units can be addressed by a number of synthetic strategies. Additionally, self-organization concepts can be employed to tailor the shape and size of nanoparticle systems.[5]

In particular nanoparticle systems consisting of different polymer subunits have gained significant interest during the last years.[6] Depending on their architecture they are able to form well-defined nanoparticle systems featuring a core-shell structure, i.e., by forming a hydrophobic core which is surrounded by a hydrophilic shell. While the hydrophobic core can potentially be used to host hydrophobic drug moieties the shell can govern the interaction of the nanoparticle with its environment and can, e.g., facilitate enhanced uptake of the nanoparticles into (specific) cells or cell organelles.[7]

The uptake of nanoparticle conjugates into cells has been found to be one of the most critical steps for targeted drug delivery.[8] Nature has developed sophisticated and dedicated uptake pathways for materials to enter the cell. In general uptake processes can be divided into active and passive uptake mechanisms.[9] Some of these uptake processes require the direct interaction of the material with the cell at the plasma membrane with specifically designed receptors, which allow the entrance of the material into the cell.[10] Such active uptake mechanisms include, e.g., the controlled uptake of sugar moieties into the cell. For this purpose, a number of transmembrane glucose transporters (GLUT) is present on the plasma membrane of cells, which specifically can interact with different glucose molecules.[11] This is of relevance

for cancer treatment because cancer cells show high levels of sugar uptake regarding to their need of energy for a faster rate for rapid proliferation and some of these GLUT receptors are overexpressed in many cancer types.[12]

Other uptake pathways of materials into the cell are more complex and depend on a large number of different parameters. Small molecules can pass the plasma membrane by diffusion if they are sufficiently small and form intimate contact with the plasma membrane.[13] Larger molecules or even nanoparticles rely on a deformation of the plasma membrane. These processes can be categorized as pinocytosis, which includes, e.g., micropinocytosis, clathrin dependent pinocytosis, receptor mediated pinocytosis, and clathrin independent pinocytosis. Additionally, endocytosis processes are used, including adsorptive endocytosis and caveolae dependent endocytosis.[14] The uptake also critically determines the localization of the internalized material within the cell and might determine their metabolic pathway as well.[15]

The basis for designing efficient polymer conjugates or nanoparticle systems for targeted drug delivery is the fundamental knowledge of the complex processes taking place in the cell, i.e., the interaction of the polymer drug conjugate with the cell, their metabolic pathway and the fate of the drug and drug carriers inside the cell as well as their association with different cellular compartments.[16] Some of these issues can be studied well by suitable imaging techniques, i.e., optical or electron microscopy.[17] In particular the development of electron microscopy techniques to investigate the internal structure of cells boosted the understanding of cellular uptake processes.[18] These investigations were pioneered by Albert Claude, Keith Porter and Ernest Fullam,[19] who, for the first time in 1945, could demonstrate the presence of mitochondria, the Golgi apparatus, and discovered the endoplasmic reticulum. Since then, improved sample preparation and staining protocols continuously enhanced the possibilities to study cellular uptake and the response of intracellular features toward drug uptake. It became evident that the cellular uptake is a complex process which can be influenced by several peculiar parameters of the drug delivery system, including, e.g., their size, shape, charge, material composition, aggregation state and surface chemistry.[14, 20] In particular the possibility to introduce tailor-made interaction sites, e.g., interacting with specific receptors on the plasma membrane of a cell or which can participate actively into metabolic processes, opens up attractive possibilities for targeted drug delivery.[21]

For electron microscopy the utilization of easily traceable markers, i.e., electron dense colloidal gold nanoparticles, represents a powerful tool to study targeted uptake processes in detail.[22] Colloidal gold provides in this sense the additional advantage that the nanoparticle surface can be easily tailored with small molecules, e.g., by utilizing molecular self-assembly and ligand exchange strategies, or can even be used to graft polymer conjugates to the nanoparticle surface.[23] Basic considerations for optimized imaging conditions for transmission electron microscopy (TEM) of such systems and suitable preparation protocols are summarized in

Chapter 2. The utilization of functionalized colloidal gold nanoparticles allows studying different aspects of cellular internalization and intracellular metabolism. This thesis will specifically discuss three different systems for studying three important issues for targeted drug delivery and drug release (**Chapter 3**). Each system addresses a different targeting strategy which include:

1) The modification of gold nanoparticles with sugar containing polymers to enhance and control their uptake into HEK-293 cells. This system also investigates the influence of the aggregation state of the nanoparticles by introducing a thermoresponsive polymer unit. Four different types of sugar functionalized polymers are selected and attached on the surfaces of spherical Au nanoparticles surfaces. The differences in the intracellular distribution, uptake rate and their localization with respect to the type of sugar functionalized polymer are summarized. (**Section 3.3**).

2) The application of pyruvate functionalization of the gold nanoparticles to allow the guided uptake of the nanoparticles in the mitochondria of cells to stimulate mitophagy (**Section 3.4**).

3) The utilization of a metal-polymer hybrid nanoparticle system, which can trigger the release of a potential target molecule along the endocytic pathway and which utilizes the gradually increasing pH value of the nanoparticles' environment to stimulate the release of the nanoparticle content from the endosome into the cytosol of the cell (**Section 3.5**).

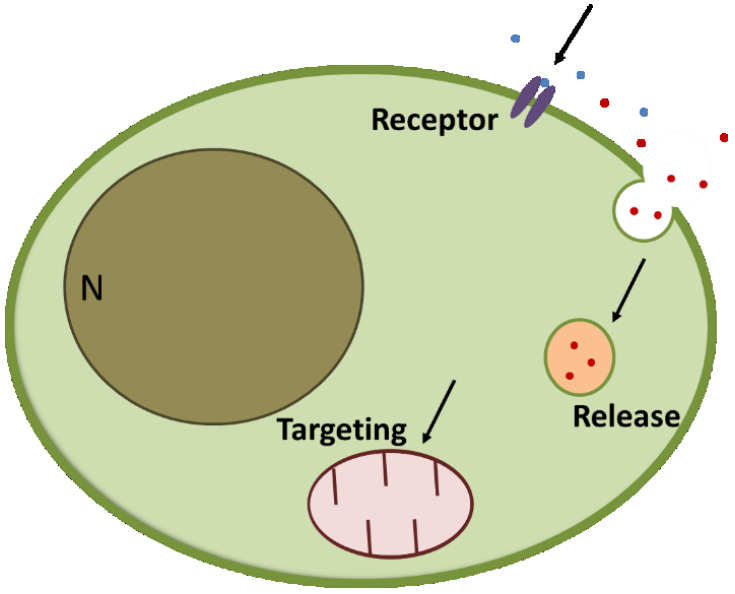

Figure 1 – 1 *Particle uptake by addressing three different strategies studied in this thesis.*

The performed investigations target aspects of the physico-chemical activity of the functionalized colloidal gold nanoparticle systems, utilize advanced and improved imaging

capabilities of transmission electron microscopy and are supplemented by biological tests. The rationalization for the chosen nanoparticle systems are discussed in detail in **Chapter 3** in relation to a discussion of the biophysical and biochemical processes which control the particle uptake.

The utilization of colloidal gold markers resembles a certain limitation in the presented studies. They are mainly used as easily traceable model systems to prove the concepts of the different targeting strategies. Ultimately, polymer nanoparticles are supposed to further improve the drug delivery performance. This is rationalized by the fact that stable gold colloids can only indirectly respond to external triggers (see for example **Chapter 3**). As a consequence, a number of different polymer systems has been investigated, which could potentially replace the colloidal gold markers. These systems are introduced in **Chapter 4**. In particular their morphological properties and the possibilities to tune the structure of the obtained structures as well as their response to external triggers, e.g., pH value and temperature, have been studied by means of cryo transmission electron microscopy (cryo-TEM) investigations. In this chapter additional possibilities emerging from advanced microscopy and preparations are highlighted.

2. Transmission electron microscopy

In this chapter the basics of transmission electron microscopy, used in this thesis as the main investigation tool, will be summarized. This includes, next to a discussion of the fundamental principles, also an in-depth discussion of advanced measurement modes used in this thesis. Specifically, the utilization of scanning transmission electron microscopy (STEM), energy dispersive X-ray (EDX) analysis, tomography and the requirements for sample preparation and preparations at cryo-temperature conditions will be discussed.

2.1. History of TEM

The era of electron microscopy started with the invention of the first instruments in the early 1930th by Ernst Ruska and Max Knoll.[24] Their studies focused initially on the possibilities to manipulate electron beams by magnetic fields, but it soon became evident that it is also possible to obtain visible images of matter with a resolution of 10 to 50 nm.[25] Technical improvements regarding increased acceleration voltages, improved electron lens technology, which drastically reduced aberrations, a better vacuum and brighter electron guns quickly pushed the resolution limit down to 2 nm already in 1944.[26] With Knoll and Ruska pioneering the development of transmission electron microscopy, soon it was recognized that electron microscopy had the potential to provide a high resolution method with interesting capabilities for many different research fields. Ladislaus L. Marton used a simple electron microscopy setup to produce the first micrograph of a biological specimen.[27] Early progresses in material science in the 40th addressed mainly the study of small particles and pigments and it became possible to study their size, shape, number but still could not be possible to reveal their internal structure. The following years showed continuous improvement of the instrumentation resulting in improving the resolution and, at the same time, researchers learned also how to prepare samples suitable for electron microscopy and how to interpret the data.[28]

It has to be stated here that the advancement of electron microscopy has been always an interplay between new technical improvements but, at the same time, also the establishment of new preparation techniques equally contributed to the improvement of electron microscopy studies.

While the first images of cells were conducted on specimens, which were solely fixed with osmium tetroxide, gradually the sample preparation techniques were improved. Milestones of this development include the development of the ultramicrotome between 1948 and 1953 which improved the section quality. Starting from metal blades and glass knives, diamond knives were introduced in 1950s to obtain uniform ultrathin slices from a sample block.[29] Since then, sectioning at room temperature and even at cryo-temperatures provided opportunities for improved sample preparation.[30] In 1955 important contributions were made regarding negative staining protocols, first on virus structures, which resulted finally in the possibility to

stain tobacco mosaic viruses.[31] This procedure was further improved and refined and developed ultimately into a technique of negative staining for high-resolution electron microscopy.[32] During this time, also the selective staining to identify antigen sites was developed by Singer.[33] This method utilized ferritin coupled with immunoglobulins and provided the molecular specificity to visualize a particular protein in the specimen. These studies later developed into immunogold labeling and immunoenzymatic labeling.[34] While many structural analyses on intracellular structures initially were conducted on fractionated cell samples, which separates the intracellular species into fractions of purified materials by centrifugation, the fixation of tissue and cells posed more demands on the sample preparation since the materials to be fixed are relatively thick. The proper choice of embedding medium materials and their compositions are important points connected to the chemical fixation and sectioning.[35] Various embedding media offer different properties such as solubility in dehydrating agents, good penetration into the sample, uniform polymerization, good preservation, good sectioning and stability in the electron beam.[36]

As an alternative for the applied embedding strategies, which are still commonly used today, cryo-fixation methods, e.g., plunge freezing and high-pressure freezing were developed.[37] High pressure freezing is used to vitrify thicker samples up to 200 µm under high pressure. Plunge freezing is performed to freeze macromolecules, drug delivery vehicles and 2D protein crystals very rapidly in a cryogen.[38]

Another breakthrough is marked in 1981 when Dubochet and McDowall[39] introduced cryo-techniques to improve the sample preservation (for details see **Section 2.3.2**). This development was awarded the Nobel prize in chemistry (2017).[40] The prize was shared with J. Frank, who introduced the fundamentals of single-particle reconstruction techniques to reconstruct three-dimensional images of uniform objects by imaging of a large number of these identical particles. 25-Å cryo-EM density maps of the *Escherichia coli* ribosome could be obtained by J. Frank in 1995.[41] Also R. Henderson, who utilized the single-particle reconstruction to obtain atomically resolved three-dimensional structure of bacteriorhodopsin, was awarded the Nobel prize.[42] Current developments enable to reach near atomic resolutions for the determination of protein structures by cryo-tomography.[43] These developments are currently emerging into new routine tools for cryo-electron crystallography and will in the future, be a useful addition to classical X-ray crystallographic techniques. The next challenging step will certainly have to address high resolution studies of proteins interacting within cellular structures.

2.2. Working principle

The working principle of TEM is comparable to the operation principle of conventional light microscopy as illustrated in Figure 2 – 1. The three-lens design as well as the beam path are comparable in both instruments. It consists of a condenser lens, which renders a divergent

beam from a point source into a parallel or converging beam to illuminate an object, and the objective and projection lenses produce a magnified image of the specimen on the viewing screen. In TEM the image is projected either on a phosphorescence screen for visualization or is recorded by means of a charge coupled device (CCD) camera. The main difference between a classical optical microscope (OM) and the TEM is the type of illumination used to investigate a sample (see Figure 2 – 1).

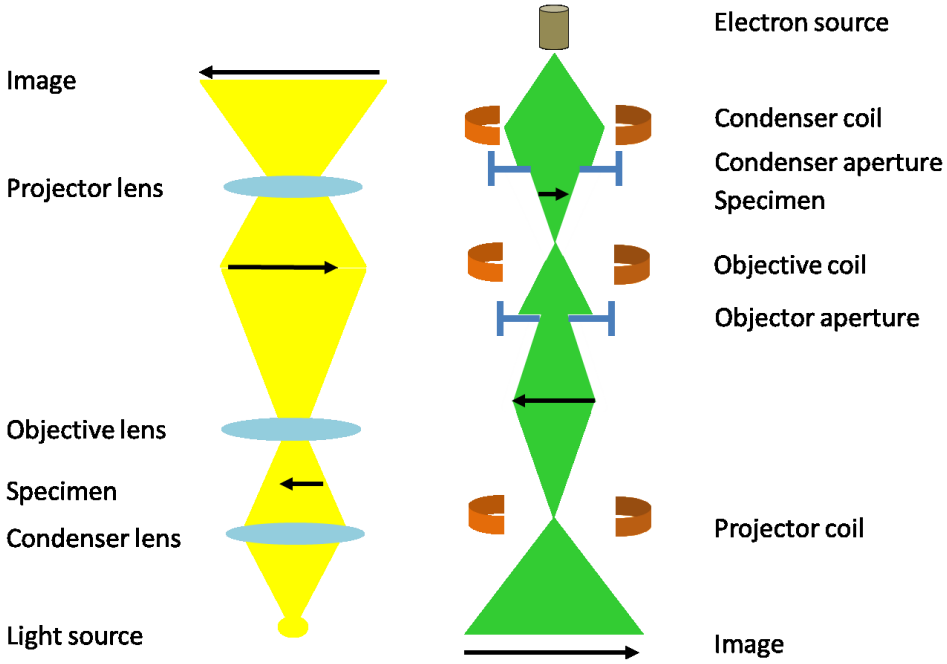

Figure 2 – 1 *Comparison of the beam path of an optical microscope (left) and the transmission electron microscope (right).*

While a light source is used in OM, an electron beam is used in TEM. The utilization of electron beams requires the implementation of electromagnetic lenses to shape and focus the beam, which essentially fulfill the same role as the glass lenses in an optical microscope and requires operation at ultra-high vacuum conditions.

The utilization of the electron beam is the key point why the resolution of TEM is higher compared to OM. In optical light microscopes the resolution limit is defined by the Abbe's formula.[44] It relates the numerical aperture (n·sinα, where n is the index of refraction of the medium and α is the half angle of the maximum cone of light that can enter the microscope) of the microscope and the wavelength (λ) of the illumination source to the minimum resolvable dimensions (d).

$$d = \frac{\lambda}{2n \cdot sin\alpha}$$

The advantage of electron microscopes becomes clear when one takes into account the wavelength of electrons accelerated by high voltages. At higher acceleration voltages relativistic effects have to be taken into account and the wavelength can be calculated according to:

$$\lambda[pm] = \frac{h}{\sqrt{2m_0 eE^*}} = \frac{1.23 \cdot 10^3}{\sqrt{E(1 + 9.78 \cdot 10^{-7}\, E)}}$$

where h is the Planck constant, m_0 is the rest mass of the electron, e is the elementary charge of the electron, E is the accelerating voltage before the relativistic correction and E^* is the acceleration voltage after the relativistic correction.

In this case one derives at a wavelength of ~2.5 pm for electrons in a 200 kV acceleration field. This is regarded as the main reason for the extraordinary resolution power of an electron microscope. It has to be mentioned here that the practical resolution power usually does not meet these values but is in the range of 0.1 to 0.2 nm due to imperfections of the lens system, non-monochromatic electron beams, or due to limitations created by the sample system itself.[45]

The electrons are produced in an electron gun. These electron guns consist nowadays mainly of LaB_6 crystals, where electrons are thermally extracted from the filament or are produced in a field emission gun.[46] The latter offer the advantage that the beam is brighter, more coherent and more stable and can be focused into a finer beam profile. On the other hand, these electron sources are rather expensive and require better vacuum conditions within the instrument. The TEM investigations summarized in this thesis have been conducted on an instrument operating with a LaB_6 filament. This compromises the achievable resolution but is entirely sufficient to resolve the targeted structural details of biological specimens and can reveal even the crystalline structure of colloidal gold nanoparticles.

After the electrons are extracted from the electron gun they are accelerated by means of a Wehnelt cylinder to the requested acceleration energy levels. The beam transverses through a condenser electron lens which converts the beam profile into a homogeneous, quasi parallel electron beam. Utilization of a condenser aperture can improve the beam quality but also minimizes the beam intensity. After that, these electrons are transmitted through the sample. Here the interaction of the electrons with the matter of the sample results in scattering effects as illustrated in Figure 2 – 2. The scattered electrons are deflected out of the beam, while some pass directly through the sample. The scattered electrons are divided into two classes, namely, elastically scattered and inelastically scattered electrons. Elastically scattered electrons are scattered at the nuclei of the target atom by Coulomb forces without energy transfer and they contribute to the contrast in TEM. The angle of scattering depends directly proportional on the atomic number and is inversely proportional to the electron energy. Inelastically scattered

electrons transfer their energy to the sample and cause emissions, e.g., of X-rays, visible light and secondary electrons.

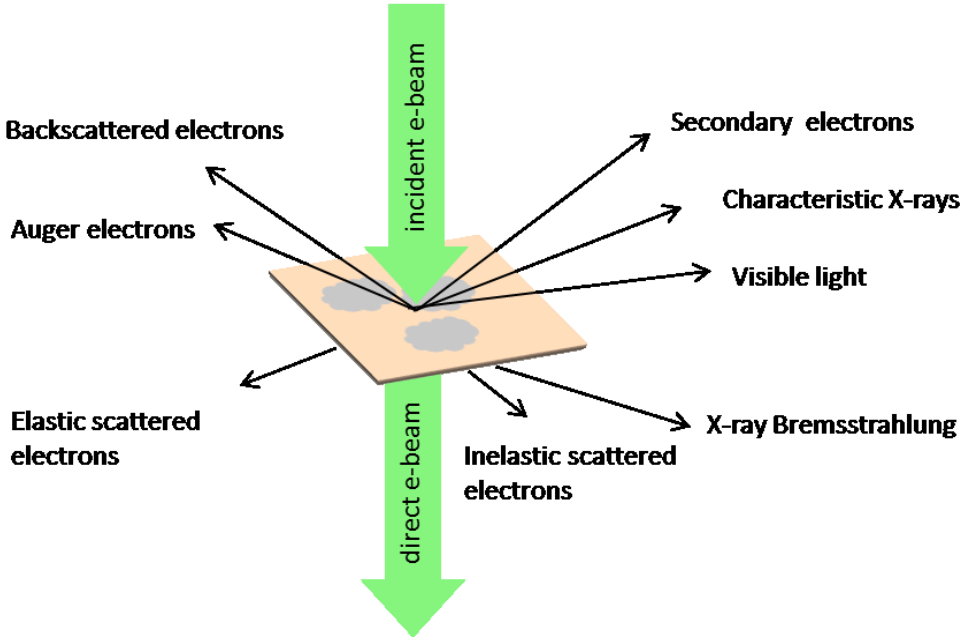

Figure 2 – 2 *Interaction between the electron beam and the sample in the TEM.*

The transmitted electron beam is directed to the objective coil to magnify the image and is further enlarged by the projection lens. Magnifications up to 700.000× up to 1.000.000× can be realized in modern TEMs.

The simple observation of the "shadow" image of the sample resembles the bright-field measurement mode. Highly scattering areas of the sample appear with a dark contrast whereas undisturbed electrons passing through the sample are creating a bright background or bright contrast, respectively. The contrast of the final image is governed in the first instance by the atomic weight and thickness of the sample.[47] Heavy elements of the specimen scatter the electrons stronger and appear darker in the final image. The contrast generated by this effect is called Z-contrast or mass contrast. Thicker regions of a sample (supposed they are providing the same average Z contrast) appear also darker with respect to thinner regions. The image contrast can be significantly increased by the use of a contrast aperture, which is located in the beam path after the beam transversed through the sample.[48] The purpose of this aperture is to block elastically scattered electrons from the beam. The size of the aperture relates to the contrast enhancement and determines which electrons finally can contribute to the image. For smaller inserted apertures an improved imaging contrast can be observed.

However, in particular biological samples require the artificial staining of the cellular structures by heavy elements (for details see **Section 2.3.1**). Sometimes this procedure can produce artifacts or masks the contrast of objects within the cellular framework.[49] Therefore, modern TEM instruments provide a number of alternative measurement modes which can generate, e.g., a more pronounced material specific image contrast. One possibility to achieve improved contrast of electron dense features is provided by Scanning Transmission Electron Microscopy (STEM).

2.2.1. Scanning Transmission Electron Microscopy (STEM)

In this measurement mode the sample is not illuminated with a parallel electron beam but the beam is focused into a very small spot. This electron probe is scanned across the sample by means of dedicated beam coils. In each point the electron probe interacts with the sample and electrons either transverse directly through the sample with no or only minimum deviation from the incident direction, or electrons, hitting areas with higher electron density, are scattered towards higher angles. These electrons are used in STEM for image generation. This is implemented by utilization of a ring detector as illustrated in Figure 2-3.

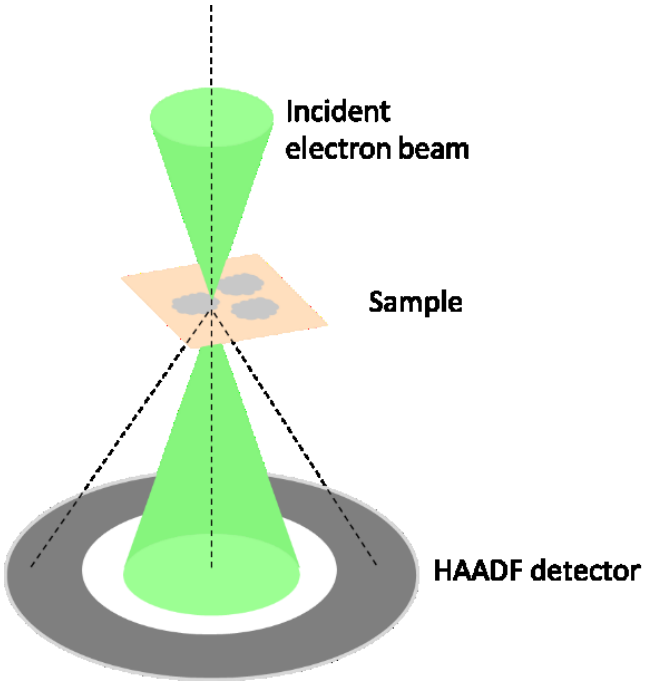

Figure 2 – 3 *Illustration of STEM mode and the ring detector (HAADF = high-angle annular dark-field).*

The ring detector registers all electrons which are scattered out of the beam and the intensity of this signal is ascribed to the scan position of the beam. This information basically reconstructs the structural features of the sample. Materials contrast can be generated within this measurement mode taking advantage of the fact that the scattering angle of electrons is larger if the mass of the scattering atom is larger. This generates a material dependent contrast in

STEM imaging and enhances weak contrasts, which are barely visible in bright-field TEM investigations.[50] For biological samples the utilization of a high-angle annular dark-field (HAADF) detector, i.e., a ring detector with large diameter, is beneficial as it is in particular sensitive to relatively heavy atoms. This can be nicely demonstrated by a comparison of bright-field and STEM investigations performed on the same cell structure as depicted in Figure 2 – 4. The cell sample under investigation was in this case only mildly stained during the post fixation step, which includes only the exposure to osmium tetroxide.

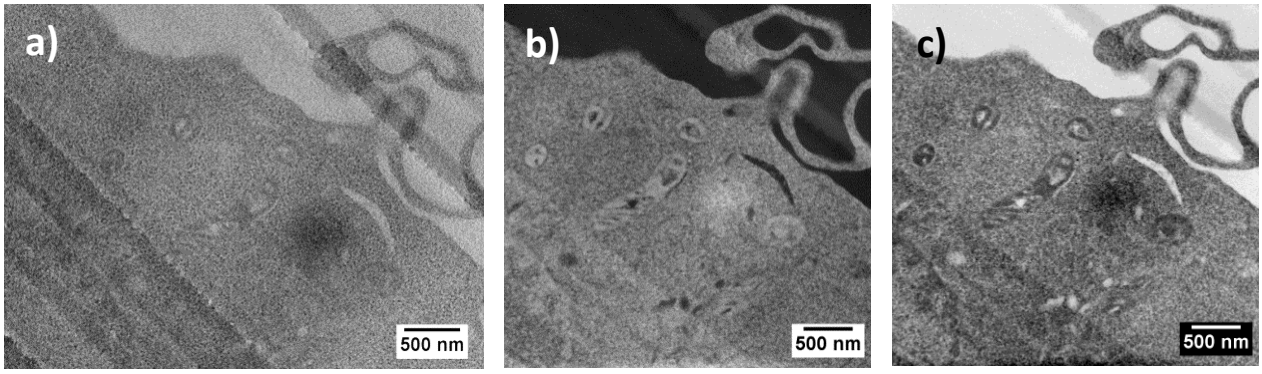

Figure 2 – 4 *Comparison of TEM and STEM mode for contrast improvement. Ultrastructural details of a cell are only slightly visible in BF-TEM (a), while the HAADF-STEM mode presents even the details of mitochondria clearly (b). c) The image is inverted for visibility reasons. (Images were reproduced from the Master thesis.[51])*

2.2.2. EDX analysis

While STEM is capable of highlighting heavy atoms in a sample or areas of higher concentration of such atoms (e.g. stained membrane structures), the illumination scheme of a focused electron beam can also be used to perform chemical analysis.[52] Essentially two different methods can provide the chemical fingerprint of an illuminated area. Energy dispersive X-ray analysis (EDX) or electron energy loss spectroscopy (EELS). The latter is more sensitive towards lighter elements, whereas in the framework of the present thesis EDX investigations have been performed to unambiguously identify gold or calcium phosphate nanoparticles in the cellular framework. EDX makes use of the fact that electrons might induce the emission of characteristic X-rays when irradiated with the electron beam. In this case, the beam electrons can occasionally eject electrons from the inner electron shells of the target atom as depicted in Figure 2 – 5.

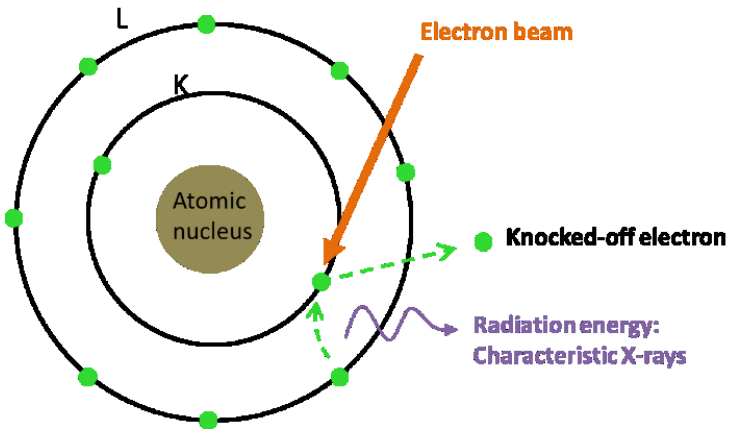

Figure 2 – 5 *Schematic representation of the characteristic X-ray emission from the target atom.*

The created electron hole is subsequently filled up with an electron occupying an outer shell of the atom. The differences in the energy state are compensated by the emission of an additional X-ray photon, whose energy depends on the characteristic energy differences of the energy levels. These are characteristic for each type of atom and provide a clear signature of the nature of the atom itself or of the chemical composition of the sample.[53] The chemical information can be extracted as a spectral information, or by using the STEM scanning mode, also as a chemical mapping where the presence of certain atoms is highlighted in the images.[54] A representative example can be seen in Figure 2 – 6. A cell of Saccharomyces cerevisiae incubated with Au nanoparticles was imaged in the STEM mode (Figure 2 – 6a) and a chemical mapping was recorded (Figure 2 – 6b). The locations of the Au nanoparticles are indicated by the green points on the image, which show that the Au nanoparticles are mostly found on the cell membrane. Spectral information from isolated measurement areas, e.g., inside of the cell (Figure 2 – 6c) and on the cell membrane (Figure 2 – 6d), prove the preferential localization of the Au nanoparticles on the cell membrane.

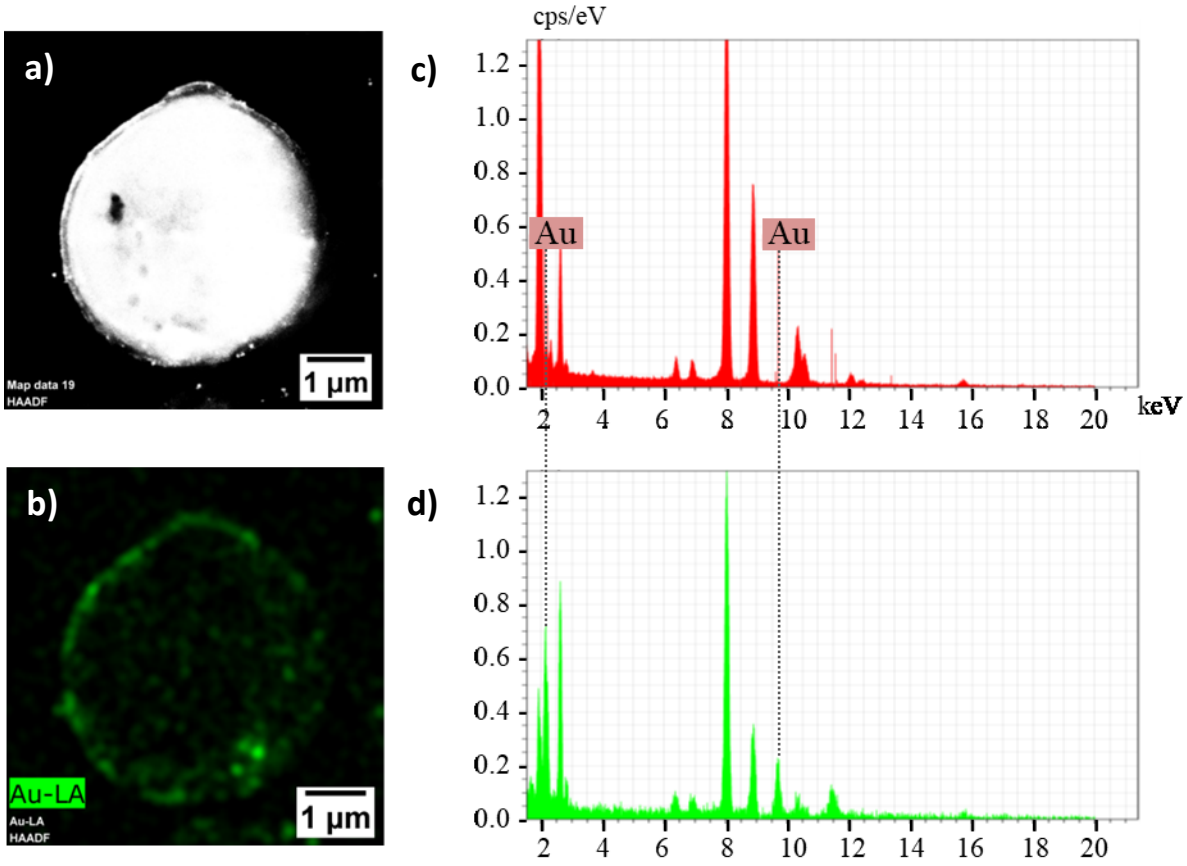

Figure 2 – 6 *a) STEM image of a cell of Saccharomyces cerevisiae. b) Chemical mapping of the same cell. c) Elemental spectrogram recorded inside of the cell. d) Elemental spectrogram recorded on the cell membrane. The image is inverted for visibility reasons. (Images were extracted from the Master thesis.[51])*

2.2.3. Tomography

One major drawback of electron microscopy studies is the fact that the three-dimensional structure of objects is lost due to the projection step during imaging. The limitation that we only can visualize the "shadow" image of the sample makes it, e.g., difficult to directly localize a nanoparticle at its characteristic position (e.g. when associated to actin filaments or interacting with membranes). With the availability of advanced software routines, which allow handling of large data sets and improved imaging possibilities, new techniques to access the three-dimensional structure of samples have significantly advanced.[55] To date sophisticated routines to perform single particle reconstruction or tomography protocols are implemented as state-of-the-art methods in modern electron microscopy. While single-particle reconstruction procedures are limited to identical objects (e.g. proteins), TEM or STEM tomography has been introduced as a method to reconstruct the three-dimensional structure of arbitrary, non-regular specimens.[56] For this purpose, an image series of a sample area has to be obtained, which is acquired under different viewing angles. For this purpose, the sample is tilted within the TEM

and respective images of the sample area are recorded. All these projections are subsequently reconstructed to provide the three-dimensional structure of the area under investigation. The quality of the obtained reconstructions critically depends on the number of images, the maximum obtainable tilt angles and the quality of the images itself.[57] Typically, an image series for reconstruction comprises at least of a set of images acquired between –60° to +60° with an increment angle of $\leq$ 1°. The algorithm for reconstruction relies in particular on the images obtained at high tilt angles. Since, technically, the obtainable angles are limited to –70 ° to +70 ° the reconstruction of the structure can never be perfect. The images which are missing to make a full turn will always limit the quality of the reconstruction.[58]

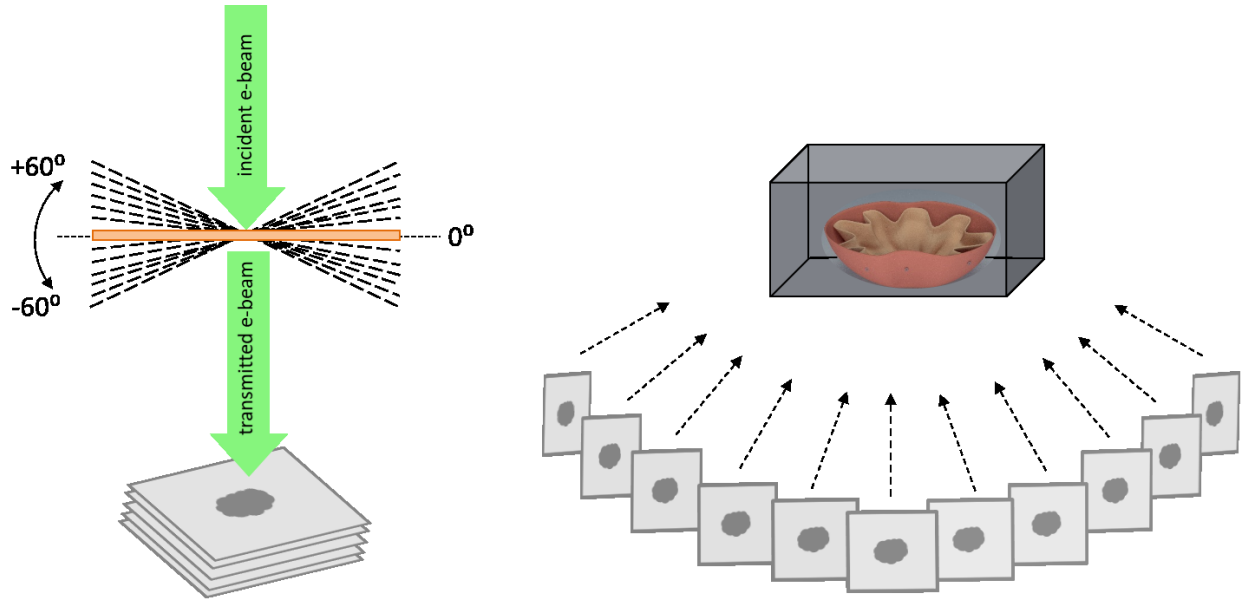

Figure 2 – 7 *A set of images acquired between –60° to 60° is recorded and the object is reconstructed.*

Modern TEM instrumentation provides the operator with useful tools to acquire the tomography series. It basically can automatically adjust the focus, re-center the region of interest and perform the tilting in an automated fashion. If necessary, also the image intensity for higher tilt angles is automatically adjusted, as in this case the apparent film thickness increases due to the tilting.

A major concern of applying TEM or STEM tomography is the stability of the sample. This is less critical for embedded samples, even though beam damage or shrinking of the cellular structures might be observed sometimes, but it is certainly an issue for more sensitive samples. One example is, e.g., the elucidation of the three-dimensional structure of polymer nanoparticle systems. These are extremely beam sensitive, nevertheless a set of $\geq$ 120 images is required to successfully run a reconstruction. Therefore, the stability of the samples always has to be evaluated or sophisticated preparation protocols or imaging techniques, i.e., low dose imaging,

have to be applied.[59] In the case of polymer nanoparticles cryo-TEM preparation should be considered (see **Section 2.3.2** for more detailed information).

2.3. Sample preparation for TEM investigations

As mentioned before, the quality of TEM imaging depends not only on the available instrumentation but also strongly relies on suitable sample preparation methods. These are always implemented with the aim to preserve the structure of the samples in the best way and, at the same time, to allow their investigation by TEM. This can be a demanding task, in particular for cellular systems, which are a particularly challenging sample system. These systems are addressed in **Chapter 3** of this thesis. Also, the characterization of self-assembled polymer nanoparticle systems, which have been studied in **Chapter 4**, requires specialized preparation protocols.

2.3.1. Sample preparation of cellular systems

Cells resemble a challenging system for TEM investigations. This can be rationalized by the fact that cells are natural systems, which consist of dynamic and fragile membrane structures, which are easily destroyed. Moreover, cellular systems contain a large amount of water. When such systems are transferred into a vacuum environment, the water tends to rapidly evaporate, and the cellular structures are altered and easily destabilized. Moreover, the electron beam can easily damage the structures of interest and, at the same time, cellular samples and tissues resemble systems which inherently provide only weak electron contrast. These problems can be addressed by suitable sample preparation protocols.[60] Many of these were developed already in the 1960th and have been since then only marginally modified. This is related to the fact that each processing step potentially can also alter the intracellular structure due to the chemical modification of the cellular constituents. This has to be prevented with the consequence that each variation of established protocols has to be carefully evaluated and approved. For this reason, a standardized preparation protocol was chosen in the experiments summarized in this thesis, which is regarded as a standard protocol for the preparation of cells for TEM measurements. The main preparation steps for the chosen protocol are summarized as follows: Fixation, post-fixation and staining, dehydration, infiltration and embedding in a resin, and slicing.

Fixation is the first important step for sample preparation. Chemical fixation is applied in order to preserve the cells in a native-like state by crosslinking their proteins. Fixation reagents should crosslink the intracellular structures fast and should not induce undesired alterations of the intracellular membranes and organelles. The success of a good fixation can be described moreover by preserving the cells in their native-like state with a minimum shrinkage. There are several chemicals to obtain well preserved cells. These include: Formaldehyde, glutaraldehyde, mixtures of formaldehyde and glutaraldehyde (GA), and osmium tetroxide.[61] The choice of a

fixative chemical critically depends on the type of sample and the aim of the study. In this thesis, glutaraldehyde was mainly used for fixation of HEK-293 cells. Glutaraldehyde was introduced in the field of electron microscopy in 1963 by Sabatini.[62] It is a small molecule which penetrates quickly into the cell. It consists of two aldehyde groups, providing C–HO groups at both ends.[63] These allow, for instance, crosslinking between the C–HO and $–NH_2$ groups being present in the sample, e.g., within proteins, as depicted in Figure 2 – 8. Reactions between phospholipids containing free amino groups and glutaraldehyde are also possible.[64]

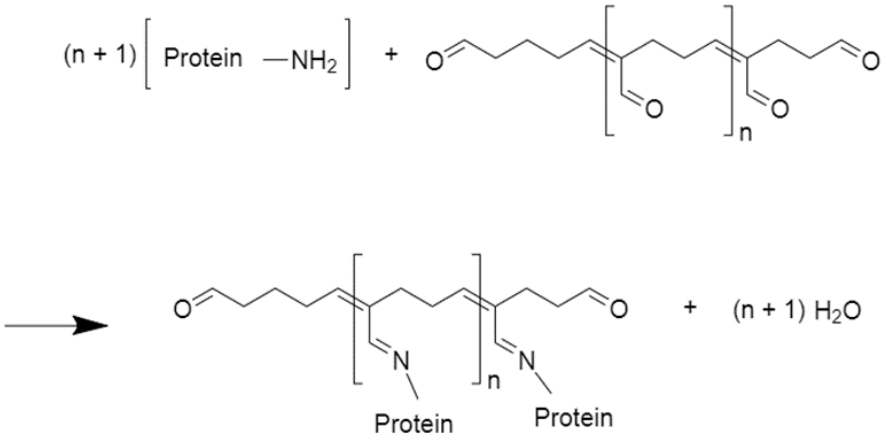

Figure 2 – 8 *Schematic representation of the crosslinking of proteins by glutaraldehyde. (Adapted from Microscopy Today.[63])*

Post-fixation and staining can be achieved by applying osmium tetroxide at a defined concentration and duration.[65] Osmium tetroxide can penetrate into cells and interact with the C=C double bonds of unsaturated lipids of phospholipids, as depicted in Figure 2 – 9. This step is formally referred to the post-fixation, but due to the fact that Osmium is a heavy element staining of the cells for electron microscopy is introduced at this preparation step at the same time.

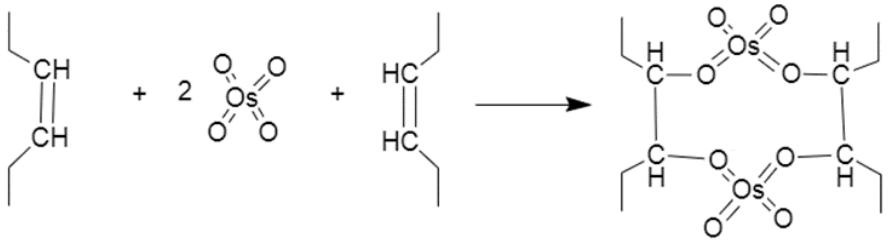

Figure 2 – 9 *Schematic representation of the post-fixation of unsaturated fatty acid chains by osmium tetroxide.*

The next step is to replace the water being present in the cells to ensure that the embedding medium can infiltrate into the cells properly and polymerization of the resin embedded samples can occur. Dehydration can be performed with a graded concentration series of increasing ethanol, acetone, or propylene oxide concentrations.[66]

After dehydration the cells are infiltrated with the resin. There are several options to harden the cells. These can be listed as follows: EPON resin, Spurr's resin, London resin (LR) white and LR gold resin.[67] The choice of the embedding medium is highly related to the sample and the aim of the study. Spurr's resin infiltrates better into plant and insect materials than EPON due to its low viscosity. Spurr's resin and EPON behave similarly with respect to sectioning, staining and contrast properties. For the studies which requires post-staining steps, the type of resin has an impact on the staining efficiency. LR white is widely used in this case because it can preserve antigenicity, which is important, e.g., for immunogold studies.[67] Generally, they all infiltrate into cells and are polymerized at elevated temperatures or by illumination with UV light. Parameters for good infiltration and hardness can be optimized by changing the ratio of ingredient chemicals of the resin. Curing agents, e.g., *tris*(dimethylaminomethyl) phenol (DMP-30) and benzyldimethylamine (BDMA) are used to accelerate the reaction. The amount of the curing agent has an effect on the color, brittleness and hardness of the final resin block.[68]

After sample hardening the embedded sample block has to be sliced down into 80 to 120 nm thick slices. An ultramicrotome can be used to obtain such thin slices. The wet cutting method is used to slice the block with a mounted diamond knife and to float the obtained ultrathin slices on the surface of a water reservoir, as seen in Figure 2 – 10 (right). The swimming slices on the water bath can be easily transferred onto TEM grids by using a loop. With this method the fragile slices can be handled with minimal mechanical forces and the surface tension of the water ensures that the slices are stretched and no folds are formed.[30] In this thesis, all the sample blocks were sliced by utilization of the wet cutting method.

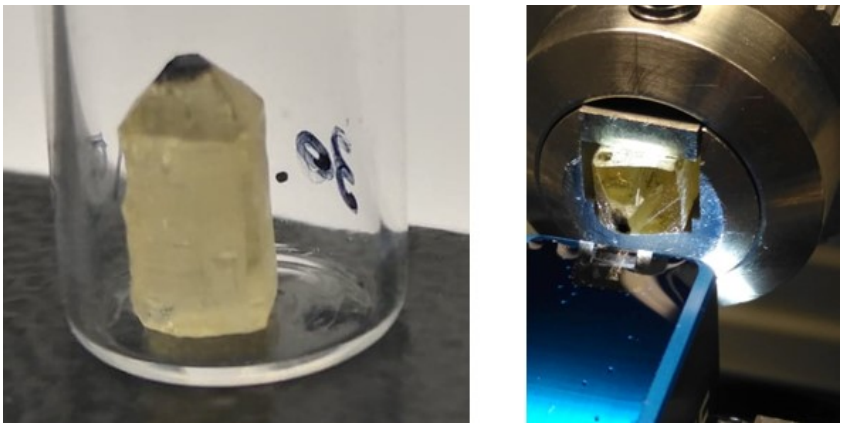

Figure 2 – 10 *Photography of cell pellet, which is embedded in a resin (left) and sliced by a diamond knife mounted on an ultramicrotome (right).*

Sometimes it is necessary to apply post-staining to the samples in order to further improve the contrast. Uranyl acetate (UA) and lead citrate are widely used post-staining agents.[69] The high atomic number of Uranium enables to improve the contrast of cell membranes since its ions bind to proteins and lipids, with sialic acid carboxyl groups, such as, glycoproteins, and also interact with the nucleic acid phosphate groups of deoxyribonucleic acid (DNA) and ribonucleic acid (RNA). Uranyl acetate provides the highest electron density due to its high mass. Most commonly, it is applied as a dilute aqueous solution. Typical concentrations used for post-staining are in the range of 0.5 to 3% and the pH value varies between 4.2 to 4.9. In these conditions, uranyl acetate stains well negatively charged molecules. Disadvantages of uranyl acetate are the sensitivity to light and the formation of precipitation, and its toxicity. Lead citrate also causes an improved contrast due to the interaction of lead ions with polar group being present in the molecules. Lead citrate staining is observed to be most efficient if previous treatments with other staining agents have been conducted. Reduced Osmium and also uranyl acetate can improve the staining capabilities of Lead citrate significantly. Hence, lead citrate staining is always applied after uranyl acetate. Lead citrate can stain a wide range of cellular structures, e.g., ribosomes, lipid membranes, the cytoskeleton and other compartments of the cytoplasm.[70] Here it should be mentioned that staining might cause confusion if the stained structures are in the same size range and provide similar shape as, e.g., the drug delivery systems. This can happen, e.g., when lead citrate is used, which can efficiently stain ribosomes. These structures feature a round shape and the protein structure shows a rather similar size like many colloidal gold nanoparticle systems.[71] As a consequence, the colloidal gold nanoparticles and the stained ribosomes appear with a similar contrast. This can complicate a proper assignment of the structures.

Similar to cell preparation, special considerations have to be taken into account for the characterization of nanoparticle systems. In the case of the mainly utilized colloidal gold nanoparticles, which are relatively non-critical in terms introducing artifacts during sample preparation, this statement is not valid for nanoparticles consisting of soft materials, like polymer nanoparticles. These systems have been characterized in **Chapter 4** of this thesis and deserve special attention as sophisticated preparation strategies have to be applied in order to preserve their structure and to characterize their morphological features in a solution-like state. For this purpose, the utilization of cryo-TEM investigations is recommended.

2.3.2. Sample preparations for Cryo-TEM

Normally, the easiest way to visualize nanoparticle systems by TEM is to drop a small amount of the sample on a carbon coated TEM grid and let it dry. However, in terms of nanoparticles consisting of soft matter, drying the sample on a surface may cause morphological changes of the nanoparticles or cause changes in their aggregation state. As a consequence, alternative

preparation techniques are required. Cryo-TEM is the best technique so far to image the sample in a solution-like state.[72]

Cryo-TEM is based on vitrifying the sample in an ice film and imaging it at liquid nitrogen temperature. In 1986, Dubochet *et al.* presented their imaging results on successfully thin vitrified layers of unfixed, unstained and unsupported virus suspensions.[73] The technique showed that water can be cooled so rapidly that it is solidified in its liquid form without the formation of ice crystals. With this achievement and also further improvements in detectors and software, in particular, low dose imaging modes, applications of cryo-TEM spread into various fields of science.[74]

For cryo-TEM preparations, a small amount of sample solution is applied on a carbon coated TEM grid and blotted with a filter paper to remove excess solution and form an approximately 100 nm thick sample film on the grid. The grids used in cryo-TEM measurements are mostly not a simple carbon coated mesh but consist of a carbon film with regular holes of defined size as depicted in Figure 2 – 11. Alternatively, lacey carbon films can be used for cryo-TEM preparations.

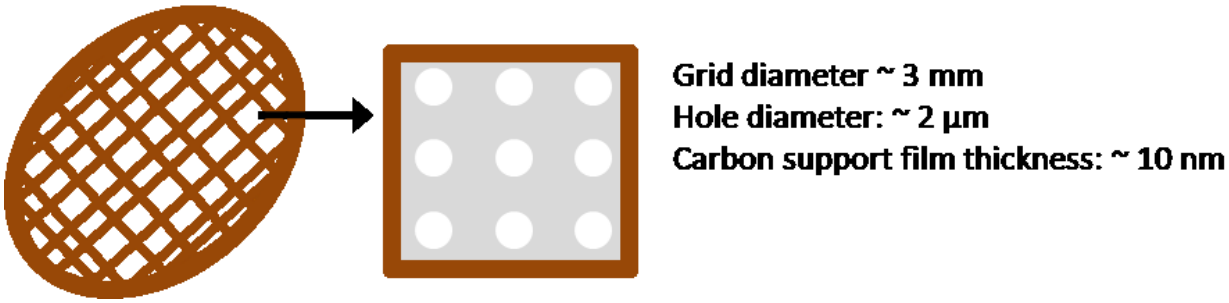

Figure 2 – 11 *TEM grids used for cryo-TEM measurements.*

The film formation can be controlled by means of special devices and tools (Figure 2 – 12a) to ensure a reproducible vitrification process. One can control very easily the temperature, humidity and other parameters, such as the force and time applied during the removal of the excess water during sample preparation for a better formation and preservation of the thin liquid sample films. The grid is subsequently plunged very quickly into liquid ethane cooled at liquid nitrogen temperature (Figure 2 – 12b). The water molecules in the sample are rapidly vitrified and preserve the samples in a solution-like state (Figure 2 – 12c). The grid is transferred into a microscope sample holder, which is kept at liquid nitrogen temperature (Figure 2 – 12d, e).[75] The steps of sample preparation are summarized in Figure 2 – 12.

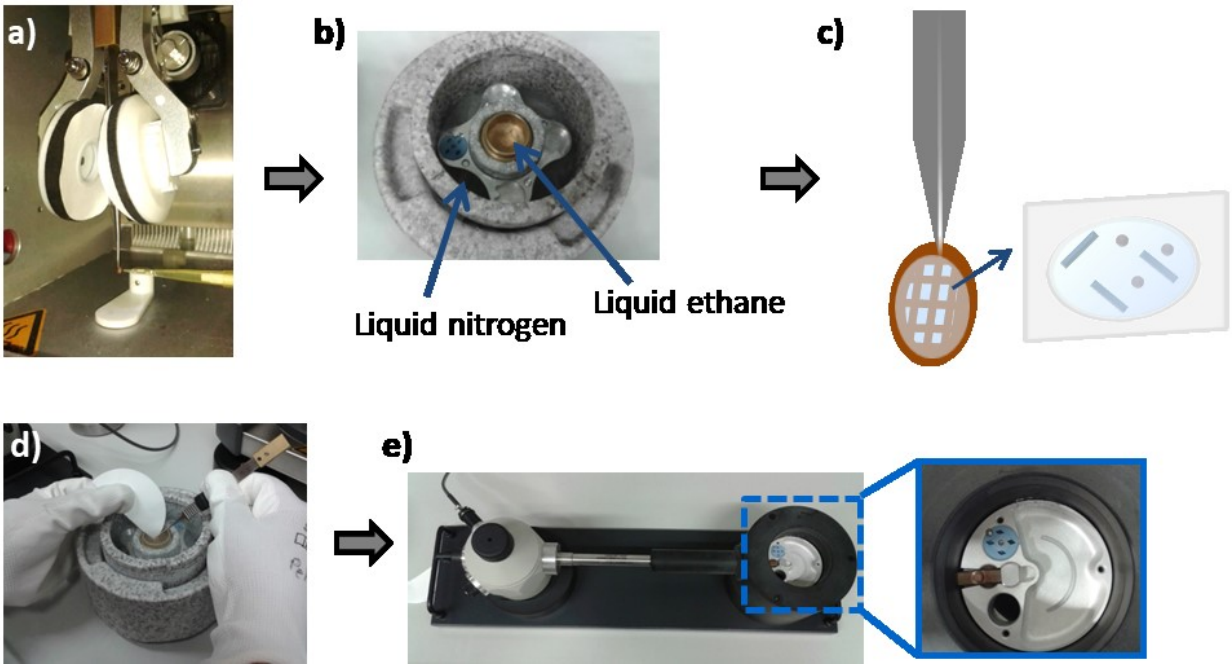

Figure 2 – 12 *Steps of sample preparation for cryo-TEM measurements. a) A small amount of the sample solution is applied onto the TEM grid and blotted by filter paper. b) It is plunged directly into liquid ethane kept at the temperature of liquid nitrogen. c) A thin film of vitrified ice is formed within the holes of the TEM-grid. d,e) The grid is transferred to the microscope sample holder, which is also kept at the temperature of liquid nitrogen.*

Although the preparation technique looks simple, there are several challenges to overcome during sample preparation and TEM measurements.[75] The first, and most important, issue is the formation of the vitreous film. Depending on the temperatures experienced by the sample different forms of ice can be obtained: Hexagonal ice, cubic ice and vitreous ice. Hexagonal and cubic ice appear as structures, which may cause confusion with the objects of interest and even can block the view on the sample as depicted by the arrows in Figure 2 – 13a. Liquid ethane cooled at liquid nitrogen temperature is commonly used to vitrify water because liquid ethane provides a higher thermal conductivity and a better heat capacity compared to liquid nitrogen. A high thermal conductivity is necessary to vitrify the solution as rapid as possible during plunging into the cryogen. A high heat capacity is also necessary to compensate for the Leidenfrost effect. The Leidenfrost effect can be described as the formation of an insulating gas film surrounding the object caused by the rapid boiling of the cryogen. Another critical issue to avoid artifacts in the vitrified sample film is the deposition of atmospheric water vapor from the environment during the transfer of the grid to the sample holder (Figure 2 – 13a). Therefore, one should avoid air contact to the grid during sample transfer. At the same time, mechanical influences, i.e., transferring the grid by tweezers, may impair the straightness of the grid.

Breaking of the grid or the film on the grid may be observed later during imaging (Figure 2 – 13b).

Another issue is the distribution of the sample suspension on the TEM grid. Generally, TEM grids are coated by carbon to form a support film containing a hole-like structure. Slight variations in the film thickness of the prepared films can occur across the individual holes resulting in thicker samples formed at the edges of the holes. Hence, larger particles are preferentially observed to be localized within the thicker film at the edges. Smaller particles are more frequently found in the middle of the holes. Even deformation of the film may happen due to large particles. To remove surface contamination as well as to improve the wettability of the grid, argon-plasma cleaning of the grids prior to the sample preparation is applied.

Another important issue is electron beam damage, which has to be avoided as much as possible. The energy of the electron beam is high enough to break the bonds of the objects as well as to melt the vitrified film. Long time exposure with the electron beam on the sample results in the formation of bubbles on the objects and leads to a destruction of the objects of interest (Figure 2 – 13c).

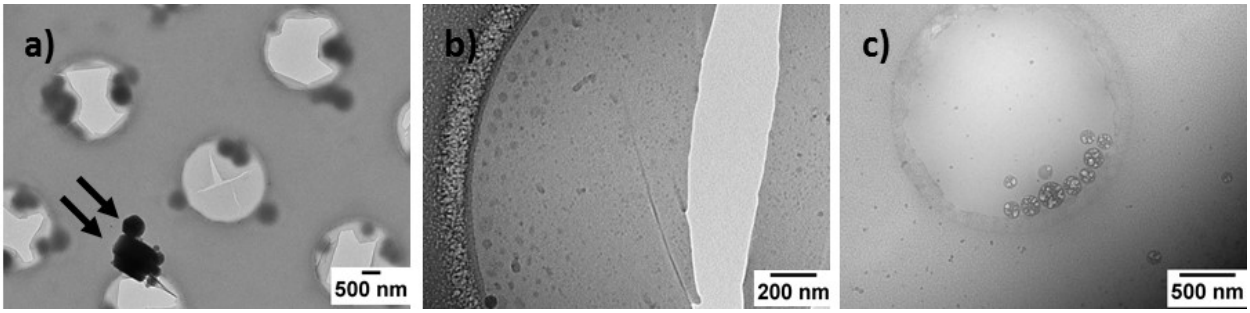

Figure 2 – 13 *Some examples of experimental problems sometimes encountered during cryo-TEM measurements.*

With the development of the sample preparation techniques and instruments, cryo-TEM started to be used in many fields, e.g., in polymer chemistry.[76] This preparation technique was used in this thesis mainly for the characterization of different polymer drug delivery systems. By synthesis and combination of polymers, one can obtain various shapes and can introduce structural changes of the systems by changes of the nanoparticles' environment. As such, polymers and polymer nanoparticles are often used in drug delivery systems to encapsulate the drugs, so that the drug can be protected during the uptake pathway and even be released at specific environmental conditions. Changes on the morphology of the polymer structures may occur also by changing the pH value and the temperature. Important issues in this field include the question of determining the polymer morphology and to visualize the changes of their appearance under such condition. For this purpose, cryo-TEM represents a very promising

imaging technique for the characterization of aggregation state and morphology of polymeric suspensions in a solution-like state.[77]

The results on the structural investigation of polymeric drug carriers are presented in **Section 4.4,** next to a detailed motivation and discussion as to why polymer nanoparticles can replace surface modified colloidal gold markers and are more versatily applicable.

In summary, simple TEM investigations as well as advanced imaging modes for the acquisition of TEM images have found a large number of applications in science these days. It provides structural information with a resolution that is still unmatched by any other microscopic technique and has been customized for the investigation of very different sample systems. In particular, in the field of biology, the impact of the availability of dedicated TEM preparation techniques strongly pushed the understanding of cellular architectures and their response to external stimuli tremendously and could reveal peculiarities of cellular uptake mechanisms. Additionally, attractive possibilities to study the uptake and metabolization of nanoparticles can be addressed with a resolution that allows to trace a single nanoparticle within the cellular environment. These advantages are used in this thesis to investigate three different drug delivery systems, which are designed to interfere with the uptake processes at cellular membrane and the metabolization cycle of human embryonic kidney cells (HEK-293). Nanoparticle characterization as well as the assessment of their uptake mechanism and their fate in the cellular environment are mainly performed by TEM investigations and advanced imaging routines have been implemented in order to improve the understanding of the mode-of-action of the designed particle systems. In **Chapter 3** surface functionalized colloidal gold nanoparticle systems will be introduced, which have been tailored by functional materials which can mediate the uptake of the nanoparticles at the plasma membrane (**Section 3.3**), can stimulate the targeting of the mitochondria (**Section 3.4**), and introduce a polymeric matrix which facilitates endosomal escape (**Section 3.5**). The key requirements of the intracellular metabolic cycle are first outlined to motivate the utilization of the chosen nanoparticle systems (**Sections 3.1** and **3.2**).

3. Targeted drug delivery and endosomal release

3.1. Main requirements for targeted drug delivery

Targeted drug delivery faces several critical issues. Drug delivery systems might be designed in such a way that only specific cells are addressed by the nanoparticle systems or their uptake is mediated by specific interactions. In order to outline the possibilities to establish targeted drug delivery strategies to cells a general overview of uptake and metabolic pathways taking place is provided in the following.

Cells consist of a number of specialized cellular compartments which fulfill dedicated tasks. These are included into a plasma membrane, which forms the interface of the cell interacting with the environment and separates the interior of the cell from the extracellular matrix.

The plasma membrane consists of a lipid bilayer mainly formed by phospholipids which contain embedded proteins. The cell membrane is responsible to establish the transport of substances in and out of the cell, governs cell adhesion, ion conductivity and cell signaling processes. The transport of materials entering or leaving the cell across the plasma membrane is facilitated either by passive or active transport mechanisms. These include: passive osmosis and diffusion, transmembrane protein channels and transporters, endocytosis and exocytosis. Diffusion processes are generally limited to small molecules or small nanoparticles. The later have been found to translocate the plasma membrane if their size is smaller than 25 nm.[78] This processes are mainly unspecific to the materials entering the cell. Transmembrane protein channels and transporters on the other hand extend through the lipid bilayer and can transport nutrients, such as sugars or amino acids, into the cell or can excrete products of metabolism. Such an exchange can proceed either passive through protein channels by diffusion or substances are actively pumped across the membrane by transmembrane transporters. Protein channels, also referred to as permeases, are usually specific and recognize as well as transport a limited variety or even only a single molecular species of chemical substances. Examples of such selective transmembrane transport proteins are, e.g., glucose transporters (GLUT), which catalyze the transport of glucose or fructose into the cell.[79]

In **Section 3.3** the selectivity of the GLUT transporters with respect to the uptake of different sugar molecules is studied as an example for the selective and enhanced uptake of sugar functionalized drug carriers. It represents an example where the targeting takes place due to direct interaction with the plasma membrane of the cell.

For larger objects to enter the cell alternative uptake pathways are employed. Endocytosis refers to the process in which cells internalize materials by engulfing them. Therefore, the plasma membrane deforms and creates an inward-directed invagination in which the materials to be taken up are captured. The invagination formation is established by proteins located at

the extracellular side of the plasma membrane, acting as receptors and cluster into depressions that can promote the gathering of proteins and lipids on the inner side of the lipid membrane.[35] These deformations form a vesicle containing the material to be taken up. The size range of materials to be taken up by endocytotic processes is rather large and can span from small molecules and macromolecules up to solid particles (macropinocytosis) or even bacteria, e.g., phagocytosis, which takes place only in specialized cells like macrophages. Next to macropinocytosis also other types of pinocytosis can be involved: Namely, clathrin dependent / receptor mediated pinocytosis, clathrin independent pinocytosis, adsorptive endocytosis and caveolae dependent endocytosis. Exocytosis is the reverse process, which shuttles undigested material out of the cell. In this process vesicular structures, such as, food vacuoles or secretory vesicles or secondary lysosomes, move to the plasma membrane. Once the vesicle membrane gets in contact with the lipid bilayer membrane of the lipid bilayer of the plasma membrane both bilayers start to fuse by rearrangement of the two membranes. In this way, a passage is formed and the vesicles discharge their content out of the cell. Endo- and exocytotic processes are thus associated with characteristic changes of the plasma membrane structure which can effectively be visualized by means of TEM investigations.

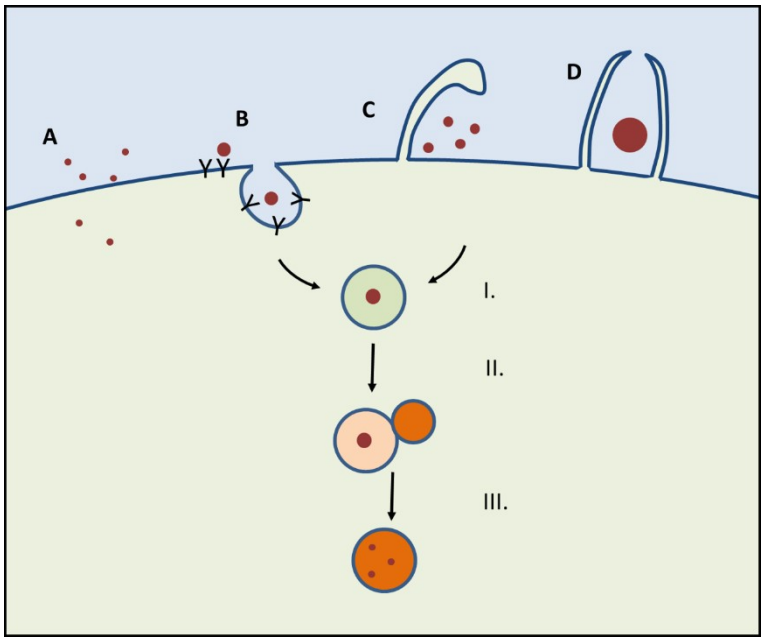

Figure 3 – 1 *Illustration of different types of cellular uptake: Diffusion (A), receptor mediated uptake (B), macropinocytosis (C), phagocytosis (D). The endocytotic pathway follows subsequently different stages of endosomal maturation. In this process the substances are first encapsulated into an endosome (I). They fuse with a lysosome (II), where the degradation of the material takes place in the lysosome (III).*

The form of intracellular uptake also governs the fate of the materials in the intracellular context. Materials taken up by passive diffusion can move freely into the cytosol, whereas materials taken up by endocytosis are engulfed by vesicular structures. These vesicular

containers undergo a development process in which these endosomes convert from early endosomes, just after the uptake, into late endosomes and later fuse with lysosomes. The pH value in these organelles gradually decreases from pH 6.0 to 6.5 in the early endosomes, to a pH of 5.0 to 5.5 in the late endosomes and finally drops to a pH of 4.0 to 4.5 in the lysosome.[80] The decreasing pH value gradually degrades materials until it is completely digested into the lysosome by enzymes. These structures are regarded as the "garbage bag" of the cells and accumulate all materials which cannot be further used by the cell. These conditions are also of relevance if drug delivery cargo's are developed. The acidic pH value in the lysosome and the strong degenerative character might be harmful to the drug as well. As such, efficient mechanisms have to be established to prevent the drug carriers ending up in the lysosomes before their cargo could be released. As a consequence, endosomal escape strategies have to be implemented in order to ensure the efficacy of the transferred drug. For this purpose, a polycationic polymer system is designed, which can undergo endosomal release. This process represents a critical issue if a drug cargo is to be released into the cytosol or for gene transfection efficiency. Also here, characteristic changes of the nanoparticle structure as well as changes of the intracellular structures are indicative for the processes taking place.

Next to the organelles responsible for uptake and digestion, there are several other organelles which can be used for drug delivery applications. Drugs and materials for initiating gene transfection are supposed to shuttle to the nucleus. The nucleus functions as a center of control for all cellular processes. It contains the genetic information in form of DNA or genes, respectively. It moreover regulates the gene expression and controls the cell activity, e.g., cell growth and cell division. The nucleus is surrounded by a nuclear membrane which hosts nuclear pores which regulate material exchange from the cytosol into and out of the nucleus. This nucleolus structure is a typically small and round-shaped very efficiently stained organelle within the nucleus and contains proteins and ribonucleic acids and its main function is the synthesis and assembly of ribosomes and ribosomal RNA (rRNA).

In order to establish the function of a cell many different kinds of enzymes and proteins are required, e.g, enzymes involved in the degeneration of materials in the lysosome. These lysosomal enzymes and secreted proteins are produced in the rough endoplasmic reticulum (RER) which typically consists of several interconnected membranous cisternae, which host on their surface the ribosomes. The ribosomes produce polypeptides which incorporate into the RER membrane, move to the central region of the cisternae or can move to the Golgi complex and even further away. In the Golgi apparatus the macromolecules are sorted and packaged for the delivery to other organelles within vesicles, which are transported to their final destination (other organelles or secretion from the cell via exocytosis). Of course many more processes are involved in keeping the cellular function in progress. For all these processes energy is required. This energy is generated in the mitochondria. They also are responsible for

regulating calcium signaling, hormonal signaling, apoptosis and maintaining the membrane potential. As such they play a key role in cellular metabolism and are, thus, an attractive target to control the cellular fate. Taking into account that dysfunction or damage of the mitochondria can even result in apoptosis this cellular organelle is a particularly attractive target site for the development of efficient drugs.

In **Section 3.4** a targeting strategy to guide the uptake of nanoparticles into mitochondria is introduced. It addresses the question, how nanoparticles can be directed towards specific organelles within a cellular system. Besides the uptake and localization also the intracellular fate of the nanoparticles and their influence on the integrity of the mitochondria was studied. The response of the cell towards nanoparticle induced damage of the mitochondria is strongly associated to characteristic changes of the cellular structure, which is a question, which can be well addressed by TEM studies. This is based on the fact that the organelles of a cell can be efficiently recognized in the intracellular environment and deviations from their typical appearance are indicative for the role of the drug delivery vehicle of the drug cargo respectively. Figure 3 – 2 displays an assortment of representative images of individual organelles which their characteristic features.

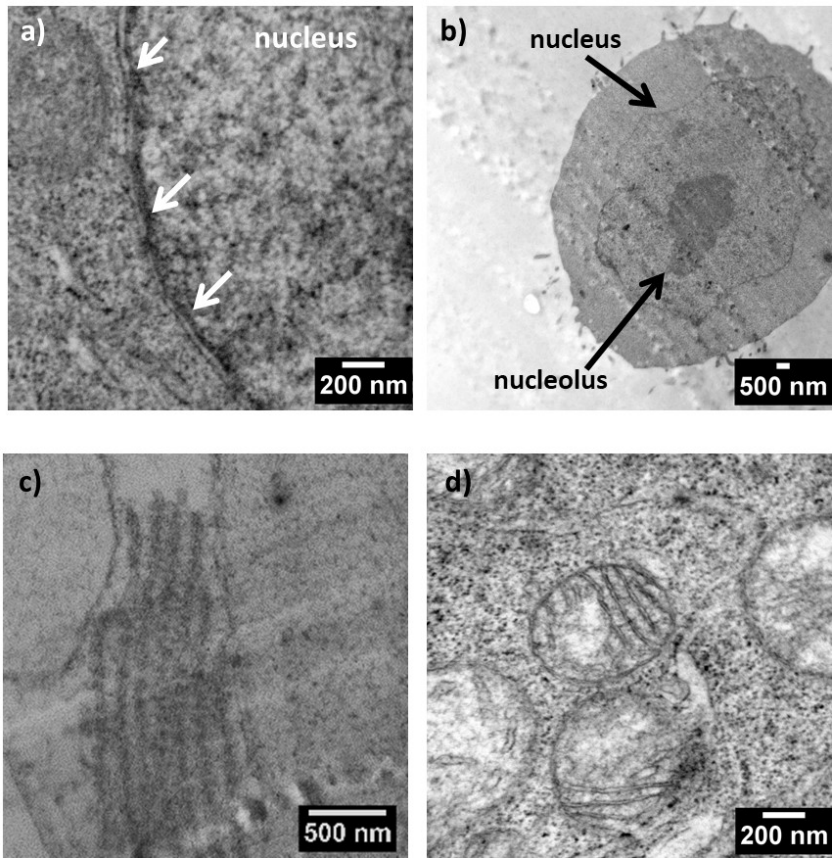

Figure 3 – 2 *TEM images of nuclear membrane (a), nucleus and nucleolus (b), endoplasmic reticulum (c), mitochondria (d) of HEK-293 cells. (Image C was taken from the Master thesis.[51])*

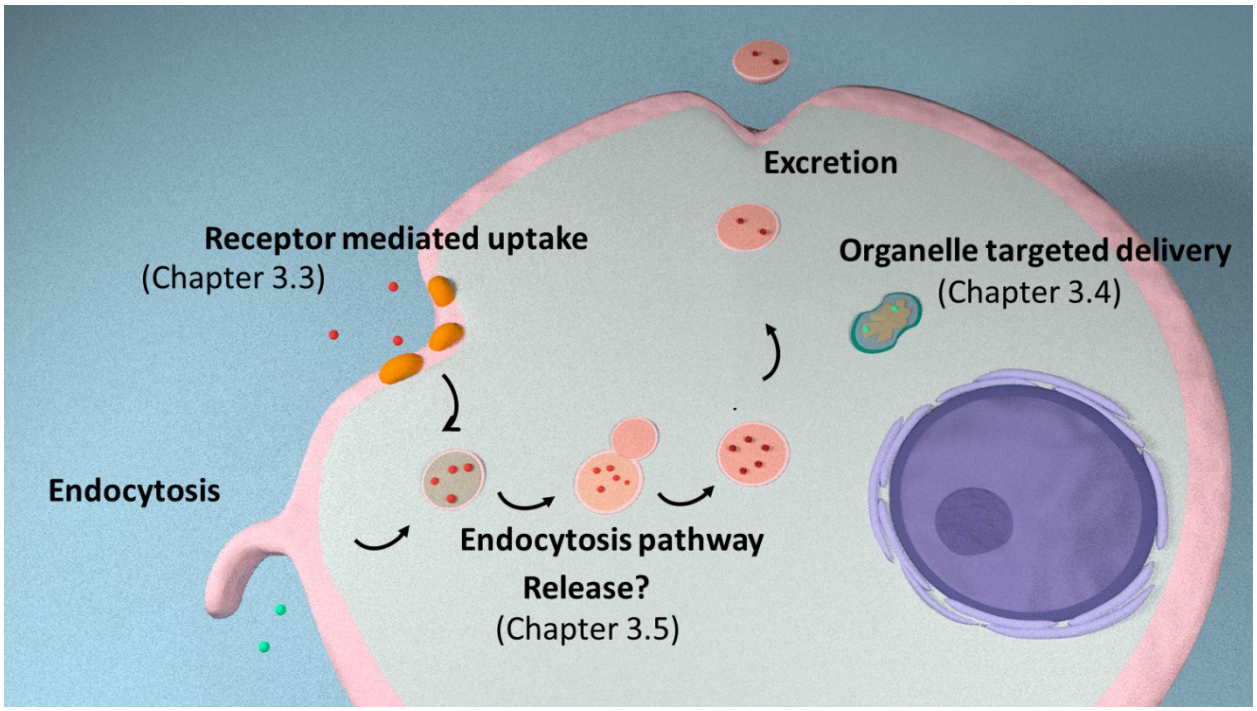

Figure 3 – 3 *Illustration of uptake mechanisms and targeting strategies investigated in this thesis.*

In all of these examples the cellular response is governed mainly by the surface functionalization of the utilized particle systems. The influence of the surface functionalization becomes evident by simple control experiments performed with non-modified colloidal gold nanoparticles of the same size.

These control experiments are very critical since they allow to discriminate between possible effects of the nanoparticles and artifacts caused by the sample preparation protocols. The cell culture with incubation of Au nanoparticles provides as well very important information on the uptake mechanism to be compared with the effects of surface functionalization. The formation of membrane protrusions, the nanoparticle localization within cell structures and uptake rate differences are very critical details for the final discussions of the projects.

For all studies model drug delivery vehicles consisting of a colloidal gold nanoparticle core have been utilized. This system is extremely appealing as it provides an inherently strong contrast for the localization of the nanoparticles in the cellular framework by TEM and renders them easy to recognize. All model systems rely on the functionalization of the colloidal surface by targeting units. These can be either sugar functionalized polymers, small molecules, i.e., pyruvate moieties, which take part in the cellular metabolism. Alternatively, the gold nanoparticles can be also embedded into the interior of polymer nanoparticles, i.e., of polycationic poly(ethylene imine) (PEI).

3.2. Surface functionalized colloidal gold nanoparticles a model system for drug delivery systems

The original method for the synthesis of colloidal gold nanoparticles was described by Turkevich[81] and was revised by other groups in order to improve the synthesis.[82] With this synthesis method, monodisperse spherical gold nanoparticles with a typical size of 10 to 20 nm in diameter can be obtained. The synthesis is based on heating up a $HAuCl_4$ aqueous solution and adding a small amount of sodium citrate as reducing agent. In addition, the citrate forms an additional capping layer around the gold nanoparticles, which protects the synthesized nanoparticles from further particle growth and aggregation. The size and shape of the synthesized Au nanoparticles can be arranged, within certain limits, e.g., by changing the amount of citrate added into the synthesis as reduction agent.

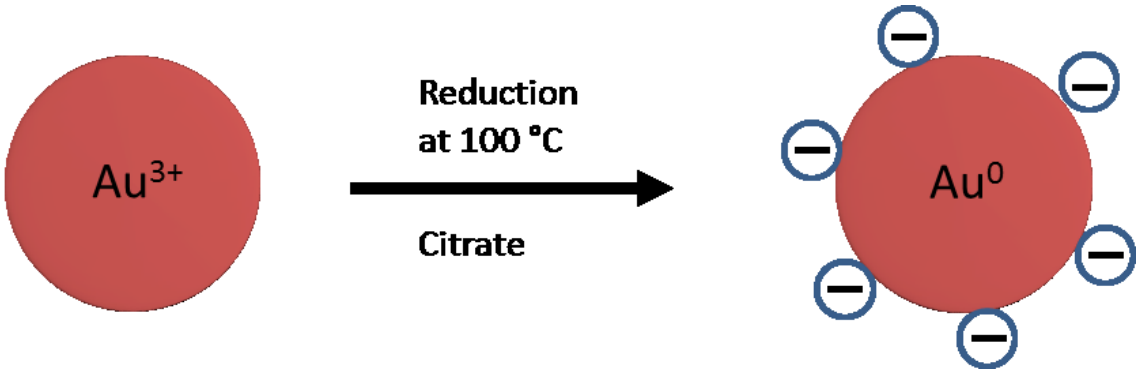

Figure 3 – 4 *Reaction of citrate stabilized Au nanoparticles.*

Colloidal gold nanoparticles offer a good platform to be used in various application. The main advantages of gold nanoparticles are their easy synthesis, tunable size and shape, and their easy detection and identification for targeting studies.[83] The surface functionalization of the colloidal Au nanoparticles provides improvements in the stability, monodispersity, biocompatibility and regarding the possibility to introduce functional groups or charges used to manipulate the biological activity of colloidal gold nanoparticles.[84] Further surface functionalization of Au nanoparticles can be achieved by ligand exchange. Due to the fact that the citrate ions are loosely bound on the Au nanoparticle surfaces they can be later exchanged with amine (–NH2) or thiol (–SH) groups. In particular the ligands containing the thiol or thiol based surfactants show the highest affinity to the gold nanoparticles.[85] By doing so, synthesized gold nanoparticles can be functionalized with small molecules, proteins and peptides, antibodies, DNA and RNA and also polymers, which can be used to enhance the uptake rate and recognition capabilities, trigger different uptake mechanism and attach to specific binding sites.[86]

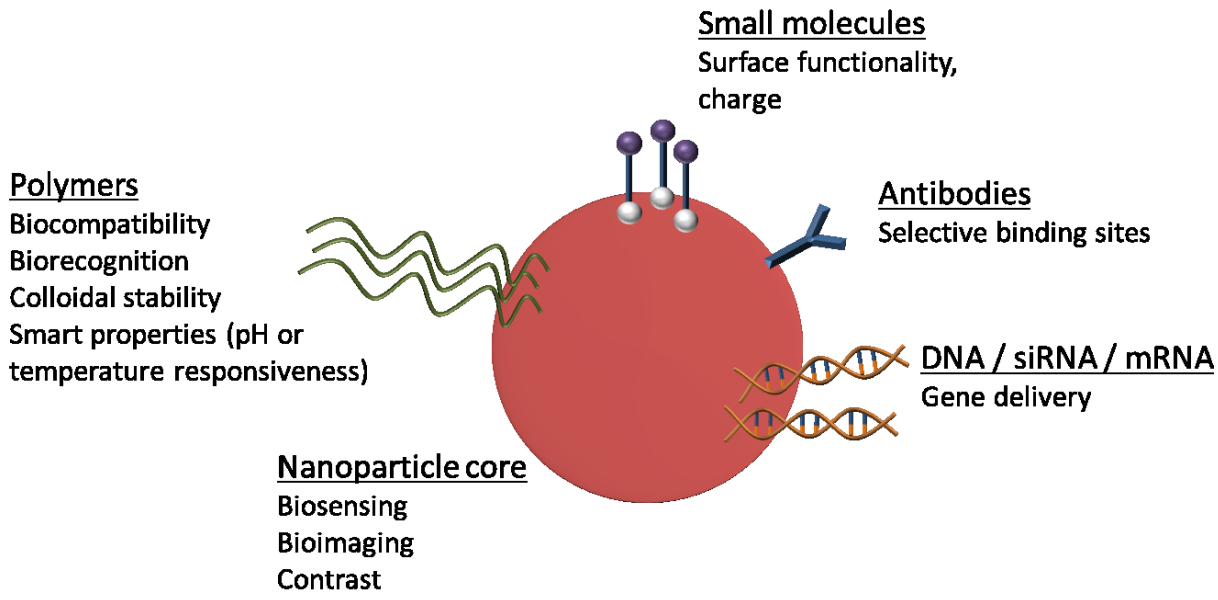

Figure 3 – 5 *Possibilities of surface functionalization of colloidal gold nanoparticles.*

Additionally, a general advantage of utilizing Au nanoparticles in electron microscopy is the high mass contrast. The high contrast of the Au nanoparticles can be easily distinguished within the cellular context.[87] This opens up new strategies towards targeted drug delivery processes by functionalizing the Au nanoparticles with tailor-made molecules or polymer systems. These systems are excellent model systems to study details of nanoparticle uptake and metabolism within the cellular context by utilizing TEM. The direct visualization of the functionalized Au nanoparticle systems combined with high resolution of TEM can be used in many fields from identification of infectious agents to targeted drug delivery systems.[88]

3.3. Sugar modified nanoparticles for targeted uptake

This project resembles the direct continuation of the work started in the Master thesis entitled "Localization of nanoparticles in cells by transmission electron microscopy".[51] During the Master thesis the nanoparticle system was established, incubation and preparation conditions were optimized, and first TEM studies could confirm their uptake into HEK 293 cells. No systematically conducted experiments were performed to further analyze details of the sugar mediated uptake process itself. These studies have been conducted during the PhD studies and are summarized in the following sections. These systematic investigations resulted in a deeper understanding of the underlying principles and could reveal also the influence of nanoparticle aggregation on the uptake and distribution of the nanoparticles into the cells.

The first approach to investigate targeted delivery addresses the utilization of GLUT transporters located at the plasma membrane of HEK-293 cells. 14 different GLUT transporter proteins have been identified so far, which are responsible for the specific uptake of different

sugar moieties. Their abundance greatly differs within different organs or tissues as summarized in Table 3 – 1. Their active role in the uptake mechanism has been outlined before, however, to date their individual roles are not completely understood. [89]

Human gene name	Protein name	Related substrates	Tissue & cellular expression
SLC2A1	GLUT1	glucose, galactose, mannose, glucosamine	erythrocytes, blood tissue barrier, blood-brain barrier
SLC2A2	GLUT2	glucose, galactose, fructose, mannose, glucosamine	liver, intestine, kidney, brain
SLC2A3	GLUT3	glucose, galactose, mannose, xylose	brain, testis
SLC2A4	GLUT4	glucose, glucosamine	adipose tissue, skeletal and cardiac muscle
SLC2A5	GLUT5	fructose	intestine, kidney
SLC2A6	GLUT6	glucose	brain, spleen, leucosytes
SLC2A7	GLUT7	glucose, fructose	intestine, colon, testis, prostate
SLC2A8	GLUT8	glucose, fructose, galactose	testis,brain, liver, lung
SLC2A9	GLUT9	urate (glucose, fructose)	kidney, liver, intestine, placenta, lung, leucocytes
SLC2A10	GLUT10	glucose, galactose	heart, lung, brain, liver, skeletal muscle, pancreas, placenta, kidney
SLC2A11	GLUT11	glucose, fructose	heart, muscle
SLC2A12	GLUT12	glucose	heart, prostate, skeletal muscle, placenta
SLC2A13	HMIT	myo-inositol	brain, adipose tissue
SLC2A14	GLUT14	glucose	testis

Table 3 – 1 *GLUT family. (The table was reproduced from the Master thesis.[51])*

As seen in Table 3 – 1, the GLUT transporters are highly selective in terms of the sugars that can be transduced through the membrane. Therefore, a study involving the functionalization of

colloidal gold nanoparticles with four different sugar moieties was conducted. The functionalization comprised the utilization of a statistical copolymer system consisting of thioglycosidic glycomonomers with four different types of sugar substituents (glucose, mannose, fructose and galactose) and *N*-isopropylacrylamide (*N*iPAm) serving as a reference sample (Figure 3 – 6).

3.3.1. Synthesis and characterization of sugar functionalized colloidal gold nanoparticles

To utilize sugar functionalization onto Au nanoparticles, a polymer system containing thiol group is required. Thioglycosidic glycomonomers containing poly-*N*-isopropylacrylamide (P*N*iPAm) were selected. P*N*iPAm is a polymer which is known for temperature responsive properties, specifically for a lower critical solution temperature (LCST) transition. The LCST transition can be described as a coil-to-globule transition of thermoresponsive polymers upon exceeding a specific temperature. This polymer is frequently discussed as a system with favorable properties for drug delivery, as temperature triggered release of the cargos can be easily established.[90] The here presented polymers were synthesized by utilization of reversible addition fragmentation chain transfer (RAFT) polymerization according to the procedure outlined in Figure 3 – 6. These polymers can be grafted onto the surface of colloidal gold nanoparticles by a simple ligand exchange reaction. For comparison of the uptake characteristics, a control sample facilitated with only the P*N*iPAm homopolymer was prepared.

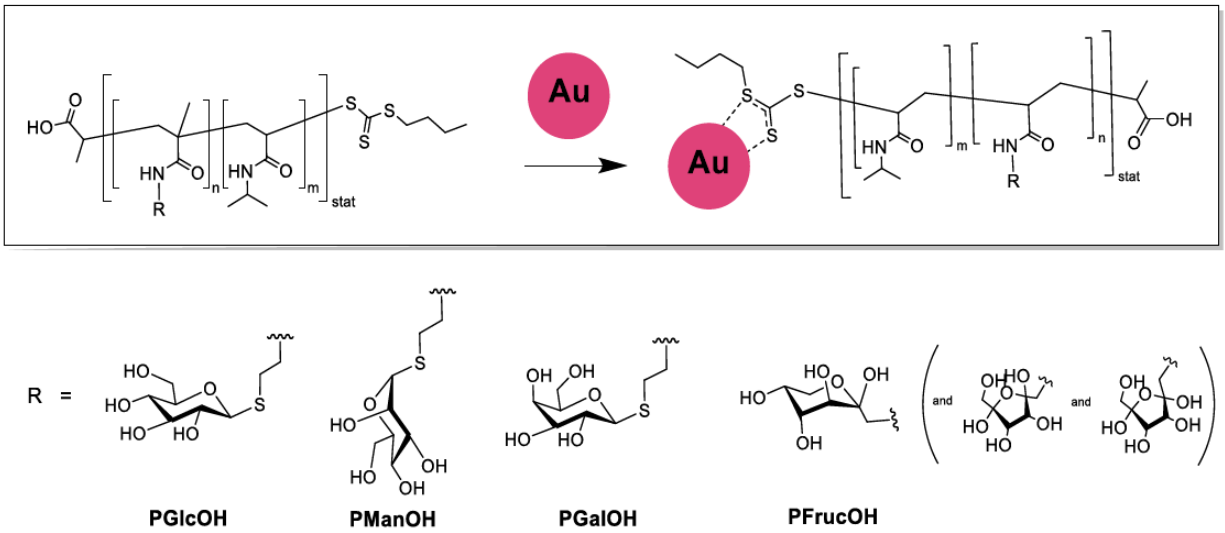

Figure 3 – 6 *Schematic representation of a copolymer functionalization of PNiPAm and sugar substituents on Au nanoparticles. (The figure was taken from Master thesis.[51])*

The synthesized polymer systems were characterized regarding their physico-chemical properties by different techniques. These involve imaging and scattering methods to determine the size, shape, surface charge as well as biological testing to investigate the biotoxicity.

3.3.2. Instrumentation and experimental details

The characterization of the nanoparticle system was performed by means of various methods. Firstly, a drop of the colloidal nanoparticles was dried on a carbon coated TEM grid. It was later imaged by TEM (FEI Tecnai G^2 20 at 200 kV) in order to visualize the polymer shell attached to the nanoparticles.

The hydrodynamic radius and polydispersity index (PDI) values of the nanoparticles were measured by means of Dynamic Light Scattering (DLS) (Zetasizer Nano ZS (Malvern Instruments, Herrenberg, Germany)). As an important parameter in bioapplications, the Zeta potential and the lower critical solution temperature (LCST) values of the nanoparticles were also measured. Zeta potentials were measured by using a Zetasizer Nano ZS (Malvern Instruments, Herrenberg, Germany) and LCST values were obtained by the turbidimetry method (Crystal 16, Avantium Technologies).

Cytotoxicity of the polymers and the functionalized nanoparticles were tested by an alamarBlue test. HEK-293 cells were seeded in a 96-well plate for 24 hours and were later incubated with polymers and functionalized nanoparticles at a series of concentrations ranging from 10 to 1000 µg/mL for 24 hours. After washing once, alamarBlue (Thermo Fischer) was applied for 4 hours. The fluorescence wavelength of excitation was 570 nm and of emission was 510 nm. The negative control cell culture was used to set 0% of metabolism inhibition which equals to 100% viability. Values below 70% were assigned as cytotoxic.

3.3.3. Incubation of the nanoparticles and sample preparation for TEM investigations

HEK-293 cells were prepared in a 12-well plate (0.1×10^6 cells/mL) in R10 medium for one day. After that, the medium was exchanged with OptiMEM for 20 minutes. The nanoparticles were incubated for 4 hours. Finally, the cells were washed twice with PBS and collected by trypsinization. A medium exchange to R10 was performed as the final step.

After one hour of fixation with glutaraldehyde (8%, Electron Microscopy Sciences) on ice, osmium tetroxide (4%, EMC) was applied for 45 minutes at room temperature. In order to dehydrate the cells, a graded ethanol series (20, 50, 60, 70, 80, 90 and 100%) was performed for 10 minutes for each step. At this stage, epoxy resin composed of 20 mL of EMBED 812 (Electron Microscopy Sciences), 9 mL of DDSA (Electron Microscopy Sciences), 12 mL of NMA (Electron Microscopy Sciences) and 15 µL/mL of DMP-30 (Electron Microscopy Sciences) was prepared. The cell pellet was infiltrated with mixtures of embedding medium and ethanol (Resin/ethanol = 1:1 v/v for 1 hour, = 2:1 v/v for overnight at room temperature). Next day it was replaced with a 100% of embedding medium and polymerized at 70 ˚C for overnight.

The hardened sample block was sliced into 80 nm thick slices by a diamond knife (RMC) mounted on an ultramicrotome (PT-XL, PowerTome, RMC, Tuscon). The slices were collected

from the pool (introduced in **Section 2.3.1**) of diamond knife and transferred onto carbon coated copper TEM-grids (400 mesh, Quantifoil, Jena).

3.3.4. Results and discussion

Glycomonomers were synthesized and later copolymerized with *N*iPAm via RAFT polymerization. The trithiocarbonate RAFT endgroups enabled the immobilization of the polymer system onto the surface of the synthesized Au nanoparticles. The characterization of the nanoparticle system was first performed by TEM imaging. The citrate stabilized colloidal gold nanoparticles feature a rather spherical appearance with a size of approximately 17 ± 4 nm. In order to visualize the polymer corona around the functionalized colloidal gold nanoparticle core, negative staining had to be performed. In this case uranyl acetate was used as a stain. Classically this staining agent interacts with the carbon coating of the TEM grid, thus, creating a dark background usually referred as negative staining. In our particular case, however, uranyl acetate increased the contrast of the polymer corona faintly, as it tends to incorporate into the loose polymeric framework. In contrast to the strong contrast which is generated by the nanoparticle itself the obtained staining contrast remains weak but the presence of the polymer shell can be visualized (Figure 3 – 7). A quantitative estimation however is not possible as drying artifacts might strongly change the appearance of the polymer shell.

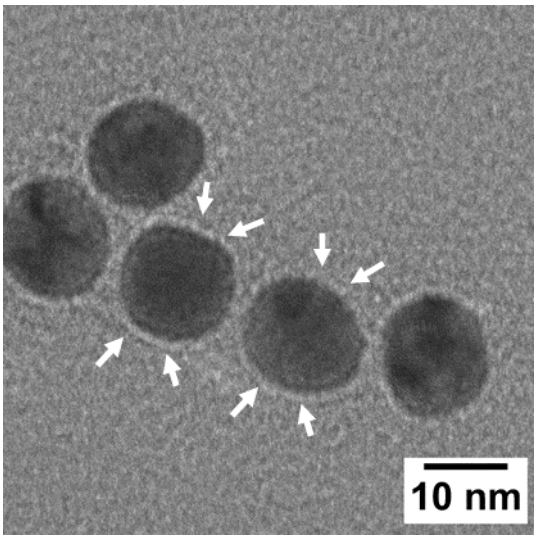

Figure 3 – 7 *TEM images of Au-*P*N*iPAm-*GlucOH nanoparticles stained with uranyl acetate.*

To address the issue of particle size and particle size distribution, DLS measurements provided the information on the hydrodynamic radius and the PDI values of the nanoparticles. Table 3 – 2 summarizes the obtained results. DLS measurements were performed by collecting the scattering fluctuations from the nanoparticles in solution which move randomly by Brownian motion. These fluctuations in the scattered signal were used to determine hydrodynamic size of the nanoparticles. Hydrodynamic radii of the functionalized nanoparticles were calculated in a

range from 28.5 to 52.8 nm. The size of fructose functionalized nanoparticles was the largest with a value of 52.8 nm, while the sizes of glucose, galactose and mannose functionalized nanoparticles are relatively similar to each other. The PDI value provides the information on the aggregation state of the nanoparticles in a solution. The smaller the PDI, the better the homogenity of the nanoparticle is. Here, the PDI values were obtained in a range from 0.24 to 0.27 for sugar functionalized nanoparticle systems, which confirmed the good uniformity. However, the PDI value of the P*N*iPAm functionalized nanoparticles, the control sample, showed relative high PDI values of 0.36. The Zeta potential values were measured as these values can provide information on the stability of the formed systems and can, moreover, offer an indication for the successful functionalization of the colloidal gold nanoparticles and also allow a prediction about the interaction of the nanoparticles with cell membranes. Here, the obtained zeta potential values revealed that the nanoparticle systems showed only a short term stability, because it is known that the absolute value of Zeta potential around 20 indicates short time stability. The negative value of the Zeta potential indicates a negative surface charge of the nanoparticles. Taking into account that biological membranes are also negatively charged, it can be excluded that the nanoparticles are internalized by electrostatic nanoparticle–cell membrane interactions.

Sugar functionalization	**R_h [nm]**	**PDI**	**Zeta potential [mV]**	**LCST * [°C]**
Glucose	28.5	0.24	-18.6	48
Galactose	35.4	0.27	-11.7	49.5
Fructose	52.8	0.27	-28.1	41.3
Mannose	32.1	0.24	-14.8	44.6
Control	44.7	0.36	-23.2	~32[91]

Table 3 – 2 *Characterization of the nanoparticle system. *Pure polymer in water. (Data were used from the Master thesis.[51])*

The utilized nanoparticle system featured two important properties. The first one is the effect of the type of sugar molecules on the uptake rate into cells. The second important property is the response of the P*N*iPAm to the temperature changes. The lower critical solution temperature triggers a coil-to-globule transition of the polymer. Among other sugar functionalized systems, the fructose functionalized system revealed an LCST value much closer to the temperature of the cell culture, (37 °C). The LCST values showed that the pure polymer system was actually incubated into the cells above its LCST value. With the combination of these two properties, sugar-cell interactions could be tested.

Cytotoxicity tests for the polymer systems and also for the functionalized nanoparticle systems were performed. Figure 3 – 8 depicts that neither the polymers nor the functionalized nanoparticle systems showed cytotoxic effects on the HEK-293 cells. A cell viability of > 70% is regarded in this case as non-toxic.

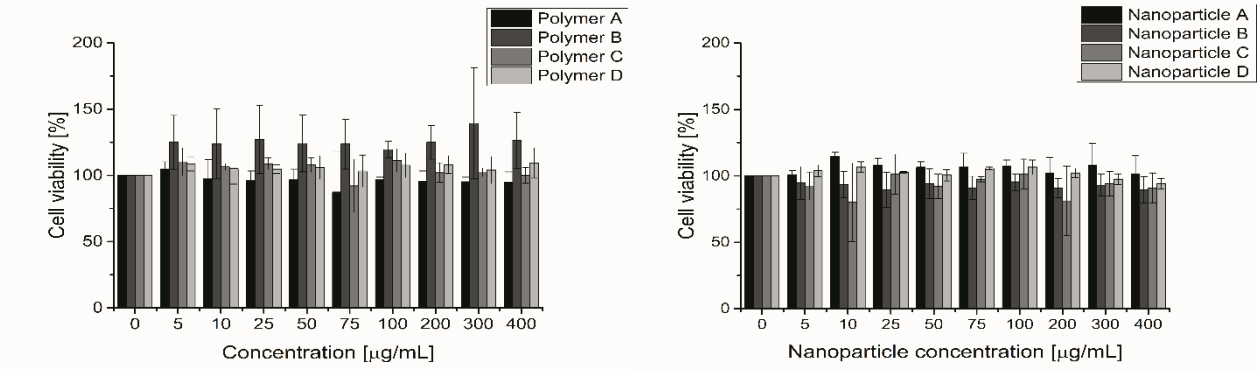

Figure 3 – 8 *Cytotoxicity results of polymer systems (a) and polymer functionalized Au nanoparticles (b). (A= PNiPAm-GlucOH, B= PNiPAm-ManOH, C= PNiPAm-GalOH, D= PNiPAm-FrucOH)*

Au nanoparticles functionalized with four different glycopolymers were incubated into HEK-293 cells and their localization in cells was investigated by (S)TEM. Each nanoparticle system was localized in encapsulated structures in the cells. These structures can be identified as endosomes or lysosomes (Figure 3 – 9). On the other hand, some free nanoparticles of Au-P*N*iPAm-GlucOH, Au-P*N*iPAm-ManOH and Au-P*N*iPAm-GalOH systems were detected in the cytoplasms, which supported the receptor mediated uptake (Figure 3 – 10).

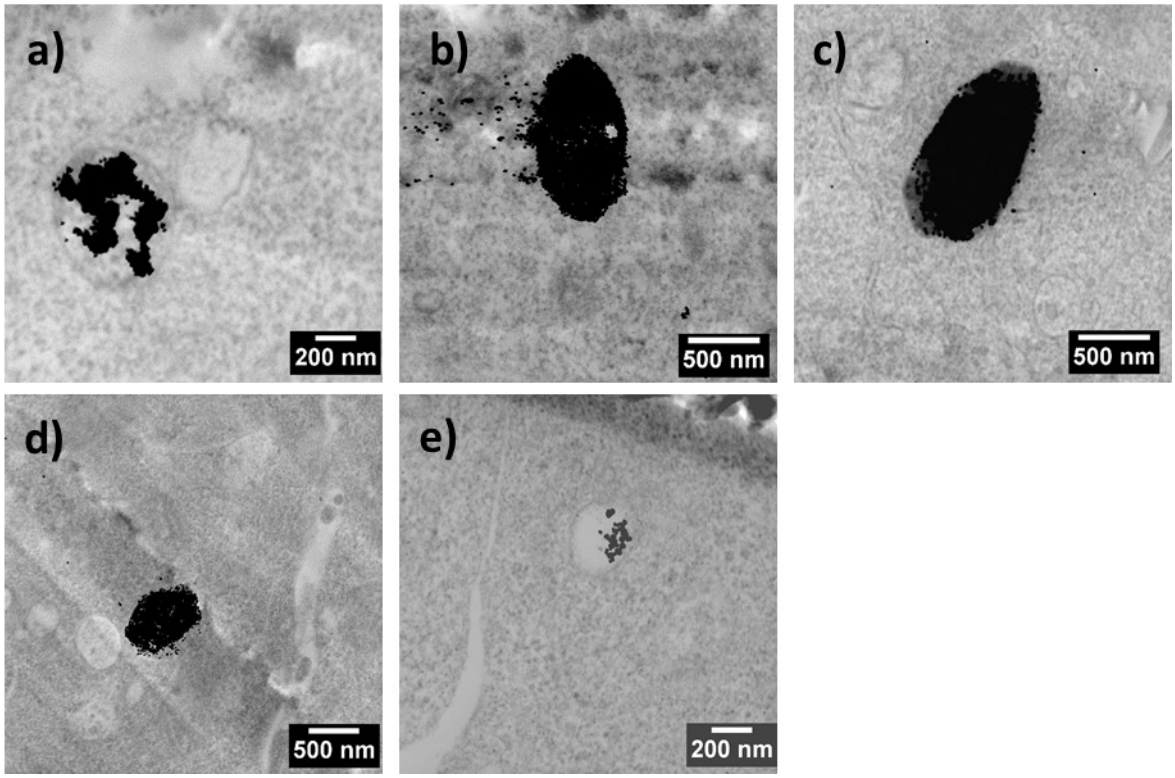

Figure 3 – 9 *STEM investigations of uptaken nanoparticles in HEK-293 cells. All of the nanoparticle systems were localized in encapsulated structures. a) Au-PNiPAm-GlucOH, b) Au-PNiPAm-ManOH, c) Au-PNiPAm-GalOH, d) Au-PNiPAm-FrucOH, e) Au-PNiPAm.*

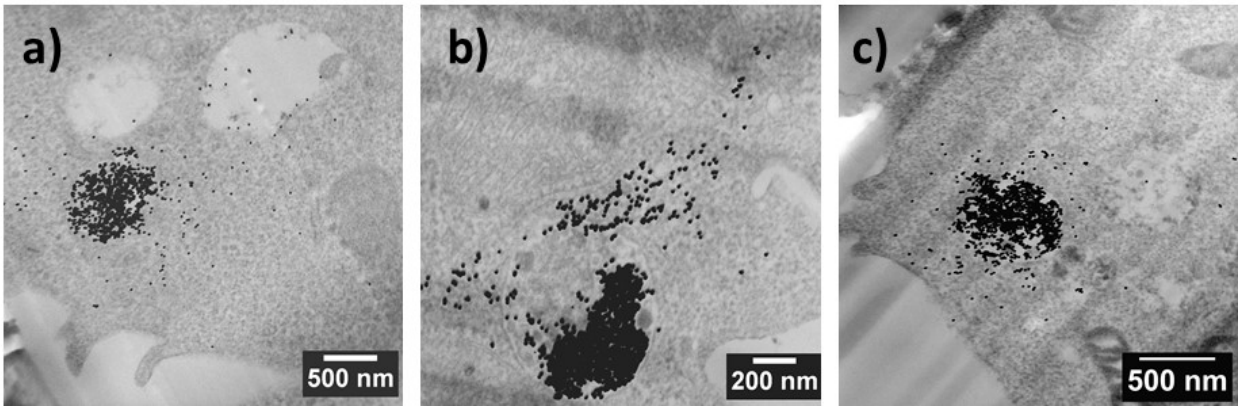

Figure 3 – 10 *Free nanoparticles in cytoplasms of HEK-293 cells were localized for the nanoparticle systems of Au-PNiPAm-GlucOH (a), Au-PNiPAm-ManOH (b) and Au-PNiPAm-GalOH (c).*

The uptake of the nanoparticle system was assumed to be a receptor mediated uptake via GLUT receptors on the cell membrane. Therefore, the observation of nanoparticle aggregation on cell membranes was very crucial. No nanoparticle aggregations on cell membranes was observed for the samples incubated with Au-P*N*iPAm-GlucOH, Au-P*N*iPAm-ManOH and Au-P*N*iPAm-GalOH systems (Figure 3 – 11). Oppositely, large aggregates of the Au-P*N*iPAm-FrucOH and Au-P*N*iPAm

nanoparticles were observed on the cell membranes (Figure 3 – 12). Additionally, channel-like structures were detected for the cells incubated with Au-P*N*iPAm nanoparticles (Figure 3 – 13). These variations on the nanoparticle aggregation and the channel-like structures on the cell membrane can be attributed to the thermoresponsive property of the P*N*iPAm to the temperature of the cell culture during incubation.

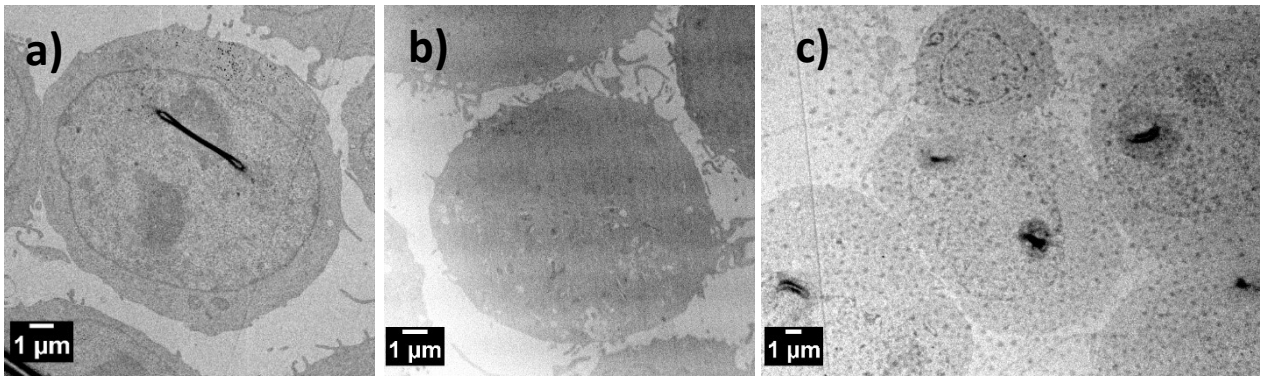

Figure 3 – 11 *No nanoparticle clusters on cell membranes were observed for the nanoparticle systems of Au-PNiPAm-GlucOH (a), Au-PNiPAm-ManOH (b) and Au-PNiPAm-GalOH (c).*

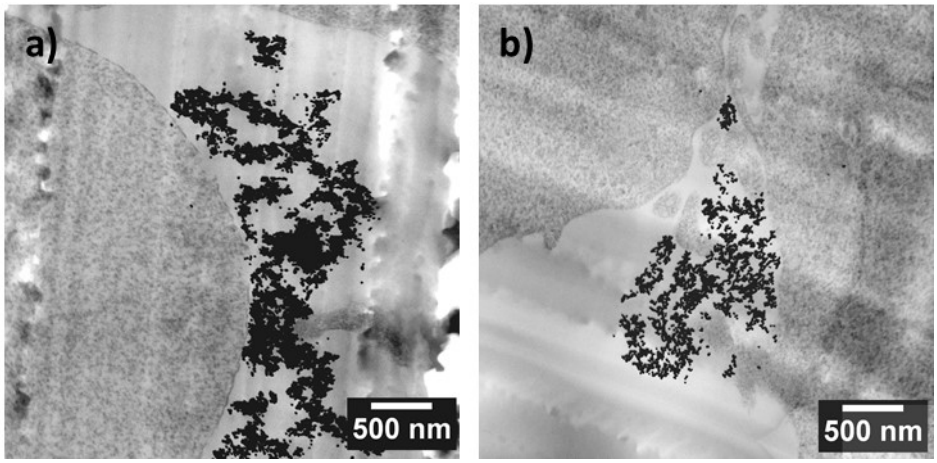

Figure 3 – 12 *Nanoparticle aggregation on cell membranes was observed for the nanoparticle systems of Au-PNiPAm-FrucOH (a) and Au-PNiPAm (b).*

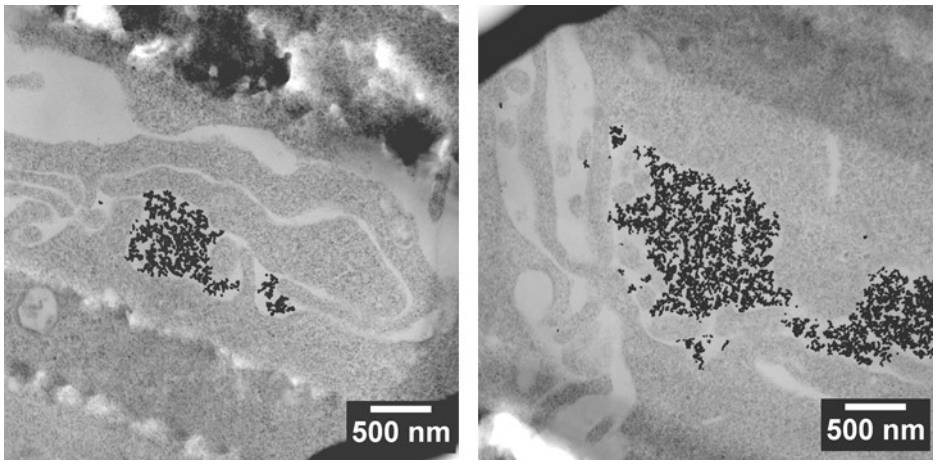

Figure 3 – 13 *Channel-like structures were observed for the uptake of Au-PNiPAm nanoparticles into HEK-293 cells. (Images were used from the Master thesis.[51])*

Furthermore, the uptake rate differences regarding to the type of sugar functionalization on Au nanoparticles were determined. It is known that the TEM measurements were performed on very thin slices of a cell pellet as described in **Chapter 2.3.1**. A slice containing endosomes filled with nanoparticles depends simply on the slicing position. As illustrated in Figure 3 – 14, a slice with a size of 80 nm may not contain the whole volume of an endosome. Therefore, it is a difficult task to perform a statistical study on uptake rate by utilizing only TEM.

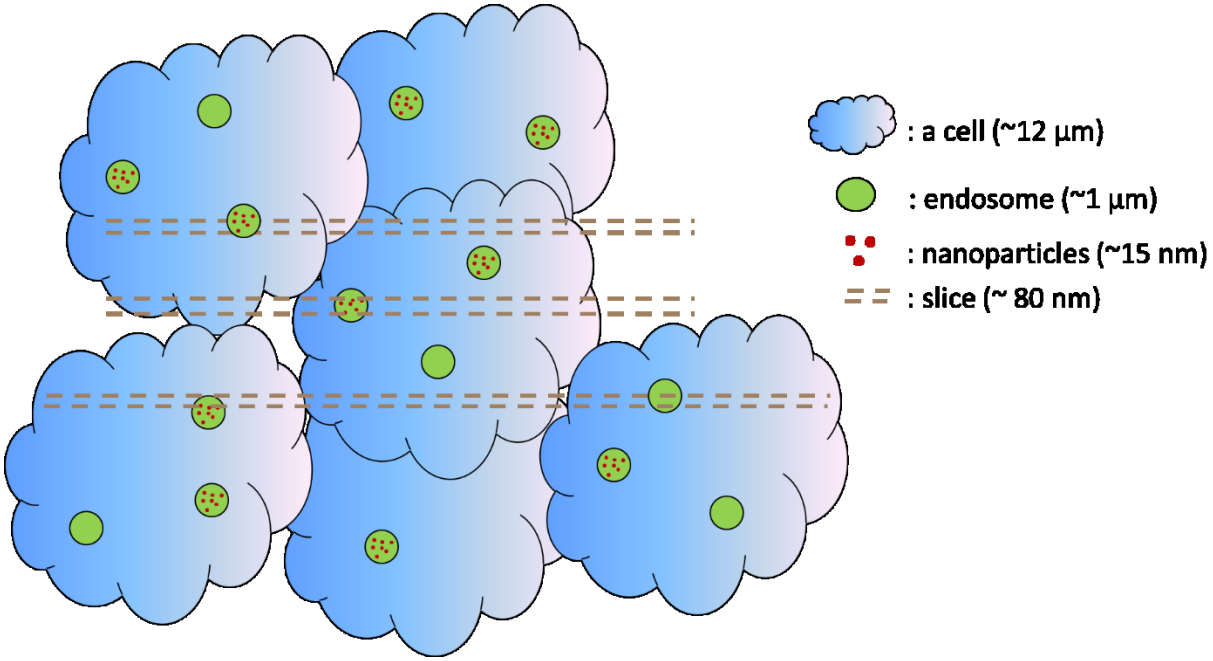

Figure 3 – 14 *The sectioning provides only a 80 nm thick slice from the cell pellet.*

To evaluate our experiments by statistical means, the cells on a slice were grouped according to three criteria: Cells containing nanoparticles, cells containing no nanoparticles and "half cells". These "half cells" describe a cell which is not completely visible due to mesh and folds. These cells were counted as half and added into the column of "no nanoparticle". One slice from three batches of each sugar type was used to count the cells. According to this analysis, it was found that the highest uptake rate with 44 ±22% was observed for Au-P*N*iPAm-GlucOH. It was followed by Au-P*N*iPAm-GalOH with 25 ±12% and Au-P*N*iPAm-FrucOH with 20 ±15%. The lowest uptake rate was found in Au-P*N*iPAm-ManOH samples with 8.5 ± 4%. A relatively high uptake rate was also observed for the polymer control system Au-P*N*iPAm as 54 ±29%. Detailed numbers on the analysis are given in Table 3 – 3.

Sugar type		Number of cells				Uptake rate [%]	Resulted uptake rate [%]
		With np	No np	Half	Total		
Glucose	Batch 1	45	55	39.5	139.5	32.2	44 ±22
	Batch 2	64	21	8.0	93.0	68.8	
	Batch 3	17	-	43.5	60.5	28.1	
Mannose	Batch 1	10	28	33.5	71.5	14.0	8.5 ±4
	Batch 2	4	35	41.0	80.0	5.0	
	Batch 3	2	12	16.5	30.5	6.5	
Galactose	Batch 1	42	32	31.5	105.5	39.8	25±12
	Batch 2	12	35	31.0	78.0	15.4	
	Batch 3	16	32	26.5	74.5	21.5	
Fructose	Batch 1	31	30	20.5	81.5	38.0	20 ±15
	Batch 2	6	46	27.0	79.0	7.6	
	Batch 3	10	23	34.5	67.5	14.8	
Polymer	Batch 1	69	9	14.0	92.0	75.0	54 ±29
	Batch 2	30	27	32.5	89.5	33.5	
	-	-	-	-	-	-	

Table 3 – 3 *Cells on each slice from different batches for each functionalized nanoparticle systems were counted.*

The chosen system resembles in this sense a rather complicated system where different aspects of particle uptake are involved. A clear discrimination of the selective uptake of sugar functionalized nanoparticles is therefore difficult to determine. Nevertheless, it can be concluded that the particles are definitely taken up by the cells by an endocytotic uptake into endosomal/lysosomal structures, however, their localization into the cytosol was also observed. The aggregation state of the nanoparticles possibly plays an important role. This factor, influencing the targeted uptake is certainly of tremendous importance as metabolic pathways determine the localization and, with that, the possibility to deliver drug carriers to predefined positions. An inspection of the plasma membrane is for this purpose a useful step in every

uptake study, which can be best performed by TEM imaging. Alternative optically based investigation tools, i.e., fluorescence or dark-field microscopy cannot provide to date the resolution required to discriminate between individual particles interacting with the membrane or smaller clusters of many particles which are interacting with the membrane.

3.4. The uptake study of pyruvate functionalized Au nanoparticles

In the second approach to establish a strategy for targeted drug delivery the guided uptake of nanoparticles in mitochondria is proposed. Mitochondria, as the energy generation site of a cell, play a key role in cell regulation of citric acid cycle (CAC) and any defects or dysfunction in mitochondria may be related to severe diseases. As a consequence, studies on targeting mitochondria represent a very promising approach to cure such diseases. Pyruvate as the trigger molecule for the citric acid cycle in mitochondria can be utilized to target mitochondria. In this project, spherical Au nanoparticles functionalized with pyruvate molecules were synthesized and incubated into HEK-293 cells. The localization of the functionalized nanoparticle systems and their effect on cell metabolism could be determined by imaging the incubated cells by TEM.

3.4.1. Introduction

Compared to other organelles, mitochondria are essential for generating energy for the cell's metabolism. Not only the energy supply but also the cell survival, cell death and homeostasis are controlled by mitochondria. This relates any mutations or dysfunctions of mitochondria to severe diseases, e.g., mitochondrial myopathy, myoclonic epilepsy, Leber's hereditary optic neuropathy or the Leigh syndrome.[92] Thus, finding efficient strategies for targeting mitochondria is widely addressed to develop suitable therapies against such diseases.[93]

A mitochondrion consists of five main parts: The outer membrane, the inner membrane, an intermembrane space, cristae and the matrix (see Figure 3 – 15).[94] The outer membrane is a double-layer-membrane surrounding the whole mitochondrion to retain its contents. Ions can diffuse into the mitochondria through, e.g., porin channels on the outer membrane. The inner membrane is also a double-layer membrane enclosing the matrix of the mitochondria and is highly impermeable to ions. The inner membrane hosts various enzymes and proteins facilitating catalytic reactions, the transport of ions into the matrix, and hosts F_1F_0 synthase, which is directly responsible for the adenosine triphosphate (ATP) synthesis. The cristae are invaginations of the inner membrane of the mitochondria. The intermembrane space, i.e., the region between the outer membrane and the inner membrane, is very similar to the cytosol but comprises a different protein composition, which is related to the energy production. The matrix, i.e., the region surrounded by the inner membrane, is highly dense due to the presence

of hundreds of enzymes involved in the CAC and contains also the mitochondrial DNA genome.

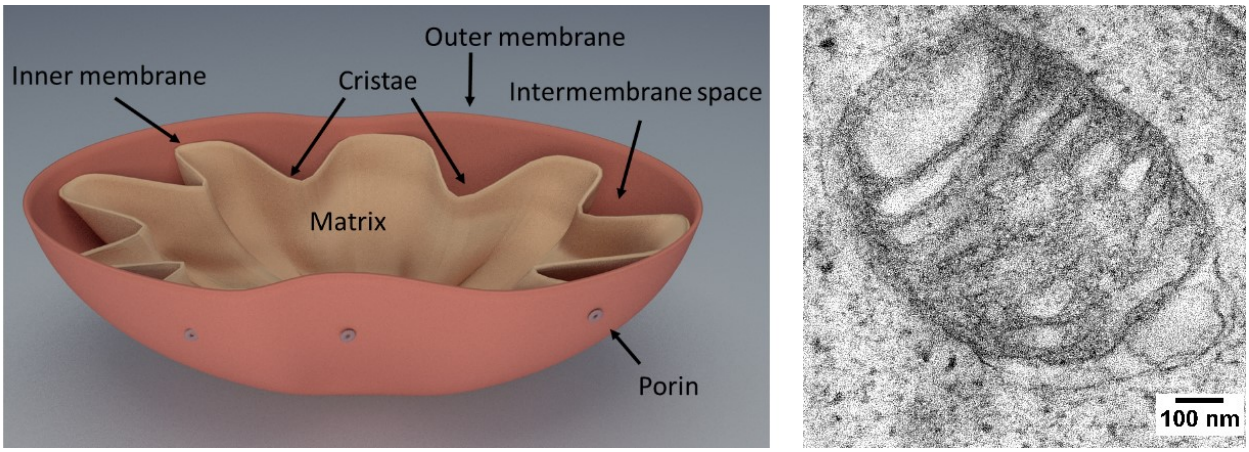

Figure 3 – 15 *Illustration (left) and TEM image (right) of a mitochondrion.*

The energy production in a cell consists of two steps, namely the glycolysis and the citric acid cycle. In the first phase, glycolysis takes place. The glucose molecules are recognized by the related proteins on the cell membrane and are taken up into cytoplasm and are converted from a six-carbon sugar into two three-carbon pyruvate and two molecules of NADH and ATP.

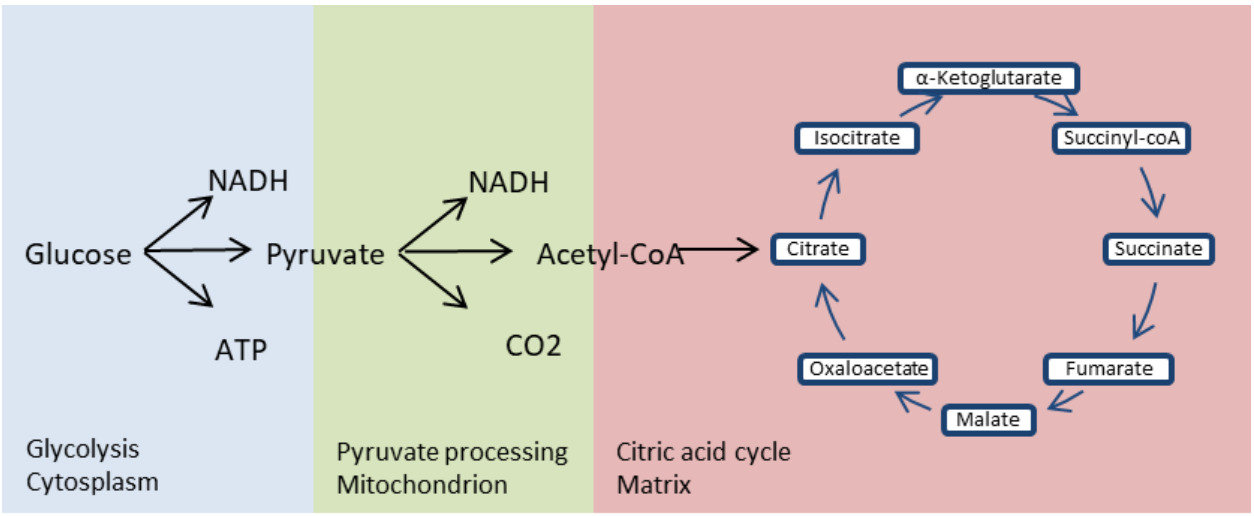

Figure 3 – 16 *The reactions for energy production starting from cell cytoplasm to the mitochondrial matrix.*

The formed pyruvate molecules are transported into the mitochondria, through the mitochondrial outer membrane and on the inner-membrane by related proteins. In the mitochondrial matrix, a conversion of the pyruvate into acetyl-coenzyme A (acetyl-CoA) takes place. Pyruvate will be used as a major reactant of the CAC for the energy production. This process shows the importance of pyruvate as connecting the reactions of glycolysis and CAC. Thus, the pyruvate represents a suitable target molecule to establish specific uptake into mitochondria. Hence, the proposal of utilizing pyruvate as targeting agent to address

mitochondria represents a good approach to add selectivity towards the uptake of the potential drug delivery system into the mitochondria.

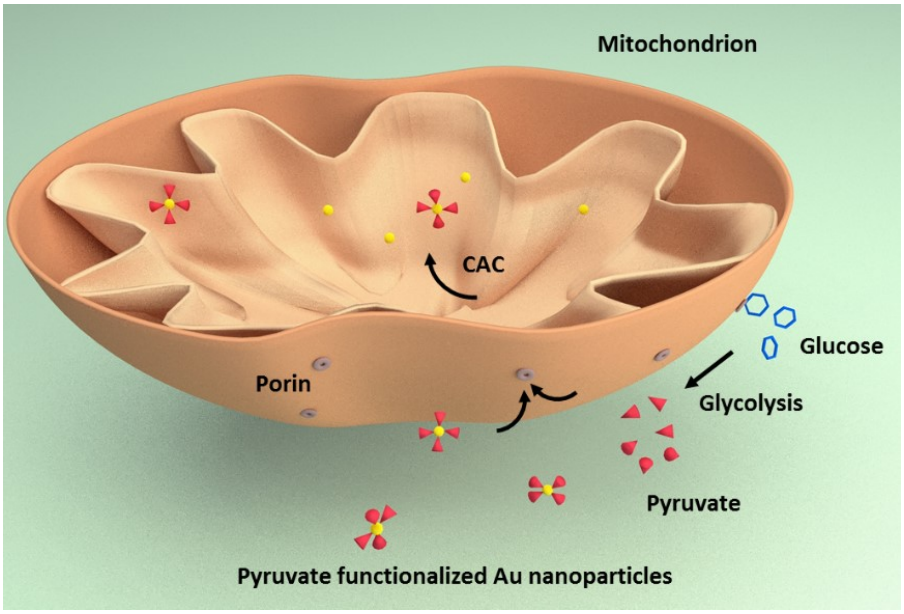

Figure 3 – 17 *Illustration of glycolysis and citric acid cycle.*

Mitochondria are not only responsible for energy production but regulate cell death and self-defense. For example, highly reactive superoxide anions are constantly generated by mitochondria as a byproduct of electron transport during oxidative phosphorylation. The danger of producing a too large amount of these reactive oxygen species being exposed to proteins, lipids and DNA can be regulated by a self-defense mechanism. Mitochondria start to degrade themselves under stress condition or damage. This process is known as mitochondrial autophagy. Mitochondrial autophagy is divided into two classes: Non-selective autophagy and cargo-specific autophagy. The non-selective autophagy occurs in nutrient deprivation in order to supply essential proteins and energy. The cargo-specific autophagy, i.e., mitophagy, refers to the degradation of mitochondria even in nutrient rich conditions. Some specific receptors such as NIX, BNIP3, FUDNC1 or the PINK1/Parkin pathway regulate mitophagy in cells. By selective degradation of mitochondria, cells can remove defective mitochondria and ensures cell survival. This specific clearance mechanism is a promising strategy to be utilized in mitochondria targeting studies, e.g., in cancer or stroke treatments.[95]

The steps of mitophagy are schematically illustrated in Figure 3 – 18. In summary, a curved membrane structure, called a phagophore, is developed around the mitochondrion and wraps it into an autophagosome. A fusion of autophagosome with a lysosome starts the degradation of the mitochondrion.

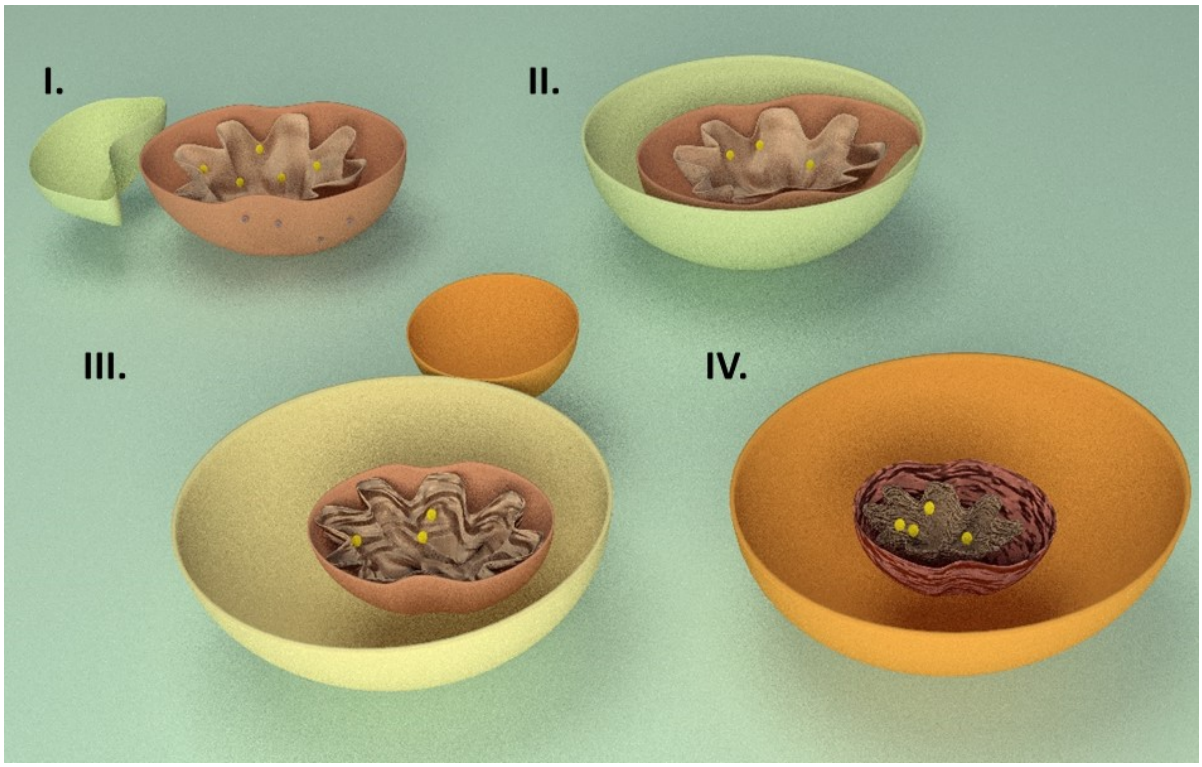

Figure 3 – 18 *Illustration of mitophagy. I. A membrane structure in close vicinity of the mitochondrion under stress or with defect of disfunction is formed. II. The mitochondrion is encapsulated into an autophagosome. III. A fusion with a lysosome occurs. IV. The autophagosome transforms into a lysosome and degradation starts.*

3.4.2. Instrumentation and experimental details

Spherical Au nanoparticles were synthesized according to a previously reported study.[91] Shortly, 200 mL of a $HAuCl_4 \times 3\ H_2O$ (99.99%, Alfa Aesar, Germany) solution in water was prepared and stirred under heating in an oil bath at 600 rpm. When 100 °C was reached, 1 mL of sodium citrate in water (0.78 M) was quickly added. Approximately after 30 seconds the color of the mixture turned reddish and the solution was heated for another 30 minutes. The colloidal nanoparticles were left for cooling to room temperature. Later, the solution was distributed into 1 mL of plastic vials and was washed once by centrifugation (Heraeus Biofuge Primo) at 5000 rpm for 90 min in order to remove unreacted reagents from the solution.

To functionalize Au nanoparticles, 1 mM of sodium mercaptopyruvate dihydrate (Sigma Aldrich, Germany) in water was prepared and added into 1 mL of the colloidal Au nanoparticles. The attachment of pyruvate onto the Au nanoparticle surface was established by the affinity of the thiol functionalities of the mercaptopyruvate to the gold metal surface. Ligand exchanged proceeded overnight, subsequently the solution was washed by centrifugation at 5000 rpm for 90 min.

The characterization of the nanoparticles was performed by TEM, UV-VIS, FT-IR and Zeta measurements. A drop of the nanoparticle solution was dried on a carbon supported TEM grid (400 mesh, Quantifoil, Jena) and measured with a FEI Tecnai G^2 20 at 200 kV. UV-Vis spectra were acquired with a Varian Cary 5000 UV–Vis–NIR double beam spectrophotometer (Agilent) with a spectral resolution of 1 nm. The sample solutions were filled into a 1 cm quartz cuvette. FT-IR spectra from nanoparticles deposited onto a silicon wafer were acquired by using a Hyperion 2000 FT-IR microscope (Bruker). Zeta potentials of the citrate stabilized and pyruvate functionalized nanoparticles were acquired in water and also in OptiMEM utilizing a Malvern Zetasizer.

The cytotoxicity of the nanoparticle system was tested by using an alamarBlue test. HEK-293 cells were prepared in a 96-well plate for 24 hours and nanoparticles were incubated at a series of concentrations from 10 µg/mL to 1000 µg/mL for 24 hours. After an exchange of the culture medium, alamarBlue (Thermo Fischer) was applied for 4 hours and the fluorescence was measured at λ_{ex} = 570 nm / λ_{em} = 510 nm. Untreated cells were measured as a control system on the same well plate. This negative control was set to 0% of metabolism inhibition and refer to 100% viability. The threshold for cytotoxicity was set below 70%.

3.4.3. Incubation of the nanoparticles and sample preparation for TEM investigations

In a 12-well plate (0.5×10^6 cells/mL) HEK-293 cells were prepared in R10 medium for 24 hours. It was followed by applying OptiMEM for 20 minutes and then the incubation of 100 µL of the pyruvate functionalized Au nanoparticles into cells for different incubation times from 10 minutes up to 4 hours were tested. After that, the cells were washed twice with PBS and were trypsinated. In the end, R10 medium was applied.

To start the fixation of cells, glutaraldehyde (2% in PBS, Electron Microscopy Sciences) was applied for 1 hour on ice. Post fixation by OsO_4 (4%, in water, Electron Microscopy Sciences) was performed for 1 hour at room temperature. A graded ethanol series from 20 to 100% was conducted for 10 minutes for each series. The cell pellet was embedded into a resin (Embed 812/EtOH = 1:1 v/v for 1 hour and 2:1 v/v overnight at room temperature). Next day, it was exchanged with embedding medium and hardened at 70 °C for 24 hours. The sample block was cut into 80 nm thick slices by a diamond knife (Diatome, Switzerland) mounded on an ultramicrotome (PT-XL, PowerTome, RMC, Tuscon) and transferred onto carbon supported TEM-grids (400 mesh, Quantifoil). The grids were imaged by TEM. A post staining step with uranyl acetate and lead citrate was also performed if necessary.

3.4.4. Results and discussion

A drop of the synthesized Au nanoparticles was measured by TEM in order to characterize the size and shape of the nanoparticles. The mean size of the nanoparticles was found to be 17 ± 4 nm (Figure 3 – 19). The pyruvate functionalized Au nanoparticles were also measured by TEM.

However, the pyruvate shell around the Au nanoparticles was not observed due to its low contrast in comparison to the electron dense metal nanoparticle core.

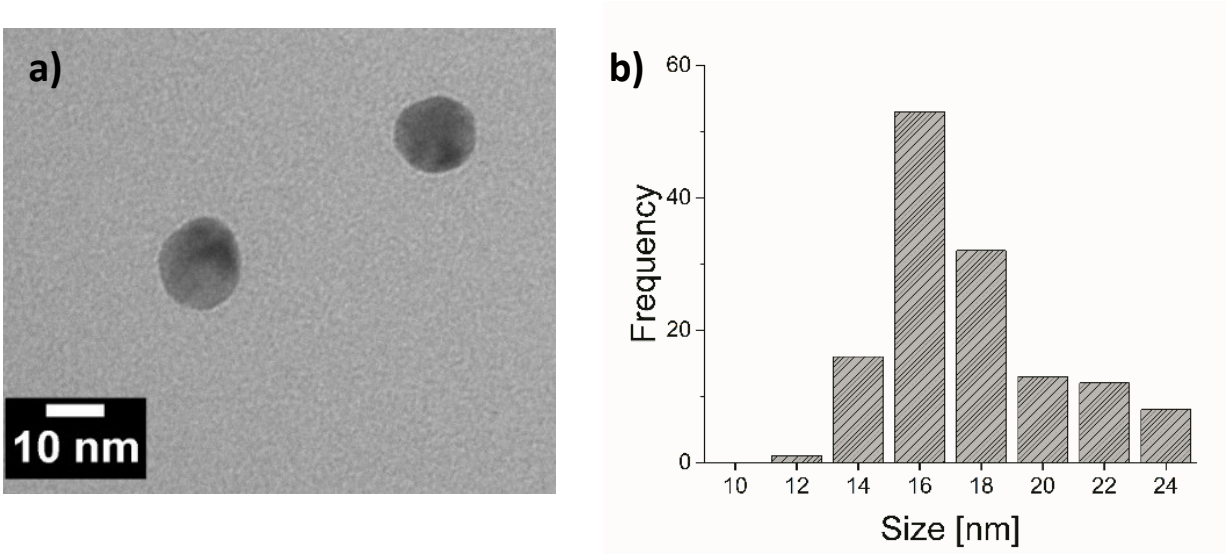

Figure 3 – 19 *(a) TEM image of the Au nanoparticles. (b) Size distribution of synthesized Au nanoparticles.*

An alternative to confirm the attachment of pyruvate molecules on the nanoparticles UV-VIS, FT-IR and Zeta potential measurements were performed. The UV-VIS spectra indicate a small shift from 524 to 526 nm of the localized plasmon resonance frequency caused by surface functionalization (Figure 3 – 20a). To further confirm the functionalization of the colloidal gold nanoparticles FT-IR characterization was performed (Figure 3 – 20b) Characteristic peaks at 1587 cm^{-1} and 1400 cm^{-1} of the citrate stabilized Au nanoparticles were obtained related to the symmetrical and asymmetrical stretching modes of COO^-. Moreover, the peak of the pyruvate solution at 1618 cm^{-1} confirmed the C=O bonds. On the other hand, a very similar peak structure was obtained due to the similarities of both molecules for the pyruvate functionalized particles. The spectrum of pyruvate functionalized Au nanoparticles however showed a slight shift of the peak positions.

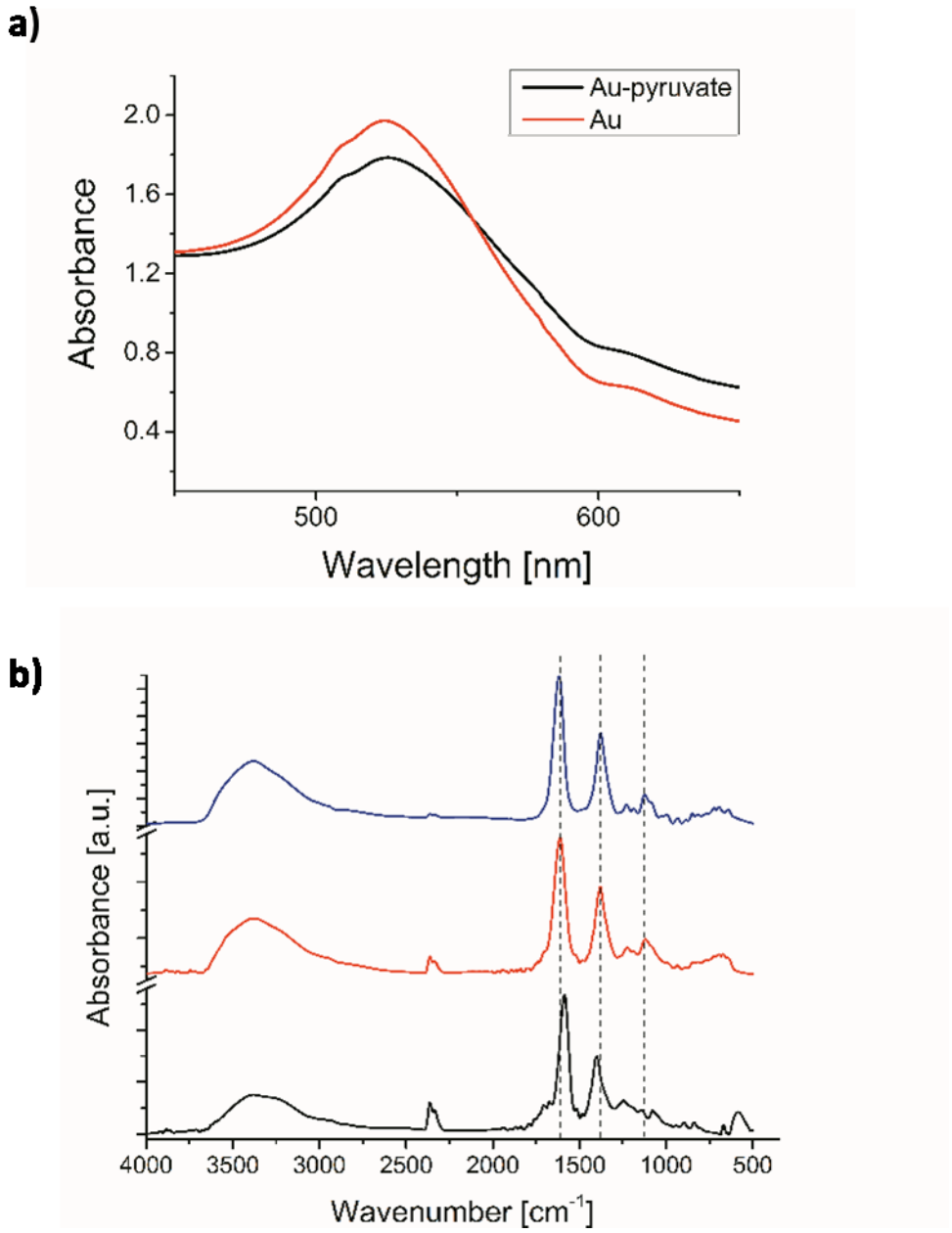

Figure 3 – 20 *a) UV-VIS spectra of Au nanoparticles and pyruvate functionalized Au nanoparticles. b) FT-IR spectra of pyruvate in solution (blue), pyruvate functionalized Au nanoparticles (red) and citrate stabilized Au nanoparticles (black).*

The strongest evidence for the functionalization of the colloidal gold nanoparticles derived from the Zeta potential measurements. They have been conducted with the aim to test the functionalization but also to determine the stability of the pyruvate functionalization towards incubation of the nanoparticles in the cell culture medium. While the citrate stabilized Au nanoparticles showed a Zeta potential of –33 mV, the pyruvate functionalized Au nanoparticles' Zeta potential decreases to –27 mV. The negative values reflect the fact that the nanoparticles

are negatively charged. Moreover, it can be concluded that both nanoparticle systems are stable, according to the guidelines provided by the supplier of the Malvern Zetasizer. In order to determine the stability of the pyruvate functionalized Au nanoparticles during cell incubation, the nanoparticles were exposed to OptiMEM medium and washed twice with water after an incubation time of 3 hours. The value of Zeta potential was found to decrease to –25.6 mV. The small difference in the Zeta potential before and after exposure to the OptiMEM medium might be indicative for the absorption of proteins, but it can be concluded that the pyruvate functionalization remains stable against the exposure to the culture medium.

Uptake investigations were first conducted for the unfunctionalized Au nanoparticles as a control measurement. Incubation times of 4 hours, 1 hour, 30 minutes, 20 minutes and 10 minutes with unfunctionalized spherical Au nanoparticles into HEK-293 cells were performed. After completing the sample preparation protocol, the obtained slices were imaged by (S)TEM. It was observed that clusters of citrate stabilized Au nanoparticles were localized in a membrane surrounded organelle, which is likely to be an endosomal structure. This indicates an internalization of the unfunctionalized colloidal gold nanoparticles into HEK-293 cells by a macropinocytosis mediated uptake process (Figure 3 – 21).

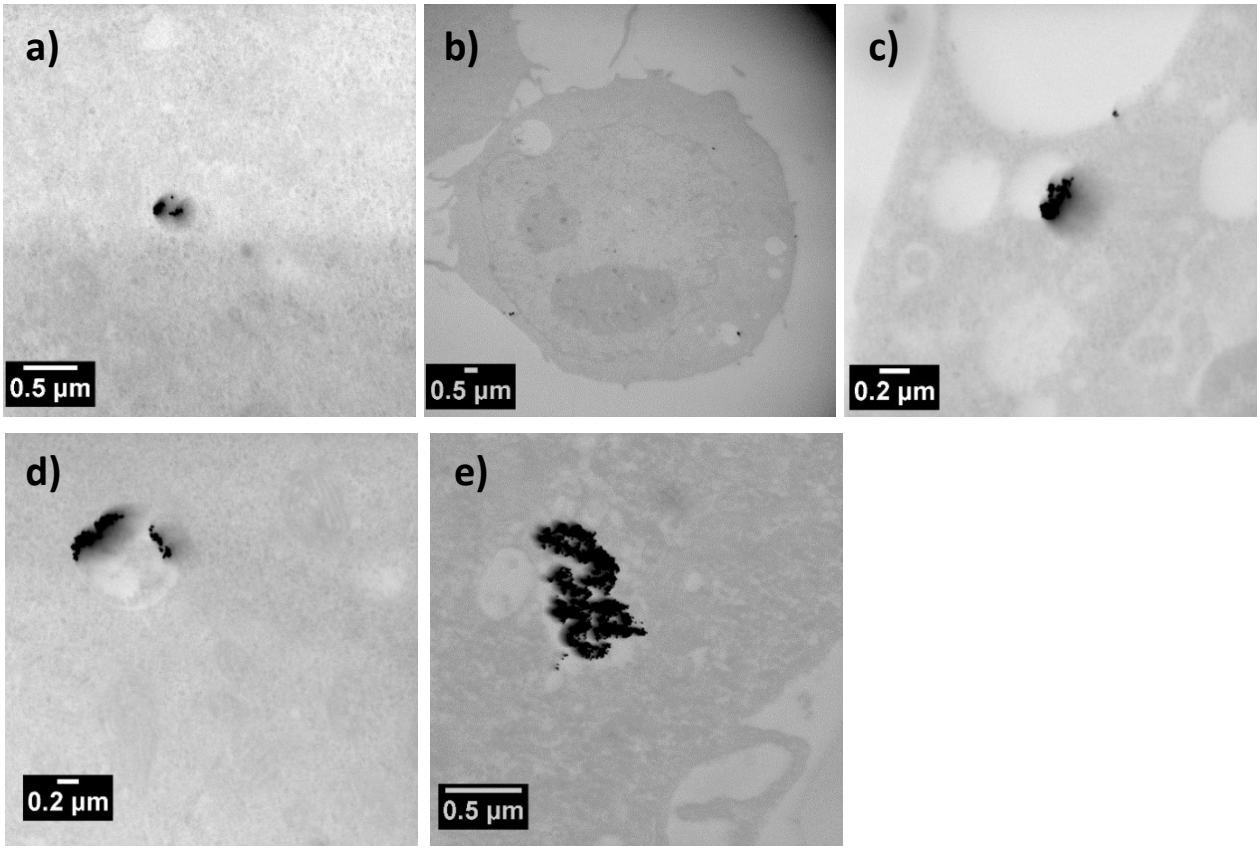

Figure 3 – 21 *STEM investigations of Au nanoparticle uptake in HEK-293 cells at 10 minutes (a), 20 minutes (b), 30 minutes (c), one hour (d) and four hours (e) of incubations.*

To study the localization and uptake of the pyruvate functionalized Au nanoparticles, different incubation times were investigated. After an incubation time of 10 minutes a slice of the embedded sample was imaged by (S)TEM and a few nanoparticles were localized in mitochondria. With the help of the STEM mode, the characteristics lamellar structure of mitochondria could be easily identified within the cell. Moreover, some changes on the mitochondrial morphology were also observed. These changes can be ascribed to a destructive impact of the nanoparticle system on the mitochondria.

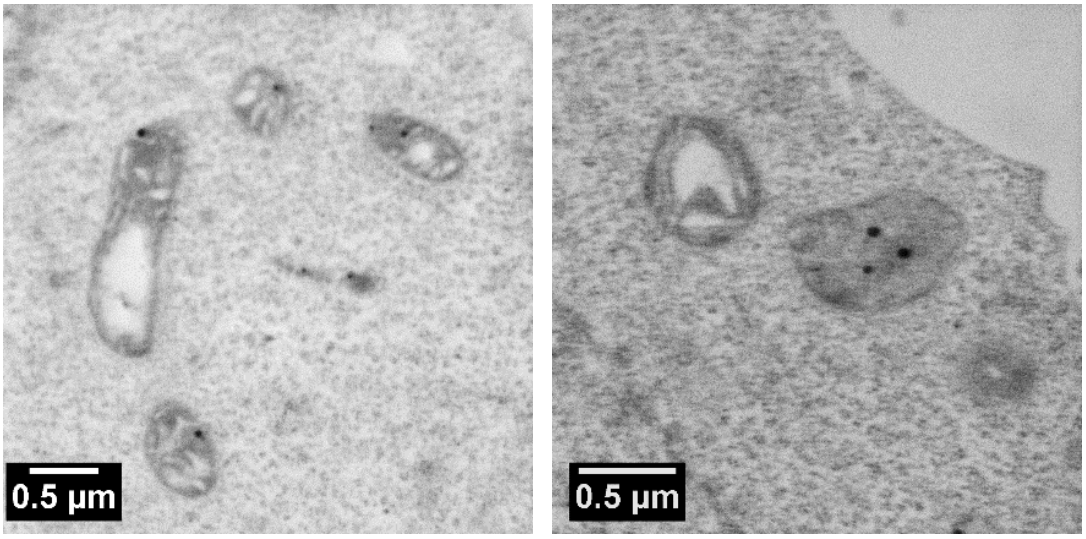

Figure 3 – 22 *STEM investigations of pyruvate functionalized Au nanoparticles incubated into cells for 10 minutes.*

In order to investigate the observed changes in the mitochondria structure on the cell viability of the entire cell, the cytotoxicity of unfunctionalized and pyruvate functionalized colloidal gold nanoparticles was investigated. It was found that neither the unfunctionalized nor the pyruvate functionalized Au nanoparticles show a significant cytotoxic effect up to concentrations of 500 mg/mL.

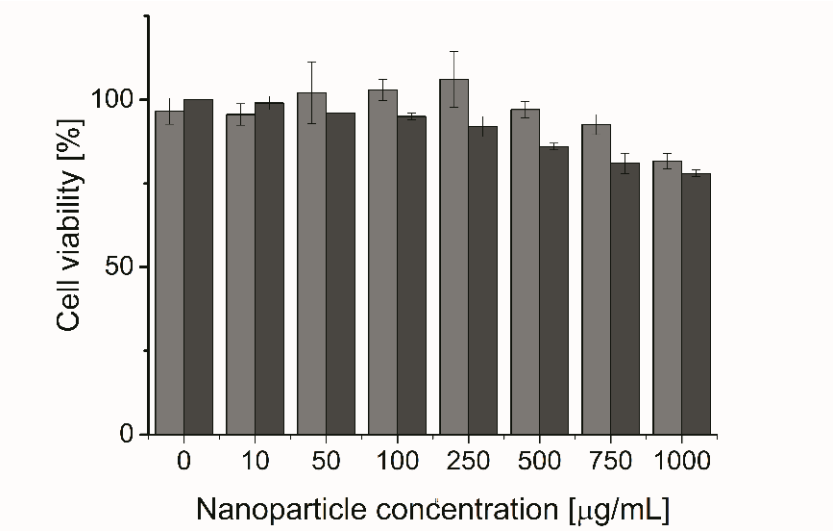

Figure 3 – 23 *Cell viability of the unfunctionalized Au nanoparticles (dark gray) and the pyruvate functionalized Au nanoparticles (gray) at different concentrations after an incubation time of 24 hours.*

Thus, it was concluded that the change of the mitochondria structures was a direct consequence of the internalized pyruvate functionalized nanoparticles. To gain a better understanding of the further fate of the nanoparticle within the HEK-293 cells, experiments with longer incubation times of 20 minutes and 30 minutes were also conducted (Figure 3 – 24). Next to the localization of the nanoparticles within the mitochondria additional structural changes were observed at these prolonged incubation times. Closer inspection of the direct environment of the mitochondria revealed the evolution of round shaped structures which show only a weak electron contrast in close vicinity to the damaged mitochondria. These structures mark the onset of the self-defense processes triggered by the damaged mitochondria. As outlined in Figure 3 – 18, this process starts with the formation of a curved membrane structure (Figure 3 – 24), a phagohore, which subsequently encapsulates the entire damaged mitochondria. These phagophores are electron-transparent and are surrounded by a double layer membrane. In these images it becomes moreover evident that the pyruvate functionalized colloidal gold particles are taken up individually at the plasma membrane, that is why individual gold nanoparticles are found in the cytoplasm. These are not yet associated to mitochondrial structures. This behavior is different from the uptake of unfunctionalized nanoparticles which are exclusively found in endosomal structures.

At the same time, taking into account the cell viability, it becomes clear that the self-defense mechanism of mitophagy was initiated in order to clear the cells for defective mitochondrial structures.

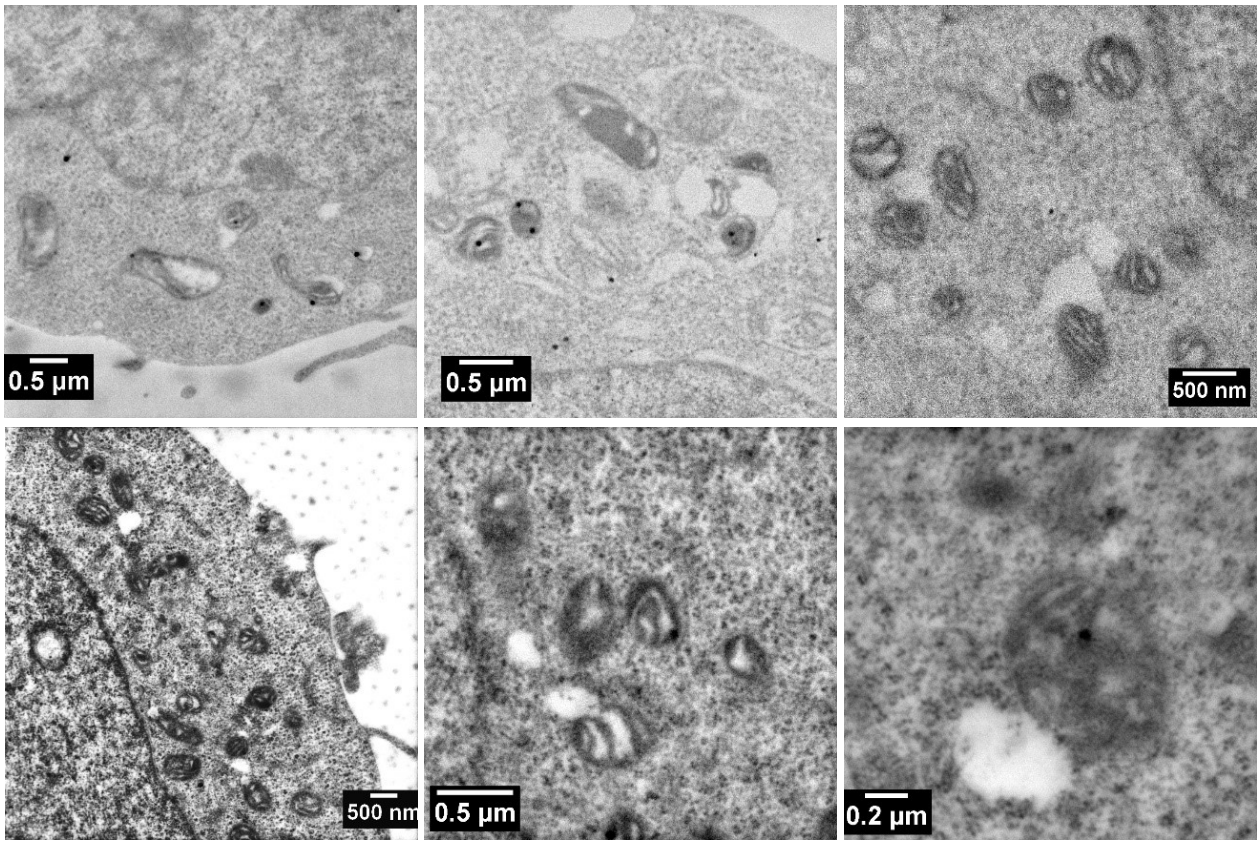

Figure 3 – 24 *STEM investigations of pyruvate functionalized Au nanoparticles incubated into HEK-293 cells at incubation times of 20 minutes (upper row) and 30 minutes (lower row).*

Consequently, the process was further investigated also for longer incubation times to also confirm the later stages of mitophagy, which would provide additional support for the proposed targeting concept. After 1.5 h (Figure 3 – 25a) the functionalized nanoparticles were localized in larger and membrane encapsulated organelles. These organelles frequently consist of electron-dense material which resembles the remainings of the damaged mitochondria in the stage of being digested. This most probably marks the stage where the phagophores have fused with a lysosome and the onset of digestion is in progress. At this stage, due to the strong electron contrast of the digested materials, the identification of the colloidal gold nanoparticles is difficult to visualize. After incubation times of 4 h only endosomal/lysosomal structure containing a large number of colloidal gold nanoparticles were observed. The increased number might hint at this stage to the occurance of lysosomal fusion processes, which occur during the progress of mitophagy. In this case identification of the colloidal gold can be performed by means of EDX studies.

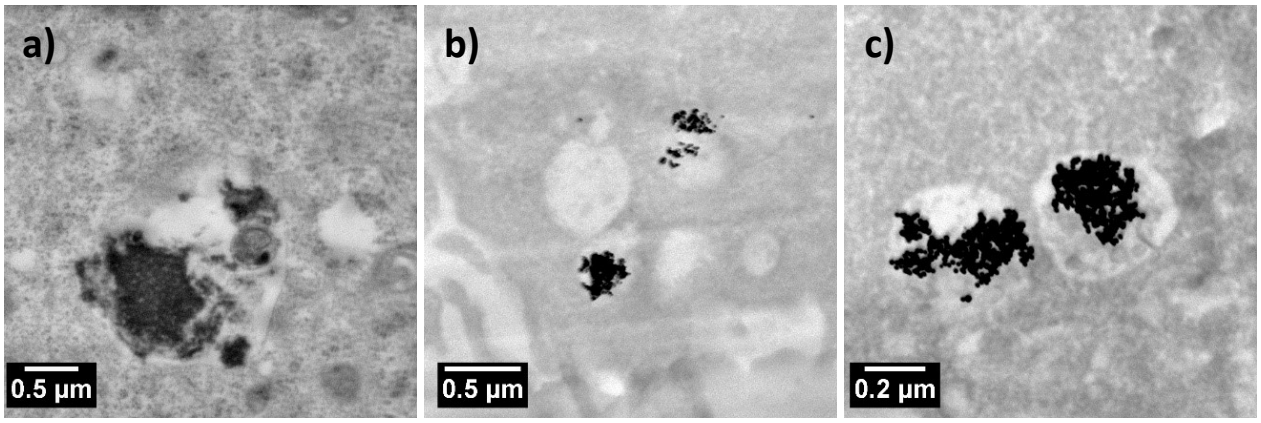

Figure 3 – 25 *STEM investigations of pyruvate functionalized Au nanoparticles incubated into HEK-293 cells at incubation times of 1.5 hours (a) and 4 hours (b,c).*

EDX analysis represents a suitable method to provide the elemental compositions of specific regions of interest on a sample. For the "black dots" localized in phagolysomal structures, a spectrum clearly indicating characteristic peaks for Au were obtained (Figure 3 – 26). The EDX spectrum additionally showed characteristic peaks associated with the conducted osmium staining as well as peaks which are associated to copper (peaks located mainly at 8.0 and 8.5 eV). These originate from electrons which undergo multiple interactions also with the copper grid used during the preparation.

Due to the weak EDX signal provided by individual nanoparticles it was however not possible to obtain EDX measurements on individual articles located in the mitochondria in the first stages of the uptake process.

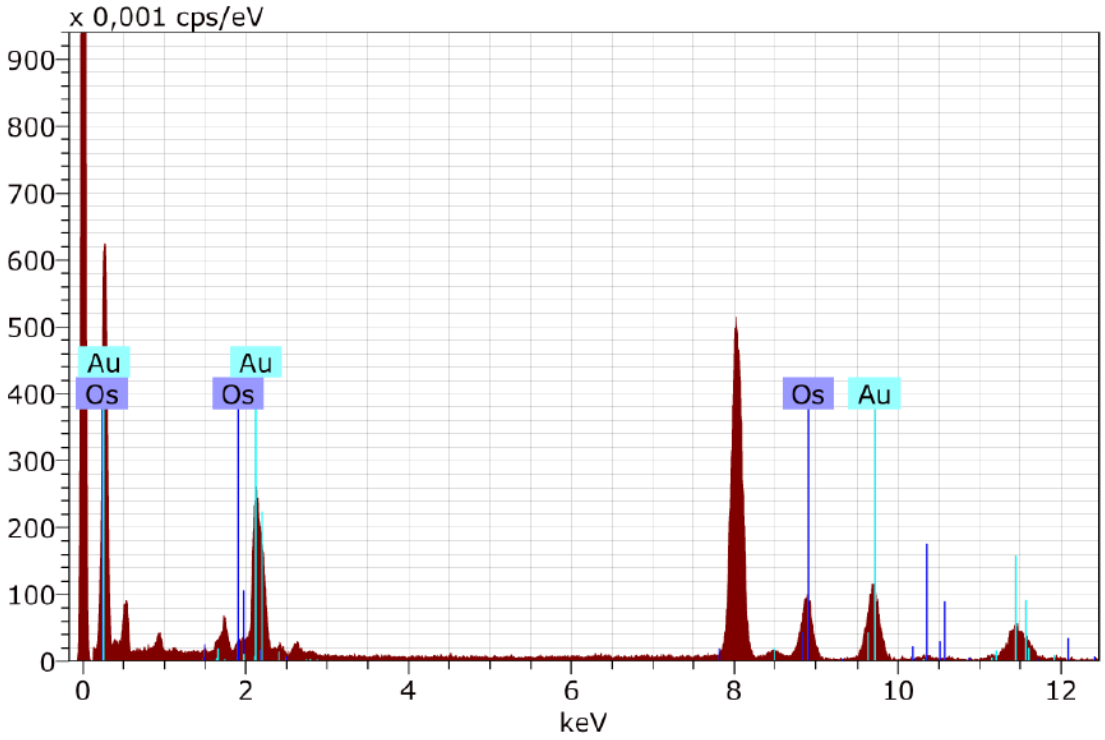

Figure 3 – 26 *EDX-spectra of "black dots" localized in endosome confirmed that they are Au nanoparticles.*

The pyruvate functionalized Au nanoparticle system was incubated into HEK-293 cells. With comparison to the other studies performed, an effect of mitophagy was observed which never was observed for other systems under investigation. Therefore, it is clear that the pyruvate functionalized Au nanoparticles caused different effects on the cells. Different incubation times from 10 minutes to 4 hours provided information how fast the mitophagy actually occurs. As a further test or control experiment to deepen the understanding of this process, pyruvate itself may be incubated into the cell culture at different incubation times. By doing so, the effect of pure pyruvate on the cells can be observed and its relation to mitophagy can be evaluated. A test will be additionally usefull to check, that, even though the nanoparticle solution was washed after functionalization, no remainings of unfunctionalized pyruvate molecules are still present in the solution. Here, improved or repetitive washing steps may be also applied and the nanoparticle system should be incubated into the cells again at different incubation times. Afterwards, the status of mitochondria and cells can be investigated to obtain more information on the delivery and mitophagy.

3.5. The uptake study of Au-PEI nanoparticle clusters by means of tomography

3.5.1. Introduction

The third system studied for targeted drug delivery covers polycationic polymer systems. These systems have gained significant attention during the last years as they represent systems which help to circumvent the excretion of the drug delivery carrier from the endosomal metabolic cycle. As previously outlined, endosomal uptake by, e.g., macropinocytosis, encapsulates the drug carriers into endosomes with increasing pH conditions during the evolution of the endosomal ripening processes and finally nanoparticles will be digested and transfer their content into lysosomes. The increasing pH environment, in particular in the lysosomes, on the one hand might be harmful for encapsulated drugs in the drug delivery vehicles. In the worst case the drugs are simple transferred out of the cell during the metabolic cycle and cannot fulfil their intended task. This is, e.g., relevant for gene transfection and optimizing gene transfection, where the encapsulated DNA has to be available in the cytosol to be transferred into the nucleus of the cell. Thus, endosomal escape represents a critical parameter which has to be established for such systems. On the other hand, the increasing pH values in the endosomal development opens up an attractive possibility to establish endosomal escape. In particular, polycationic systems are interesting in this respect.

PEI is widely used in such studies to stimulate endosomal escape via the proton sponge effect.[96] However, it has to be mentioned here that the steps of endosomal release are still under debate in literature.[97] To understand the steps of endosomal release, ultrastructural details of cells are required. In this chapter, a model system was introduced, which consists of cationic polymer and metal nanoparticles so that the model system can be localized in cell compartments by utilizing TEM.

There are sophisticated strategies to release the materials at the endosomal stage.[98] One of these strategies utilizes the proton sponge effect, which can be applied by utilizing cationic polymers because their response to the pH change in the endosome can be used to trigger endosomal release. Cationic polymers can be defined as polymers bearing positive charges or polymers possessing cationic entities. Cationic polymers are studied in literature in a way that they can build up polyplexes by binding to anionic biomolecules, nucleic acids and proteins.[99] This class of polymers can be listed as following; Poly(ethyleneimine) (PEI), poly-L-(lysine) (PLL), poly[2-(*N,N*-dimethylamino)ethyl methacrylate] (PDMAEMA) and chitosan.[100] Generally, they can be protonated on their amino functions. They can be designed also in different architectures, such as linear, branched, hyper-branched and dendritic structures. The location of their positive charge also differs. For instance, PEI carries the positive charge on its backbone. Important parameters related to cationic polymers can be listed as following; Polymeric chain flexibility, H-bond formation, hydrophobic interactions, electrostatic forces or charge transfer potential, amino group and its neighboring functionalities, p*K*a, and nucleophilic character.

Regarding to their synthesis they can be also divided into two classes of naturally derived cationic polymers and synthetically derived cationic polymers. Naturally derived cationic polymers are listed as following; Cationic chitosan, cationic gelatin, cationic dextran, cationic cellulose and cationic cyclodextrin. Synthetically derived cationic polymers can be listed as following; PEI, PLL, PAA, PAE and PDMAEMA. They can be used as therapeutics by various bioactive properties. Some of the cationic polymers exhibit stimuli responses, e.g., temperature response, pH response and ionic response or multi-responses.[101]

Among other cationic polymers, PEI or PAMAM nanoparticles are supposed to cause the proton sponge effect and they might be efficiently released from endosomes.[102] The proton sponge effect is based on the pH change and the buffer capacity of the cationic polymer. While the acidity of an endosome is increased, protonation of the amino groups of the cationic polymer, i.e., PEI, is stimulated.[103] The protonation of the amino group cause an electrostatic repulsion of the PEI chains and results in an increase of the size of the nanoparticles.[104] Meanwhile the endosome tries to maintain the acidity of the endosomal maturation and the influx of H^+, Cl^- and water is increased.[105] The increased influx, as a consequence, causes increased osmotic pressure and the endosomal membrane ruptures. In the end, endosomal escape is succeeded, and the materials are released into the cytoplasm.[106] The steps of endosomal escape are schematically illustrated with a comparison of endocytosis pathway in Figure 3 – 27.

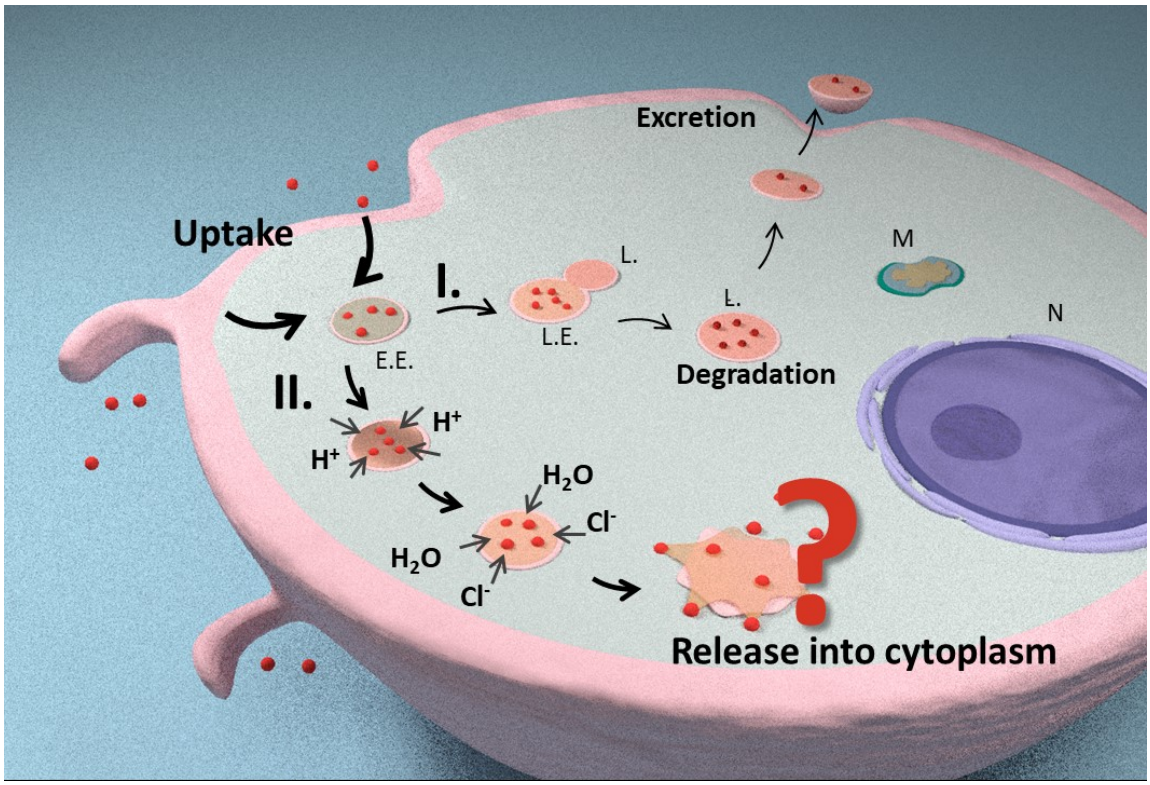

Figure 3 – 27 *I. General steps of endocytosis. II. Steps of endosomal escape.*

The important parameter for the protonation of the amino groups is the pKa value of the polymer carrier.[107] At an acidic environment, the protonation starts and the polymer chain occupies a larger volume due to the electrostatic repulsion.

Nevertheless, the proton sponge effect and its mechanism are still under discussion in literature. Some studies support the proton sponge effect while other studies claim that no pH change in the internal pH of an endosome is triggered by polycationic polymers and other mechanisms trigger actually the endosomal escape.[97, 108]

In order to study the morphological changes on the endosomal structures, transmission electron microscopy is a suitable tool to investigate the morphological changes of the nanoparticles as well as the changes associated with the release mechanisms on the intracellular structure. According to the imaging requirements of TEM, polymeric samples are almost transparent. Therefore, a model metal-polymer hybrid system was proposed, which combines a PEI nanoparticle matrix and encapsulated Au nanoparticles. With this design, the proton sponge effect, caused by PEI and the detection of PEI by the gold markers, can be studied by using TEM.

For detailed investigations of the endosomal escape process, not only TEM images but also tomograms are recorded. STEM tomography offers the possibility to localize the nanoparticles in a larger volume of the cell and delivers information on biological processes, subcellular architecture, structural details, and even drug localization.[109]

3.5.2. Instrumentation and experimental details

10 mg of hydrogen tetrachloroaurate (III) trihydrate (99.99%, Alfa Aesar) was dissolved in 1 mL DMF (anhydrous, amine free, 99.9%, Alfa Aesar). 10 mg of branched PEI (bPEI; 25 kDa, Sigma Aldrich) was also dissolved in 1 mL of DMF. 200 µL of $HAuCl_4$ in DMF, 200 µL of PEI in DMF and 5 mL of DMF were mixed in a sealed microwave vial. The synthesis was performed in a microwave reactor (Initiator Sixty Biotage) at 150 °C for 2 min. After cooling to room temperature, it was transferred into 1 mL EPIs and washed three times by centrifugation at 15 000 rpm.

20 µL of Au-PEI cluster was dropped on a TEM grid (Carbon supported, Mesh 400, Quantifoil, Jena) and imaged in TEM.

3.5.3. Incubation of the nanoparticles and sample preparation for TEM investigations

A 12 well-plate (0.1 x 10^6 cells/mL) was cultured with HEK-293 cell lines in R10 medium for 24 hours. The medium was exchanged with OptiMEM for 20 minutes before 50 µL of the nanoparticle system was incubated for 4 hours. After the incubation, it was washed twice with PBS and trypsinated in R10 medium. Cell fixation was performed by glutaraldehyde (8% in PBS, Electron Microscopy Sciences) for overnight and post-fixed by osmium tetroxide (4% in water, Electron Microscopy Sciences) for one hour. Dehydration was applied with a graded ethanol series from 20 to 100%. Embedding medium (composed of EMBED 812, DDSA, NMA and DMP-30, Electron Microscopy Sciences) and propyleneoxide (Embed/propyleneoxide = 1:1 v/v for 1.5 hours, 2:1 v/v for overnight at room temperature) were used in order to embed the cell pellet. Next day, the cell pellet was embedded into the 100% of the embedding medium firstly for 4 hours at room temperature and for overnight in an oven at 70 °C.

The hardened sample block was sliced into 80 nm, 200 nm and 300 nm thick slices by using a diamond knife (RMC) mounted on an ultramicrotome (PT-XL, PowerTome, RMC, Tuscon). Slices swimming on the water bath of the diamond knife were collected by a loop and placed on TEM grids (Carbon supported, 400 and 300 mesh, Quantifoil, Jena). Post-staining with uranyl acetate (4% for 40 minutes) and lead citrate for 20 minutes were applied in order to obtain a suitable contrast.

For tomography investigations, another type of TEM grids (PELCO slot and Athene slot, Ted Pella) was used in order to eliminate beam blocking by the meshes within the area of investigation. A support film on TEM-grids was mandatory to hold slices without folding on the large size slot of the grids. 0.375 g of formvar was dissolved in 25 mL of dichloromethane (CH_2Cl_2). A hot water pool was prepared in a beaker. Coverslips were cleaned with ethanol and

dipped into the formvar solution for 30 seconds. The edges of the coverslips were scratched by a razor blade. While dipping the coverslip into the hot water, the formvar film could be transferred onto the water surface with the help of a tweezer. After that, grids were placed on the swimming formvar film. Another coverslip was used to capture the film and grids. After drying, grids were separated from each other by using a razor blade and transferred onto a filter paper. In the end, they were coated with a carbon layer by carbon evaporating. The process is illustrated in Figure 3 – 28.

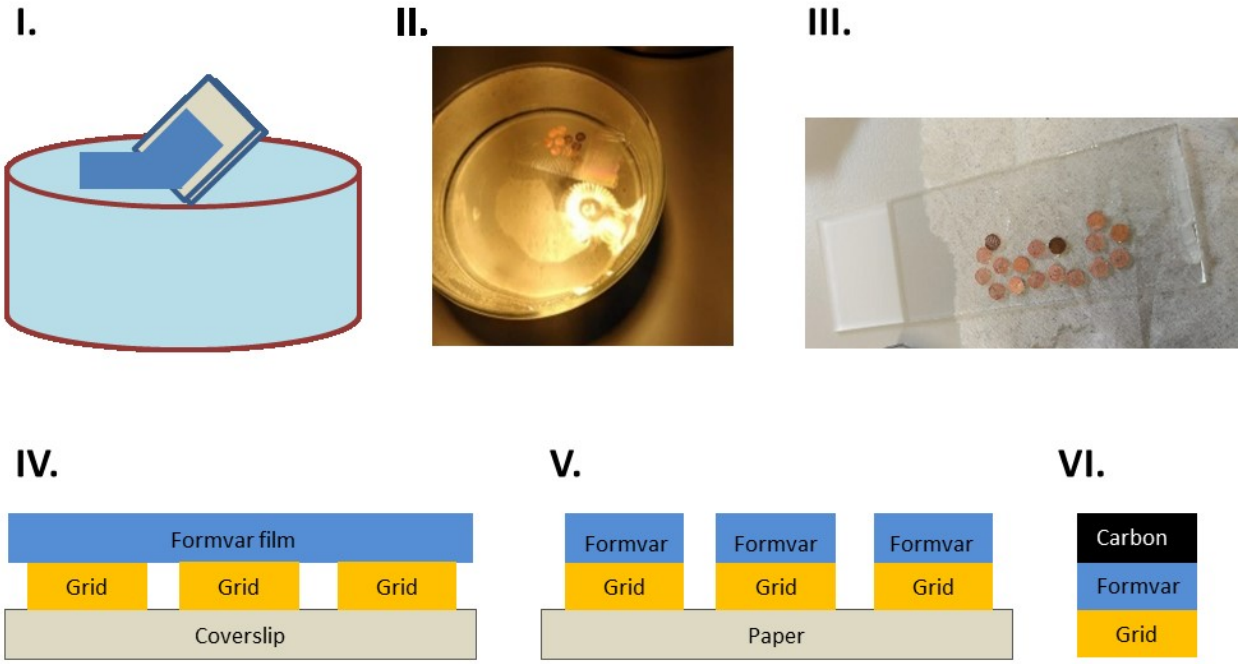

Figure 3 – 28 *Steps of formvar coating on TEM grids. I. A coverslip dipped into formvar in CH_2Cl_2 was later digged into hot water. II. TEM grids were placed on the swimming formvar film on the hot water. III. Grids on the formvar film were transferred onto another coverslip. IV. They were left to dry and were later separated from each other by a razor blade. V. Formvar coated TEM grids were placed on a paper. VI. Carbon evaporation was applied.*

The sample grids were loaded into a Tecnai G^2 20 system (FEI) and STEM mode imaging with HAADF detection at an acceleration voltage of 200 kV using a dual axis Fischione tomography holder was performed. Tomograms were recorded from thicker slices, i.e., 300 nm thick slices. Generally, the tilt angle was kept between – 60 and 60°, with a tilt increment of 1°. Images were acquired by the program Xplore3D provided by FEI and reconstructed by EM3D provided by Stanford University School of Medicine and Image J (TOMOJ plug-in) and were visualized with Chimera provided by University of California, San Francisco.

3.5.4. Results and discussion

The proposed Au-PEI nanoparticle system was synthesized as previously reported[110] but this time a microwave reactor was utilized. Heating the mixture of branched PEI and

hydrochloroauric acid in DMF started to form small gold nanoparticles embedded into a spherical PEI particle. The ratio of PEI to gold salt concentration enabled to obtain different sizes and filling ratios of the Au-PEI hybrid nanoparticles. By utilizing a microwave, the synthesis reaction time could be shortened to two minutes only. The synthesized nanoparticle system was later characterized by imaging in TEM. Figure 3 – 29a presents an overview image of the Au-PEI nanoparticles. To improve the understanding on the distribution of the Au nanoparticles within the PEI nanoparticle, a TEM tomogram was also recorded. The 3D reconstruction clearly showed that spherical gold nanoparticles are mainly located inside the PEI nanoparticle volume as seen in Figure 3 – 29b. It has to be mentioned here that the soft nature of the PEI causes also a flattening of the nanoparticles due to drying effects.

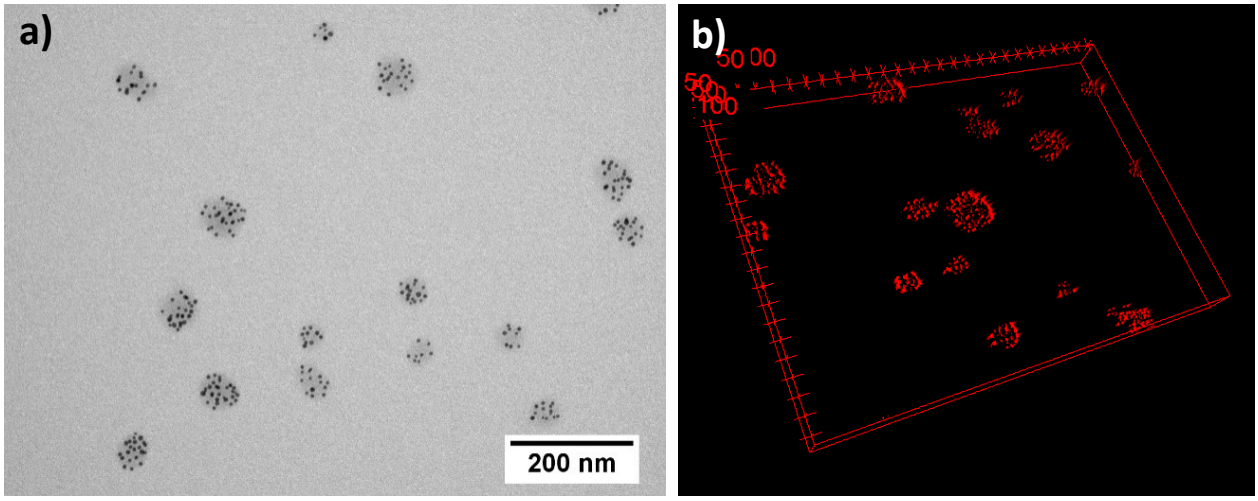

Figure 3 – 29 *TEM image (a) and TEM-tomography (b) of Au-PEI clusters.*

The Au-PEI nanoparticles were later incubated into HEK-293 cells for 4 hours. After the cell pellet was prepared for TEM measurements, it was imaged by utilizing the HAADF-STEM mode to take a closer look on the particles' and endosomes' morphologies. Images of the nanoparticles at the extra-cellular cell membrane and in the endosomal structures were acquired (Figure 3 – 30) and a histogram analyzing on the particle size differences was prepared (Figure 3 – 31).

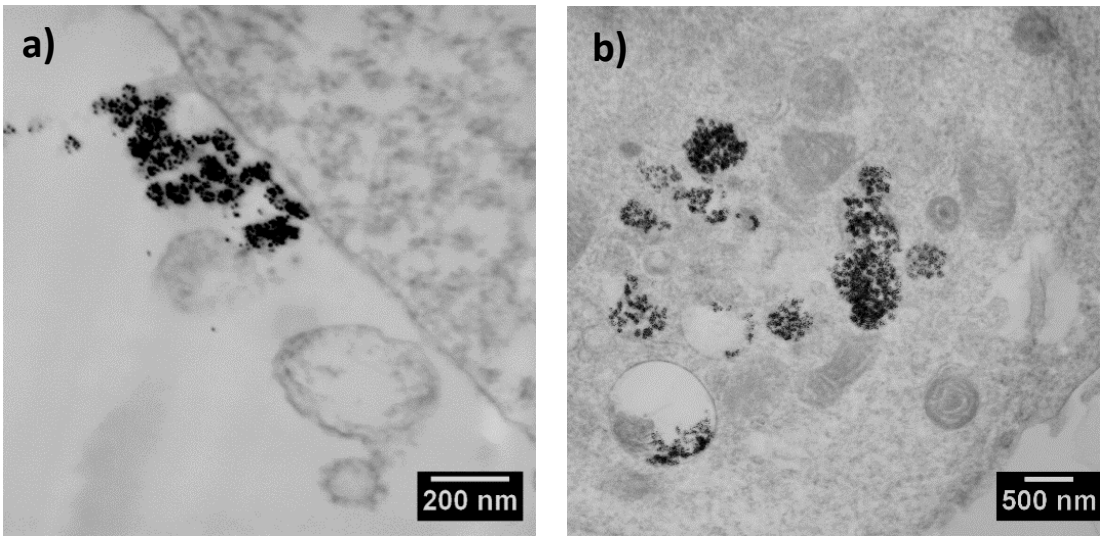

Figure 3 – 30 *Representative examples of Au-PEI nanoparticles on cell membrane (a) and in endosome/lysosome (b).*

It was found that the average size of the particles on the extracellular cell membrane is 64 ± 30 nm. Meanwhile, the uptake way was also determined as macropinocytosis, in agreement with a previous study,[111] since characteristic membrane protrusions and the engulfment of the Au-PEI clusters into endosomal structures were observed at the plasma membrane. Unfortunately, TEM is not capable to distinguish endosomes and lysosomes. However, the change on the particle size can be measured in order to examine the effect of the proton sponge effect. The average size of the Au-PEI clusters in endosomal structures was determined as 91 ± 36 nm as shown in Figure 3 – 31.

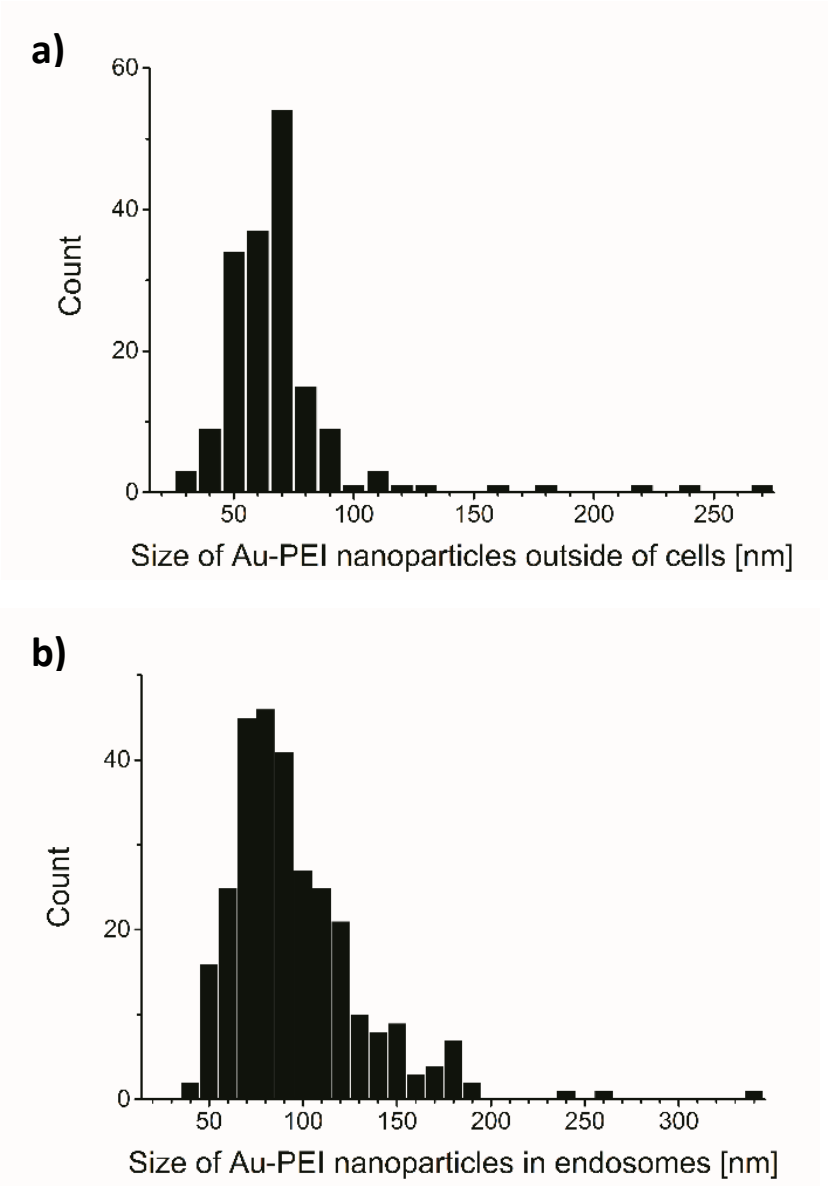

Figure 3 – 31 *Histograms of the size of Au-PEI nanoparticles on cell membrane (a) and in endosomes (b).*

These studies already demonstrate that the Au-PEI hybrid nanoparticles represent an excellent tool for uptake studies. Small Au nanoparticles provide a high contrast which can be recognized easily within the cell context. The PEI nanoparticle itself was also stained by osmium tetroxide during cell preparation, thus, also the PEI polymer matrix was nicely observable, enabling, e.g., to determine changes in the particle size. Moreover, the increased material contrast was obtained by applying the HAADF-STEM mode.

The images acquired by HAADF-STEM imaging showed that some of the endosomes were filled completely with the nanoparticles while some of the endosomes host less particles which are located mostly on/closer to the endosomal membrane. In both cases, the characteristic shape of

the Au-PEI clusters could be recognized. Additionally, endosomes located very close to each other, indicating endosomal fusion processes, were observed.

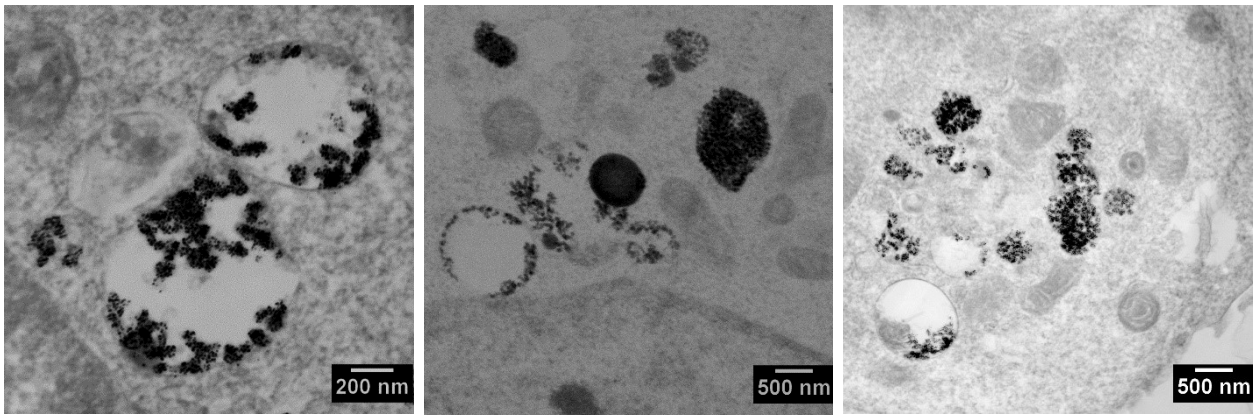

Figure 3 – 32 *Representative examples of nanoparticle filled endosomes in close vicinity to each other for fusion and nanoparticle distributions within endosomes.*

The main focus of the investigations was placed on the development of other structural features as seen in Figure 3 – 33. The original spherical and defined structure of individual Au-PEI nanoparticles evolved into much larger round features which appeared with a darker contrast. Individual Au nanoparticles were still localized in these structures, but with less density in comparison to the original Au-PEI nanoparticles. This morphological shape may indicate the degradation of the Au-PEI clusters or their extraordinary swelling due to the protonation of the amino groups which is predicted by the proton sponge hypothesis.[107] Additionally, individual Au nanoparticles were localized in the cytosol in close vicinity of the endosomal structures, which showed no dark corona which is characteristic for the PEI originally around them. This is the main indication of a complete particle degradation and release of their content into the cytosol.

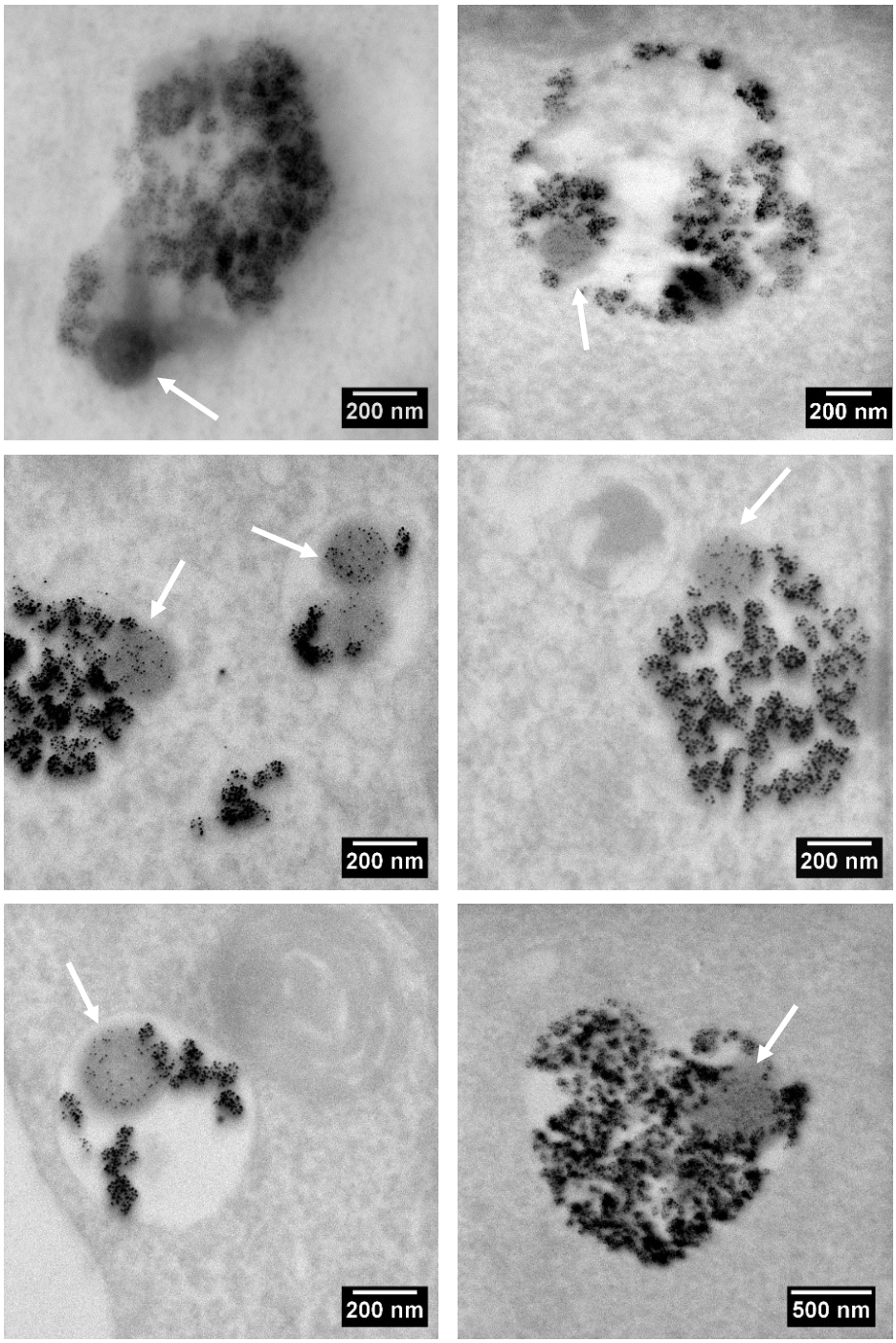

Figure 3 – 33 *Examples of changes in the morphological shape of Au-PEI clusters in endosomal structures.*

Investigations by performing STEM-tomography delivered a more detailed insight into the release mechanism. By slicing the sample block into 300 nm thick slices, tomograms with enough cell volume could be acquired to better identify the nanoparticle localization within the

cellular organelle. Selected examples of 3D reconstructions are depicted in Figure 3 – 34 and highlight the localization of the nanoparticles mostly at the endosomal membrane.

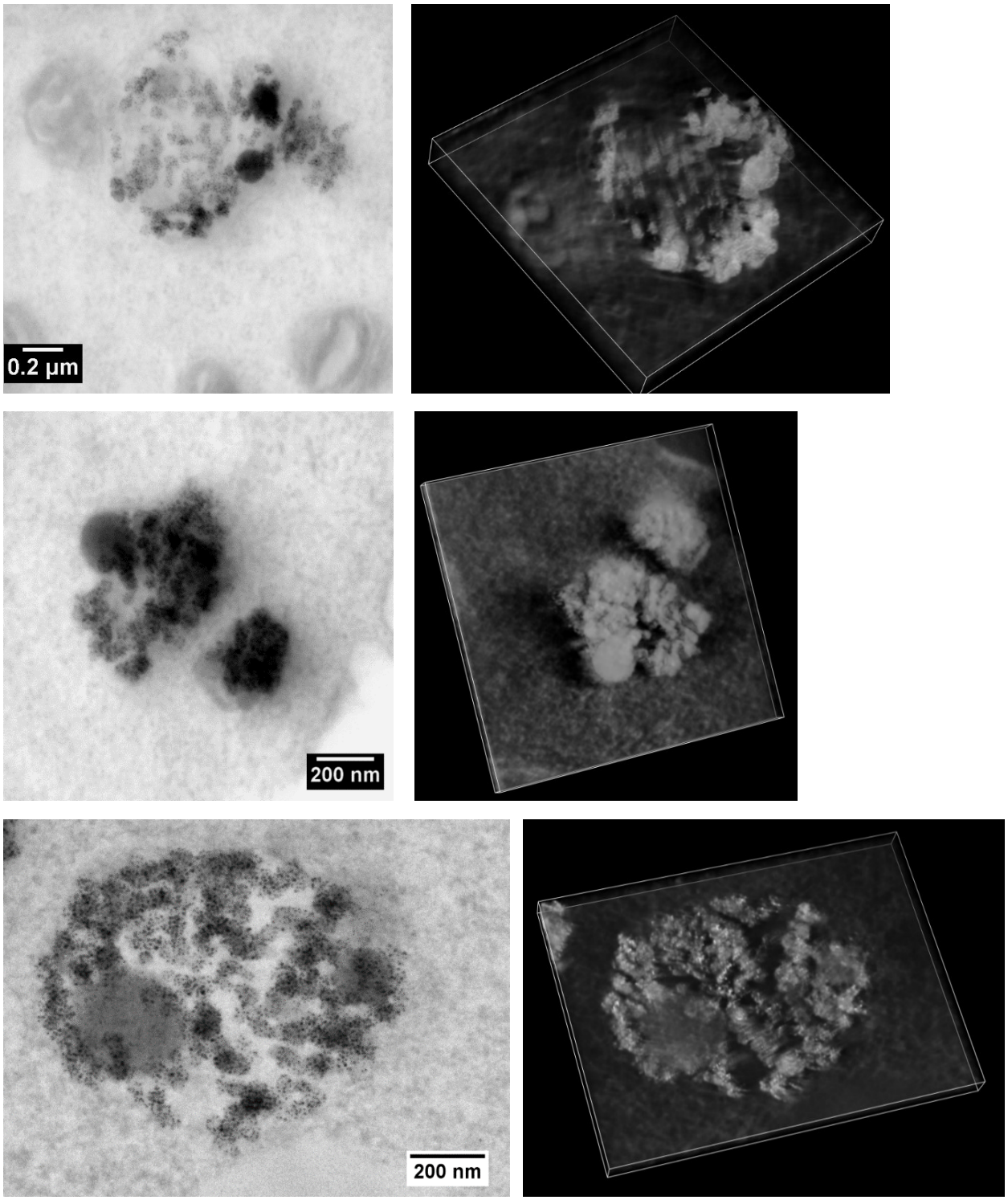

Figure 3 – 34 *Examples of reconstructed (S)TEM tomograms of Au-PEI nanoparticle filled endosomes.*

Selected tomograms were recorded at locations showing the less densely filled, enlarged metal polymer hybrid as seen in Figure 3 – 35. This behavior can be assigned to the release of the Au-PEI nanoparticles from endosome into cytosol.

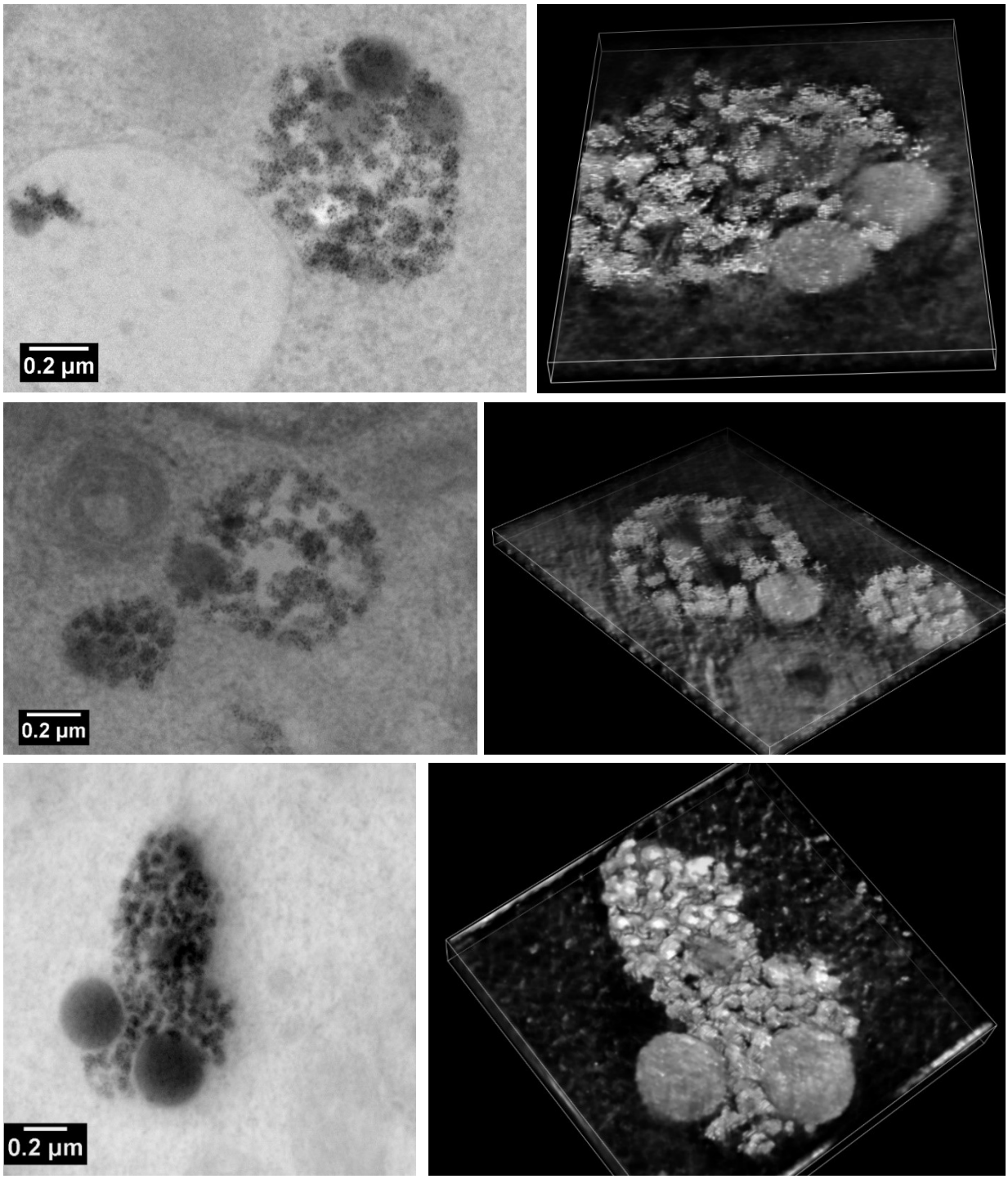

Figure 3 – 35 *Selected examples of reconstructed (S)TEM tomograms which indicate the less density of Au nanoparticles in PEI nanoparticles.*

Additionally, also a tomogram showing an endosomal fusion process was recorded as seen in Figure 3 – 36. The cell membranes of the two endosomes were clearly observable and fusion of the membranes at the junction region was visualized.

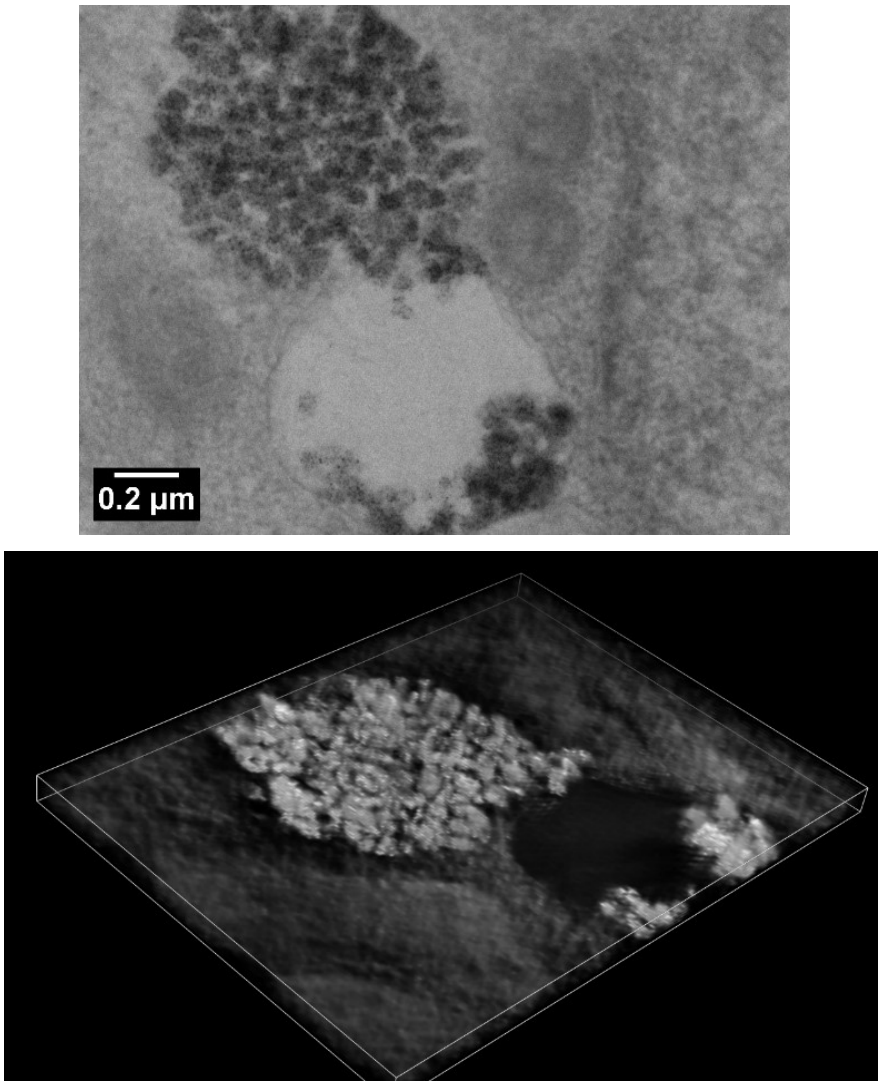

Figure 3 – 36 *TEM image (top) and reconstructed tomogram (bottom) of endosomal fusion.*

In this study a model system was introduced which allowed the in depth study of endosomal escape processes, which are an essential tool to establish drug release into the cytosol. With the applied model systems details on the nanoparticle swelling as well as on details of the release process could be identified. Extremely beneficial was in this case the utilization of HAADF-STEM tomography investigations as they tremendously increase the depth of information that can be investigated. While conventional TEM tomography is limited to the investigation of slices with a typical thickness of only approximately up to 150 nm STEM allows the investigation of thicker slices at least up to a thickness of 300 nm, as tested in these studies. These dimensions enabled

visualizing a larger volume of the endosomal structures and significantly enhanced the information that could be obtained on membrane curvature, particle localization etc.. These possibilities increase the significance of TEM tomography investigations and might provide improved insights into intracellular processes. STEM tomography has gained increasing interest with the availability of improved instrumentation during the last 10 years, however, biological studies employing this technique are still not routinely performed. In general, it can be stated here that the instrumentational progress enables these days extraordinary new possibilities, which will further expand in the future. As such TEM and STEM investigations will further gain importance in routine measurements and further capabilities to improve the significance of these investigations will evolve.

4. Advanced methods for TEM characterization

Further possibilities of advanced characterization methods performed by modern TEM were demonstrated by studying various projects with collaborators. These projects addressed specific questions which can be solved by utilizing TEM investigations, but, on the other hand, demand for specialized sample preparations and imaging methods. Results of these projects are summarized in the following paragraphs. In particular the utilization of non-standard TEM methodologies to overcome limitations of conventional TEM measurements are highlighted. The first example describes how to increase the field of view by sample stitching in order to visualize a large sample, e.g., cell spheroids. The second example demonstrates the identification of bacteria and their position in the cellular framework of immunogold labeling strategies to identify specific proteins. The third example shows the localization of calcium phosphate nanoparticles within monocytes. The fourth example demonstrates how to utilize the cryo-TEM techniques to investigate the morphology of polymer nanoparticles.

4.1. Investigations of cell-spheroids by TEM

The following studies have been performed in collaboration with Dr. Tanja Bus to study the structure of spheroids. Spheroids are three-dimensional cell cultures which can model the biological environment of tissues and mimics its microenvironment. As such, they can provide essential advantages compared to 2D cell culture models, where the intimate contact of cells is limited. In spheroids the cellular communication as well as the intricate cell-cell and cell-matrix interactions as well as transport dynamics of nutrients and drugs can be studied under more realistic conditions as it is possible in a conventional 2D cell culture. This renders them interesting systems for *in-vivo* studies to better understand the cellular complexity of tissue, e.g., as a model for tumor tissue.[112]

Typically the size of cell-spheroids can reach dimensions of millimeters involving thousands of individual cells. It has been found that the cell viability in different parts of the spheroid alters and three major regions can be distinguished. The outer shell of the spheroid consists of healthy and highly viable cells. The middle layer consists of senescent cells. The core layer, however, contains necrotic cells.[113]

For tissue model systems it is extremely important to know the internal structure of the spheroids and the state of the structural integrity of the cells within the spheroid. As such, e.g., the thickness of the individual layers represents an important information. For this purpose, it is recommended to inspect all relevant parts and, in the best case, to perform a cross-sectional investigation by TEM to visualize differences in the cell structure across the entire spheroid. This is a non-trivial task considering the typical size of a spheroid of ≥ 1 mm. These dimensions exceed first of all the field view of the TEM, and the second, new preparation strategies have to be implemented. This contains mainly the fact that normal copper TEM grids tend to cover

important parts of the spheroid and careful slicing has to be performed since the dimensions of the spheroid exceed also the typical areas which ae usually chosen for ultramicrotomy.

4.1.1. Instrumentation and experimental details

A spheroid based on human colon cancer (HT-29) cells was seeded. Since a spheroid is larger in dimensions than an usual cell pellet, optimization of the preparation protocol was necessary, e.g., by prolonging the fixation time. The optimized protocol starts with the fixation of the spheroid by glutaraldehyde (2%, 200 µL, Electron Microscopy Sciences) for two hours on ice. A post-fixation and staining was achieved by osmium tetroxide (4%, 200 µL, Electron Microscopy Sciences) for 90 minutes at room temperature. Dehydration takes places by degraded ethanol series for 15 minutes for each step. Embedding medium composed of Embed 812, DDSA, NMA and DMP-30 (Electron Microscopy Sciences) was prepared. The spheroid was embedded into the resin (Embed/ethanol = 1:1 v/v for 1.5 hours, 2:1 v/v for overnight at room temperature and 100% of resin for overnight in the oven at 70 °C).

After hardening of the sample block, it was trimmed first to reach approximately the middle section of the spheroid. Subsequently, the spheroid was carefully sliced into 80 nm thick sections by a diamond knife mounted on a ultramicrotome (PT-XL, PowerTome, RMC, Tuscon) as shown in Figure 4 – 1a. The slice was placed on a TEM grid (Pelco-slot, copper, Ted Pella). The slot-grid was selected in order to eliminate missing areas due to the meshes. However, a carbon support on the grid was required to hold the slice on the grid without folding. A formvar coating followed by carbon sputtering were performed (for details see **Section 3.5.3**). The slices were imaged with a FEI Tecnai G^2 20 TEM microscope at an acceleration voltage of 200 kV.

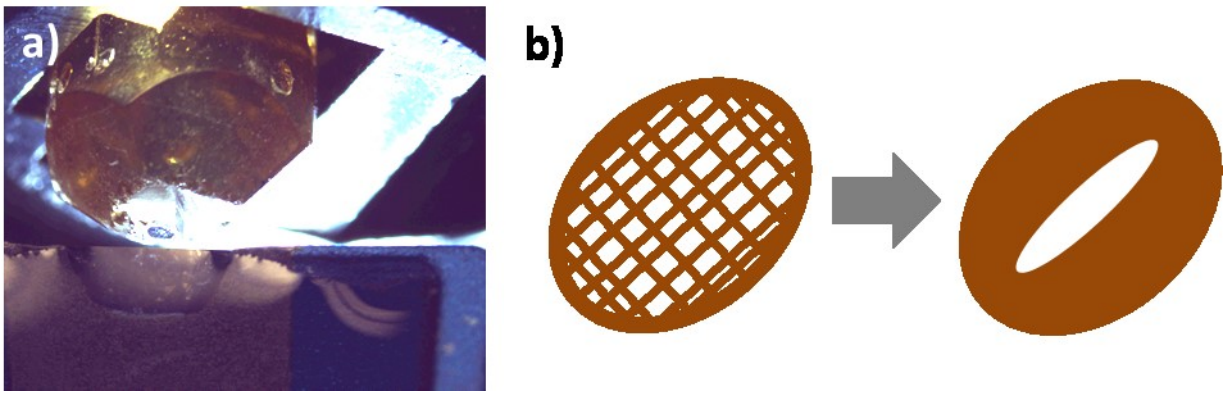

Figure 4 – 1 *a) Embedded spheroid is sliced down to 80 nm thick slices with a diamond knife using the wet cutting technique. b) For this project, a slot-TEM grid is required instead of a conventional mesh-grid.*

4.1.2. Results and discussion

By performing image stitching a whole cross-sectional view across the equatorial region of the entire spheroid could be obtained. Thus, the typical characteristics of the spheroid could be observed by TEM imaging by analyzing the structure of the cells across the spheroid. The cells in

the outer layer were highly viable, stretching their protrusions, formed by the plasma membrane, around and the organelles show their characteristic shapes (Figure 4 – 2a). The cell in the middle layer were quiescent viable, i.e., in a state where they are not actively dividing to create new cells but remain intact such that they can later be reactivate to proliferate. At this stage the cells typically show no protrusions around the cells. Moreover, large vacuoles are frequently observed (Figure 4 – 2b). As expected, the inner layer contained no living cells (Figure 4 – 2c). Imaging the slice from one end to the other end enabled to visualize these changes of the cell structure. The size of the regions for this slice were measured as following: 18 µm for the outer layer, 30 µm for the middle layer and 1 mm for the inner layer. One should keep in mind that these values may differ upon the height of slicing on the spherical form of spheroid.

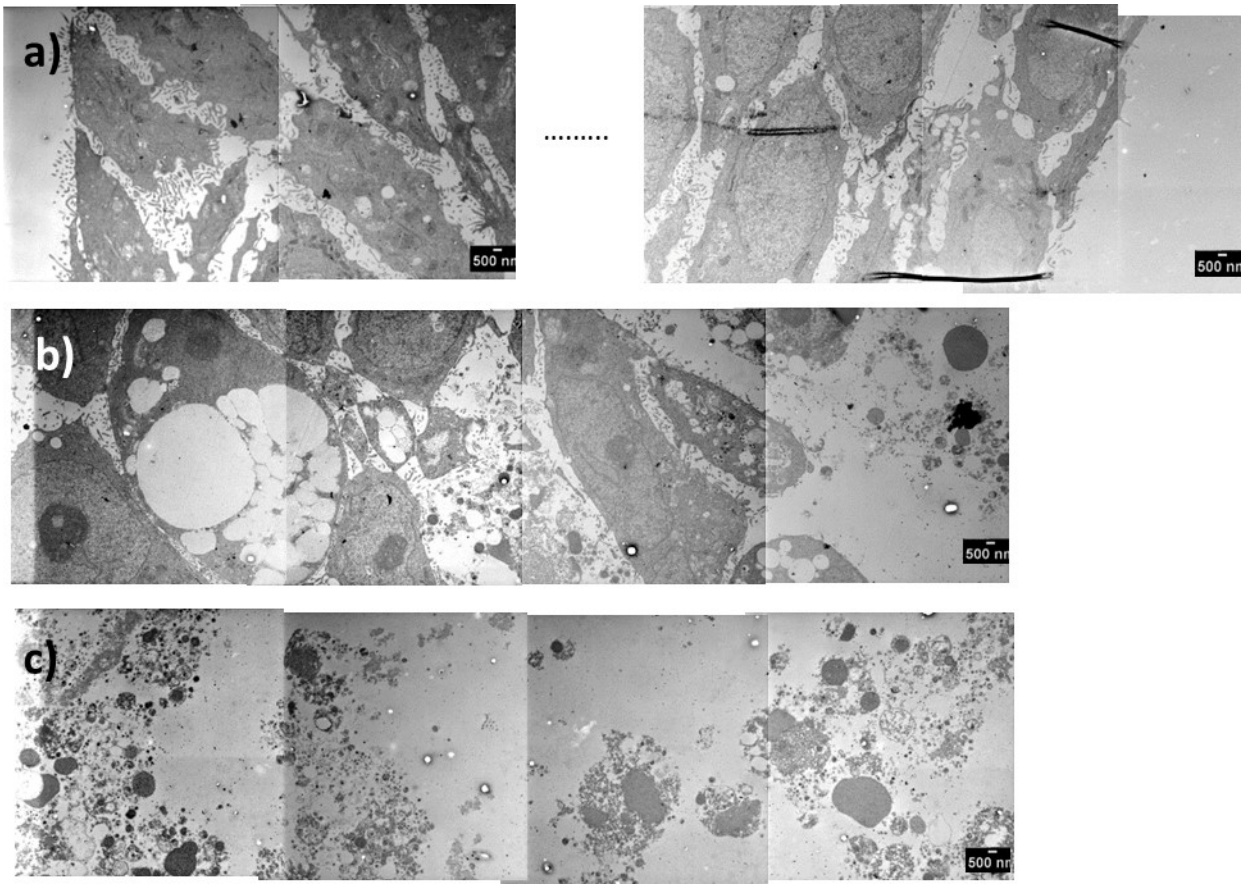

Figure 4 – 2 *The outer layers (a), middle layer (b) and inner layer (c) of a spheroid based on HT-29 cells were imaged by TEM.*

In this study, a spheroid-cell culture, which were quite large in dimensions compared to our routine cell culture, was imaged by utilizing advanced sample preparation methods. An adaptation in the sample preparation protocol, e.g., longer time of fixation and staining, was introduced. In addition, customized mesh types of TEM grids were tested to enlarge the field of view to avoid blocking of the spheroid structure by the bar of the grid and the diameter of the

spheroid could be determined. By stitching the images, the entire cross-section of the spheroid could be analyzed and the thickness of the characteristic cell layers could be determined. As suggested in literature, the variation of status of cells regarding to their position on the spheroid layers was confirmed. The preparation protocol, which was optimized for this study, can be assigned as in-house protocol and the special properties offered by cell-spheroid systems to mimic tumor tissues can be further utilized to be used in the future projects.

4.2. Localization of 15-Lipoxygenase in macrophages stimulated by *S. aureus*

TEM investigations can be also used to investigate the uptake of bacteria in cells. Specialized cells, such as macrophages, represent a special type of white blood cells and part of the immune system. Their task is to engulf and digest foreign substances, including microbes, cancer cells or bacteria and to facilitate tissue repair.[114] In collaboration with the group of Prof. Dr. Oliver Werz from the FSU Jena the uptake of *Staphylococcus aureus* (*S. aureus*) by macrophages was investigated. *S. aureus* is a round shaped bacteria found in both community and hospital settings and cause skin infections.[115] Their digestion follows the pathway of phagocytosis.[116] Phagocytosis is the uptake pathway of relatively large particles (>0.5 µm) into cells. Phagocytosis is a typical process observed, e.g., in macrophages and is based on initiating receptors or engulfment of the large particles into phagoendosomes or phagosomes.[117] First, the substance is encapsulated into a phagosome. By a fusion of phagosome with a lysosome, it becomes a phagolysosome and the degradation of the uptaken materials starts.[118]

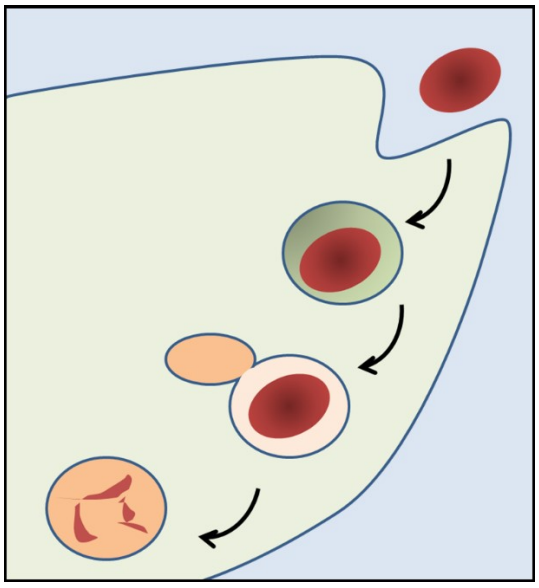

Figure 4 – 3 *Basic illustration of phagocytosis.*

Macrophages increase inflammation and stimulate the immune system or take a role in inflammatory and anti-inflammatory processes. To establish these features, there are two types of macrophages as M1 and M2.[119] M1 macrophages are classically activated by IFN-γ or

Lipopolysaccharide (LPS) and protect the system against bacteria and viruses. Additionally, they are responsible for inducing inflammation. M2 are alternatively activated macrophages by IL-4, IL-10 or IL-13, immune complexes, LPS and induce proliferation and tissue repair and decrease inflammational responses.[120] The localization of *Staphylococcus aureus* in macrophages and their association to phagoendosomes / phagolysosomes can be investigated by TEM studies.

4.2.1. Instrumentation and experimental details

M1 and M2 macrophages and *S. aureus* were prepared with a ratio of 10 (macrophages:bacteria = 1:10) for 180 min at 37 °C and were fixed with glutaraldehyde. A cell pellet was removed by centrifugation at 300 g for 4 minutes and osmium tetroxide (4%, 200 µL, Electron Microscopy Sciences) was applied for one hour at room temperature. A graded ethanol series from 20 to 100% was applied for 10 minutes for each step. Prepared embedding medium (Embed 812, DDSA, NMA and DMP-30, Electron Microscopy Sciences) at different ratios (Embed/ethanol = 1:1 v/v for 1.5 hours, 2:1 v/v for overnight at room temperature) was infiltrated into the cell pellet. The 100% of embedding medium was penetrated into cells and polymerized in the oven at 70 °C overnight.

When the resin was hard enough, it was sliced into 80 nm thick slices by a diamond knife mounted on an ultramicrotome (PT-XL, PowerTome, RMC, Tuscon). The slices were collected by a loop and placed on carbon coated copper TEM grids (400 mesh, Quantifoil, Jena). They were later imaged by TEM (FEI Tecnai G^2 20 at 200 kV).

4.2.2. Results and discussion

TEM investigations showed an obvious uptake of *S. aureus* by M1 and M2 macrophages. The bacteria were generally encapsulated separately into phagoendosomes/phagolysosomes but fusions of them were also observed. The high contrast of the bacteria could reveal its round shape and membrane structures. The phagoendosomes/phagolysosomes were also nicely seen in detail. Some of the results are depicted in Figure 4 – 4.

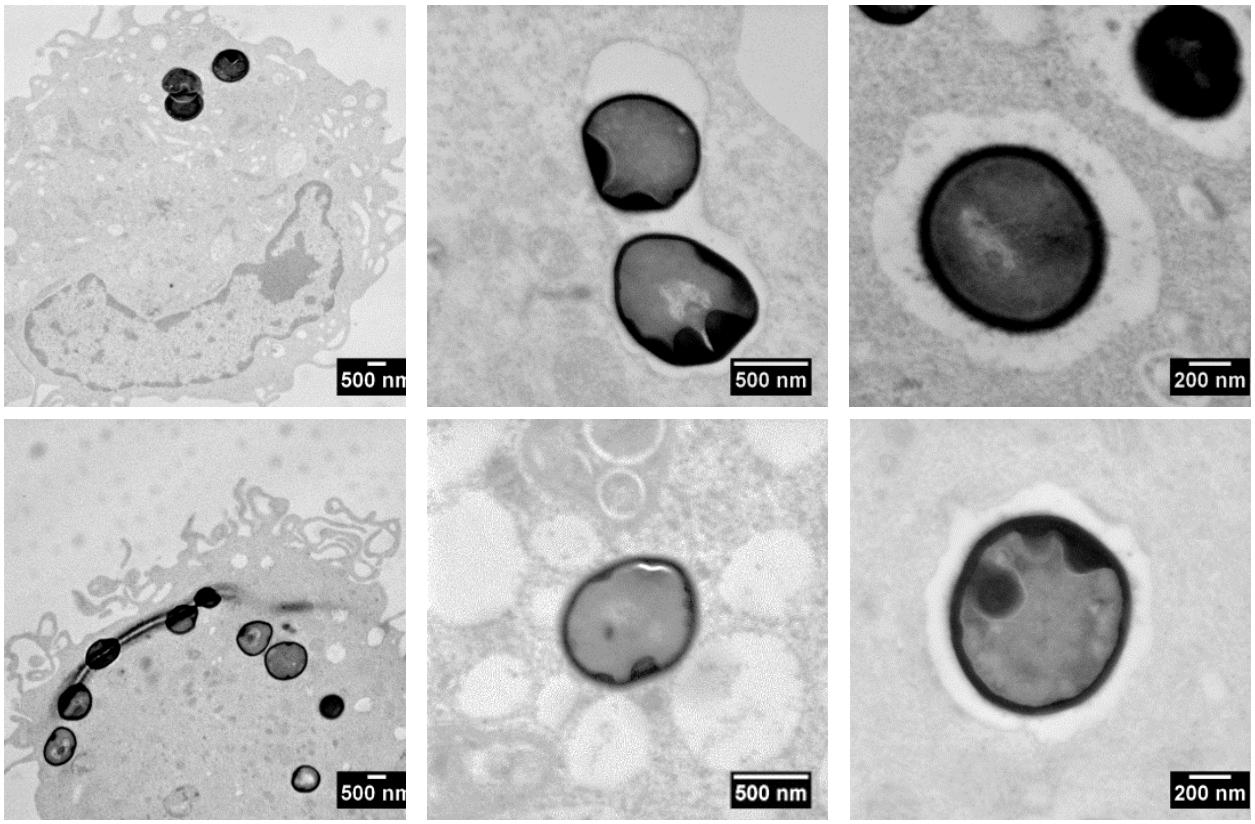

Figure 4 – 4 *M1 macrophages incubated with S. aureus (upper row) and M2 macrophages incubated with S. aureus (lower row) were imaged by STEM.*

This ongoing project will further expand into the identification of certain enzymes, such as lipoxygenase. It is known that 15-lipoxygenase exists only in M2 macrophages.[121] These are usually not observable by standard TEM preparation protocols and pose a challenge due to their rather small size and weak contrast. Common staining approaches for proteins are, moreover, generally not sensitive towards a certain protein. In electron microscopy, this issue is generally addressed by the utilization of immunogold labeling approaches. The principle of immunogold staining is to attach antibodies conjugated to Au nanoparticles to the enzymes of interest.[122] In order to improve the selectivity of the staining process, in a first step, the binding of a primary antibody to the enzyme of interest is performed. Subsequently, a suitable antigen (secondary antibody) coupled to a small colloidal gold nanoparticle is used to bind to the primary antibody. The position of the nicely observable gold nanoparticles indirectly indicates the position of the enzyme within the cellular framework as schematically illustrated in Figure 4 – 5.

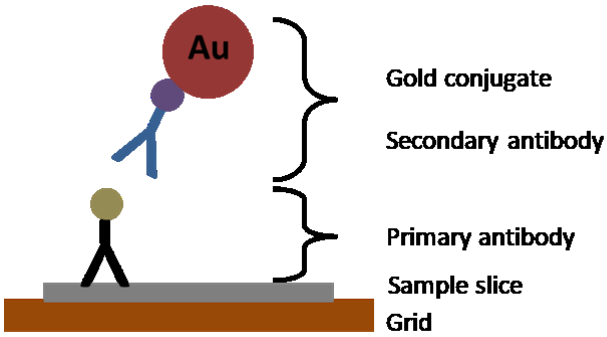

Figure 4 – 5 *Illustration of the method of immunogold labeling.*

This method represents a powerful technique which, however, requires an optimized and dedicated embedding procedure of the samples. The rather impermeable EPON resin, used so far in the previous studies, has to be exchanged by a resin which allows the permeation of the gold nanoparticle markers deep into the resin. Additionally the activity of the proteins needs to be ensured during the sample preparation process. For this purpose, LR white represents a suitable resin which can be additionally further permealized by sodium periodate. Moreover careful evaluation of the selectivity of the binding process of the primary antibody and the secondary antibody gold conjugate has to be performed to obtain meaningful results.[123]

4.3. Mechanisms of activation of the NLRP3-Inflammasomes mediated by extracellular calcium ions

Other projects, which have been performed in collaboration with other groups, target on the identification of nanoobjects with rather weak contrast in a cellular environment. In collaboration with Prof. Dr. Ulf Wagner (University Hospital, Leipzig, Germany) the identification of calcium phosphate particles within monocytes was investigated. These systems consist of relatively light atomic constituents and, thus, create only a weak contrast and are, as a consequence, only poorly recognized in the complex structure of a cell. For this project in particular the utilization of EDX mapping proved to be a powerful tool to improve the possibilities to identify the nanoparticles within the cells.

4.3.1. Instrumentation and experimental details

Nanoparticle characterization was performed first by cryo-TEM measurements to characterize the calcium phosphate (CaP) nanoparticles. For this purpose, 8 µL of nanoparticle solution was dropped on a TEM-grid (Quantifoil R2/2) and blotted by a filter paper. It was plunged into liquid ethane kept at the temperature of liquid nitrogen. The grid was later transported into the holder and imaged by TEM (FEI Tecnai G^2 20 at 200 kV). EDX analysis was performed while imaging the sample at room temperature. 15 µL of the nanoparticle solution was dropped on a TEM grid (400 mesh, carbon supported). After drying in air, it was imaged by TEM. Particle size

evolution investigations were performed by using a Malvern Zetasizer. 1000µL of Roswell Park Memorial Institute (RPMI) 1640 medium and 25 µL of $CaCl_2$ were mixed and particle formation was measured up to 24 hours.

Cell sample preparation was performed according to the following protocol. Cells were received already fixed in glutaraldehyde on ice. It was exchanged with 200 µL of OsO_4 for one hour at room temperature. Dehydration was applied with an ethanol series from 20% to 100% for 10 minutes at each step. Prepared embedding medium (EMBED 812, DDSA, NMA and DMP-30, Electron Microscopy Sciences) at different ratios (Embed/ethanol = 1:1 v/v for 1 hours, 2:1 v/v for overnight at room temperature) was infiltrated into the monocytes. The 100% of embedding medium was penetrated into cells and polymerized in the oven at 70 °C overnight. The sample block was later sliced into 80 nm thick slices and placed on TEM grids (400 mesh, Quantifoil, Jena).

4.3.2. Results and discussion

The calcium phosphate nanoparticles composed of RPMI, 10% FBS and 2.5 $CaCl_2$ form spontaneously by mixing. RPMI is a cell culture medium, which consists of glucose, pH indicator, salts, amino acids and vitamins. Fetal bovine serum (FBS) serves as serum-supplement in cell cultures. DLS measurements showed the size development over time and it was found that the particle size reached an equilibrium state after a reaction time of 7 to 8 hours. The final size ofthe particles was around 85 nm. These dimensions could be confirmed by means of cryo-TEM investigations which allow the visualization of the particles in a solution-like state. The structure of the CaP nanoparticles shows a granular-like morphology. Furthermore, a clear identification of the particles was possible by means of EDX measurements.

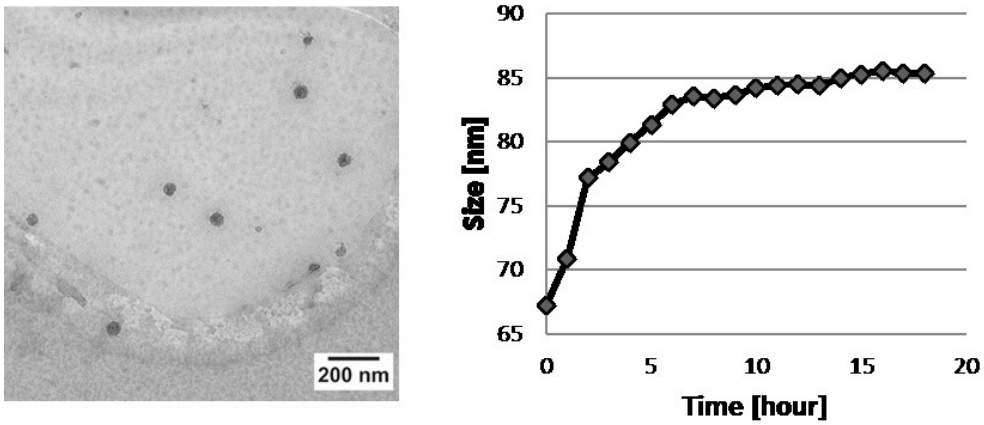

Figure 4 – 6 *Formed nanoparticles were imaged by Cryo-TEM (left) and particle size evolution was determined (right).*

Elemental analysis could be applied on TEM measurements in the dry state. Therefore, 15 µL of sample solution was dropped on a TEM-grid and was measured by TEM after dyring in air. The TEM investigation revealed again spherical shaped nanoparticles. The EDX mapping and spectrum could prove the presence of calcium and phosphate next to elements which were typically present in the incubation medium. The focused electron beam was scanned across the sample to obtain a STEM image. The X-rays emitted within this process are recorded to obtain a spectrum of the respective spot or alternatively the beam is continously scanned and the presence of certain elements was overlayed with the image. Arbitary colors can be assigned to the individual elements. In the example the Ca and P signals are plotted across the image area. They resembled exactly the shape of the particles, hence, the results can contribute to the unambigous identification of the CaP nanoparticles.

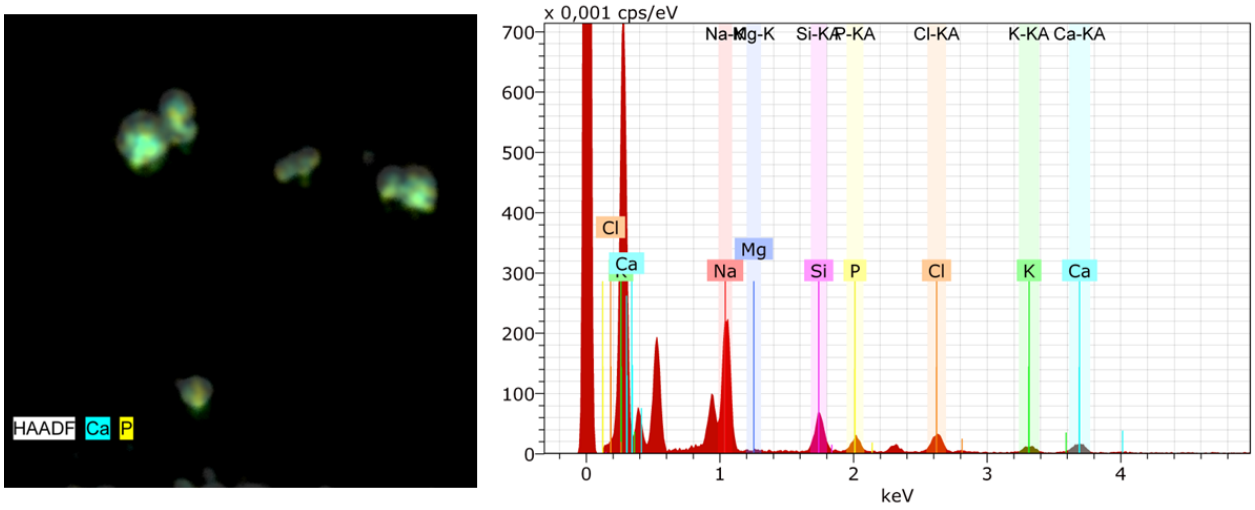

Figure 4 – 7 *EDX-spectrum presents peaks at phosphorus and calcium.*

This techique can also contribute to the determination of the nanoparticles in the more complex environment of a cell. Figure 58 shows the results of an uptake study where the formed CaP particles could be identified inside the cellular environment. The STEM image reveals the presence of two spherical species in the cell. EDX mapping clearly shows that only the moderately dark spherical objects consist of CaP and can be discriminated clearly from the other structures. The overlay image highlights the structures containing Ca. In this case the phosphate signal cannot be used for the identification of the CaP particles, since phosphor is also an abundent element being present in the cell (e.g. in form of phosolipids of mebranes and so on). Special care has also been taken for the choice of the signals which contributes to the mapping. Generally, different elements provide several peaks which orignate from electrons which have been removed from different electron shells. It has be ensured that no peaks belonging to different atoms are located in too close viscinty of the spectrum. Overlap obscures the results and prevents the unambigous identification of the individal objects. It has to be mentioned here

that the count rates for the EDX measurements are rather low. Thus, image acquisition times for a mapping typically require analysis times of >30 minutes at miniumum.

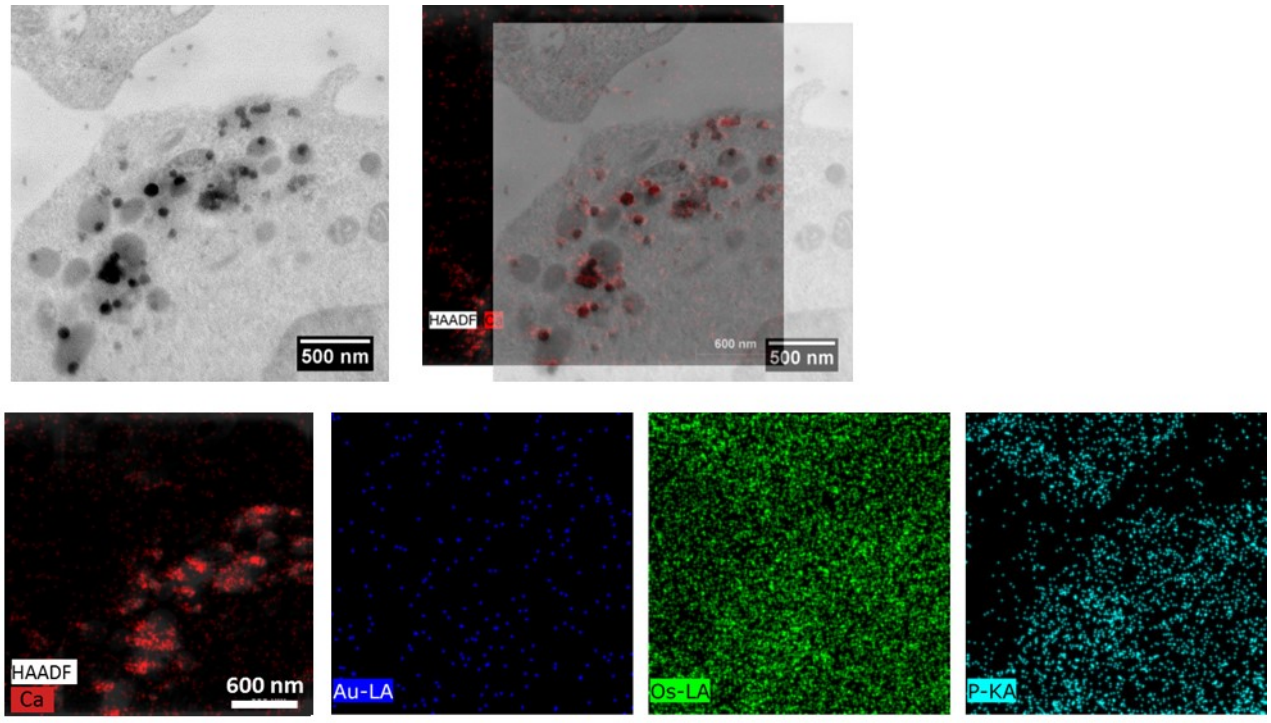

Figure 4 – 8 *TEM image of calcium particles within the cells and overlap image of TEM and EDX mapping (upper row). İndividual mapping for elemental analysis of calcium, gold, osmium and phosphorus (lower row).*

These examples demonstrate the additional possibilities emerging from the utilization of advanced TEM techniques.

As mentioned before, in particular the characterization of nanometric objects in their native state plays an increasingly important role in modern research. It becomes evident that preservation of the natural state of nanoobjects might be even more critical when they consist of soft materials, i.e., polymers. These systems suffer from a low beam stability and, in case of self-aggregated structures in acqueous environments the presence of water is essential to maintain their original shape. For this purpose cryo-TEM preparation techniques are the method of choice. In the following sections morphological studies on self-aggregated polymers are summarized. They have been investigated in collaboration projects with the aim to determine their structure. The possibility to design the shape of nanoparticle aggregates is addressed by the use of well-designed copolymer systems. The fundamentals of designing special nanoparticle shapes as well as possibilities to introduce functional polymer units, which can induce changes of the nanoparticle morphology based on external triggers (like the pH value

or the temperature of the solution) are summarized by presenting selected examples. All nanoparticle systems had to be investigated by cryo-TEM (see for example **Section 2.3.2**).

4.4. Investigations of polymer morphologies: Cryo-TEM

(Parts of this section are published in T. C. Majdanski, D. Pretzel, J. A. Czaplewska, J. Vitz, P. Sungur, S. Höppener, S. Schubert, F. H. Schacher, U. S. Schubert, M. Gottschaldt, *Macromol. Biosci.* **2018**, *18*, 1700396; T. Yildirim, A. Traeger, P. Sungur, S. Hoeppener, C. Kellner, I. Yildirim, D. Pretzel, S. Schubert, U. S. Schubert, *Biomacromolecules* **2017**, *18*, 3280; M. Sahn, T. Yildirim, M. Dirauf, C. Weber, P. Sungur, S. Hoeppener, U. S. Schubert, *Macromolecules* **2016**, *49*, 7257.)

4.4.1. General considerations for the design of polymers to form self-aggregated nanostructures for drug delivery applications

In contrast to the colloidal gold nanoparticles serving as a model system for the projects summarized in **Chapter 3**, polymer nanoparticles can be also used as drug delivery systems.[124] The utilization of self-aggregated nanoparticles consisting of polymers bears a number of advantages. Due to their flexible design different polymers can be combined, e.g., to modify their uptake characteristics (e.g., by introducing charged segments of polymers)[125], their biodegradability (e.g. by utilizing poly-L-lactide moieties in the polymer backbone)[126], or by simply controlling the shape of the formed self-aggregated particles (e.g., spherical particles *vs*. worm-like or fiber structures).[127]

Modern polymer synthesis enables the well-controlled generation of desired polymers and copolymer systems by utilizing controlled polymerization methods, i.e., Atom Transfer Radical Polymerization (ATRP), Reversible Addition/Fragmentation Chain Transfer Polymerization (RAFT) and Nitroxide-mediated Polymerization (NMP).[128] With these synthesis approaches, a large number of different combinations of polymers with designed architectures is accessible. These include block, statistical and gradient polymers, graft polymers with a comb-like structure or highly branched polymers.[129] For self-organization and self-aggregation processes in particular the class of amphiphilic block copolymers is of considerable interest. These copolymers consist of two (or more) well-defined polymer blocks of defined length, which additionally show complementary properties in terms of their solubility. While one of the blocks (or part of the polymer chain) renders hydrophilic properties the other block(s) show a more hydrophobic character.[130] The architecture of such block copolymers strongly influences the shape of the formed structures in aqueous solutions once the critical concentration for self-organization processes is exceeding the critical micelle concentration (CMC).[131] At these conditions, one part of the block copolymer is insoluble in the solvent and, as a consequence, tries to separate from the solvent. Due to the fact that both parts of the block copolymer are covalently linked a phase separation involving a larger number of molecules is formed which is spatially confined and results in the formation of self-aggregated structures. These resemble an aggregation of the

insoluble blocks in the core of the structure, which is surrounded by a corona formed by the soluble parts of the molecules. The size of the obtained structures is typically limited to a few times the radius of gyration of the polymer building blocks, which can result in structure sizes ranging from 10 to 100 nm or even more.[132]

The resulting shape of the formed structures can be predicted by utilizing a simple geometric model which was introduced by J. Israelachvili in 1976.[133]

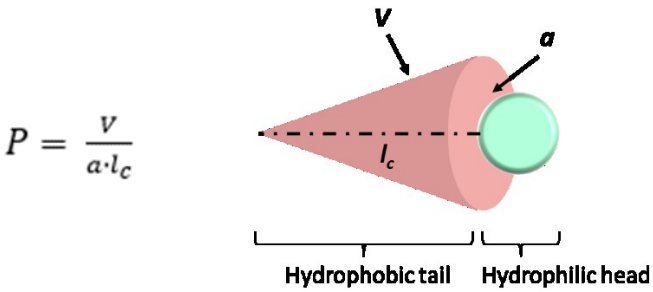

Figure 4 – 9 *The packing parameter (P) is calculated by dividing the volume (V) of the surfactant hydrophobic part by the length (l_c) of the hydrophobic group and the area (a) of the hydrophobic area.*

In this model, a packing parameter P is obtained by dividing the volume (V) of the surfactant hydrophobic part by the length (l_c) of the hydrophobic group and the area occupied per molecule at the aggregate interface (a) at equilibrium (Figure 4 – 9). This model was initially developed for simple surfactant molecules, which essentially means that the size of the hydrophilic head groups dominates the aggregate formation at equilibrium conditions (V/l_c = const. = 0.21 nm² for a single tail) and the tail does not show a significant influence on the shape of the aggregate. Nevertheless, it can be applied to copolymers as well to obtain a first prediction of the aggregate's shape. A simplified diagram summarizing the obtainable shapes by varying the packing parameter according to the Israelachvilli model is depicted in Figure 4 – 10.

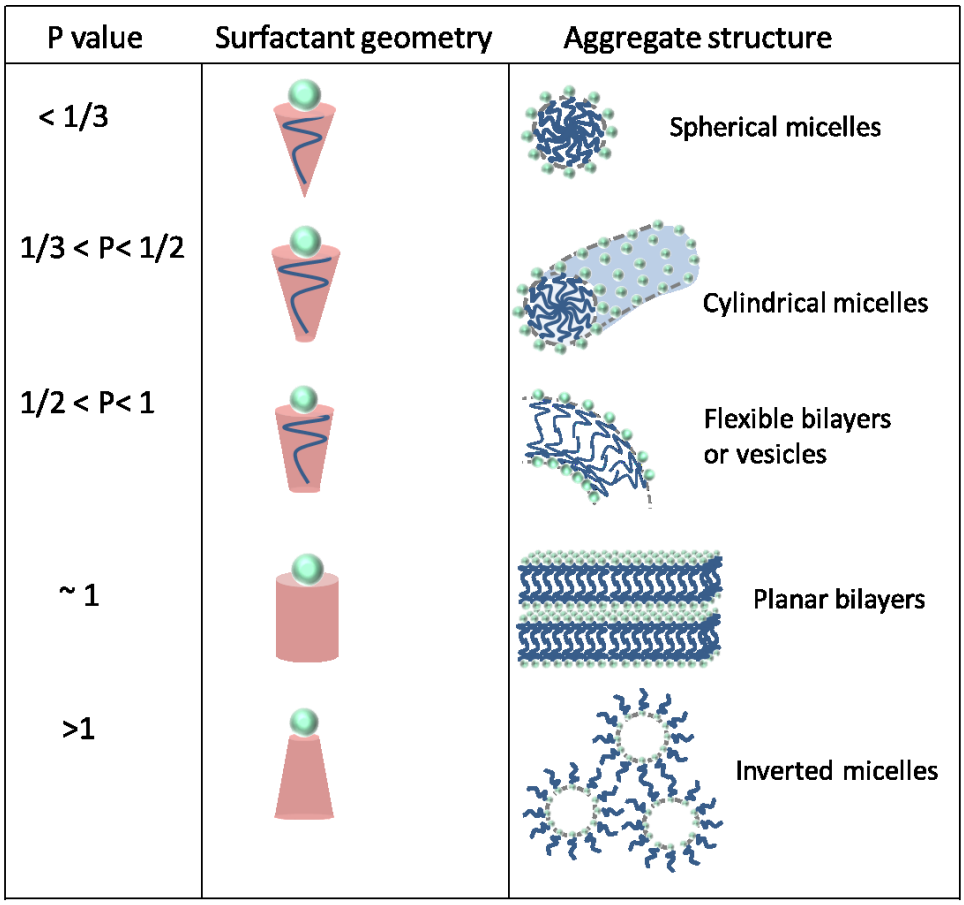

Figure 4 – 10 *The packing parameter value can help to predict the resulting shape of self-aggregated copolymers.*

The range of accessible structures includes the formation of spherical micelles at typical packing parameters P < 0.3. By increasing the packing parameter to 0.3 < P < 0.5 it is more likely to obtain worm-like micellar structures, whereas P values > 0.5 result in the formation of vesicles with increasing size due to the curvature of the membranes. A special situation is reached if the packing parameter features P = 1. In this case bilayers are formed by the system. At packing parameters P > 1 inverted micelles are formed. As mentioned before, this model simplifies the aggregation behavior and does not take into account aspects of the polymer composition, interaction of the chains, the influence of non-ionic or ionic surfactants (e.g. electrostatic interactions due to the charge of (parts) of the molecules, the sizes of the hydration shell, the type of solvents and influences of temperature or pH value.[134] As such, the predictive model can be used only as a first estimate, how to tune the morphology of copolymer aggregates.

Discher and Eisenberg defined a unifying rule accounting for block copolymer micellization.[135] This model can be applied for coil-coil block copolymers readily soluble in a selective solvent and utilize a function of the mass fraction of the hydrophilic block to the total mass of the

copolymer ($f_{hydrophilic}$). The value obtained for $f_{hydrophilic}$ can be assigned to typically observed morphologies as listed below:

$f_{hydrophilic} > 45\%$	Spherical micelles
$f_{hydrophilic} < 50\%$	Rod-like micelles
$f_{hydrophilic} \sim 35\%$	Vesicles
$f_{hydrophilic} < 25\%$	Inverted microstructures, i.e., large compound micelles

Even though this model does not take into account the chemical composition and the molar mass of the copolymer chains as well, experimental results have proven the success of this model for copolymers for molar masses ranging from 2.700 to 20.000 g/mol.[135]

Due to the fact that all introduced models are remaining on a predictive level and do not take into account important properties of the copolymer systems, the systematic investigation of polymer aggregate structures are indispensable. For this purpose, characterization tools have to be employed which can investigate the polymer structures in their native/solution-like state and provide a resolution which is high enough to obtain information on their morphology. The number of methods which can provide these information is limited. Dynamic and static light scattering (DLS/SLS) provide an ensemble average over a large number of individual objects and can poorly resolve structural inhomogeneities.[136] Small angle neutron scattering (SANS) and Analytical ultracentrifugation (AUC) provide only structural parameters which can be indirectly assigned to the morphology of the aggregates.[137] In this thesis, cryo-TEM investigations have been performed to determine the influence of the polymer composition and the response of micellar systems towards external triggers, like changes of the temperature or the pH values of the solutions. For these investigations different block copolymer systems have been synthesized in collaboration projects. First, the influence of the polymer composition and, in particular, of the length of the polymers, and their respective block ratios was studied. For this purpose a library of block copolymers was synthesized with systematically changing compositions. In the second part of this chapter, the morphological studies conducted by cryo-TEM were extended to the investigation of changes of the aggregate state with respect to external triggers. For this purpose, temperature responsive as well as pH responsive blocks have been incorporated into the block copolymer structure.

4.4.2. Influence of the polymer composition and length of polymers on the morphology

As discussed before, weight fraction changes in copolymers result in changes of their morphologies. Here, a copolymer system has been investigated to follow the morphological development of the structures in relation to different block length ratios.

The system introduced here targets the formation of worm-like micelles with the aim to improve the enrichment of administered nanocarriers in tumor tissue. A block copolymer

consisting of a poly(ethylene glycol)-*b*-poly(ethyl hexyl glycidyl ether) was synthesized by Majdanski *et al.*.[138] The polymer contained a poly(ethylene glycol) (PEG) block, which forms the main hydrophilic part of the macromolecule. These blocks are well-known to be of low toxicity, are soluble both in aqueous as well as in organic solvents and, most importantly, show stealth behavior, which renders them "invisible" to the immune system. The last feature greatly improves the blood circulation time of the nanocarriers and an enrichment of the nanocarriers in tumor tissue is possible by utilizing the enhanced permeability and retention (EPR) effect (EPR).[139] The enrichment of the nanocarriers in tumor tissue can tremendously be improved by the utilization of additional suitable targeting groups. It is well-known that tumor cells show an increased uptake of monosaccharides due to their fast proliferation and, hence, their increased consumption of nutrients. The uptake proceeds via the GLUT transporters (see also **Chapter 3.3**). GLUT5 has been identified as a fructose specific transporter which facilitates binding and uptake of fructose.[140] Moreover, the overexpression of GLUT5 transporters in breast cancer cells and tissue [141] and acute myeloid leukemia cells [142] was shown.

The polymer systems were synthesized by utilizing a protected fructose initiator, which facilitates the polymer chain with a D-fructose group at its end. Polymerization was performed by living anionic ring-opening polymerization (AROP) and the PEG group is connected additionally to a hydrophobic poly(ethyl hexyl glycidyl ether) (PEHG) chain. These hydrophobic segments represent a polyether backbone, and their very hydrophobic side chain provides high chemical stability, for example, toward strong acids, and nondegradability by enzymes or hydrolytic cleavage. The protecting groups of the sugar moiety were removed in the course of the synthesis procedure. The polymers were subsequently formulated into nanoparticles by means of an emulsion technique, utilizing polyvinyl alcohol as surfactant. Cryo-TEM characterization of D-fructose modified poly(ethylene glycol) (Fru-PEG) and fructose modified poly(ethylene glycol)-*block*-poly(ethyl hexyl glycidyl ether) (Fru-PEG-*b*-PEHG) at different weight fractions revealed the changes in their morphologies.

A low amount of hydrophilic monomer units incorporated into the block copolymer (Fru-PEG_{43}-*b*-$PEHG_{21}$) exhibited vesicular structures with diameters of 20 to 30 nm and also the formation of aggregates with diameters of 100 to 300 nm. A significant change in the morphology was observed with an increase of the PEG content (Fru-PEG_{88}-*b*-$PEHG_{21}$). The block copolymers self-assemble into filomicelles or worm-like micelles with a length of several µm and vesicles with a diameter of 50 nm were observed. When the content of PEG was strongly increased, the same behavior of forming filomicelles and few vesicles were observed and also small spherical micelles could be observed. Among the other systems, this system exhibited the largest variety of structures being formed. For comparison, also a methoxy functionalized analogue was investigated by cryo-TEM. In this case, the fructose functionalization was preplaced by a simple methyl group, thus, the formed structures cannot be used to establish a selective targeting of

the GLUT5 receptors. The system of $mPEG_{104}$-*b*-$PEHG_{13}$ formed also filomicelles but showed a significantly reduced length of the formed micelles. Due to the faint contrast around the core of the filomicelles, the distance between the neighboring micelles could be imaged and a PEG corona was measured within a distance of 18 nm. By utilizing cryo-TEM, the influence of the block copolymer composition on the resulting nanostructures were visualized. It was observed that the effect of the fructose on the resulting nanostructures was actually negligible in the presence of PEG-*b*-PEHG chains. The synthesized system resulted in two special structures as it provides bicontinuous spherical aggregates and filomicelles. The bicontinuous spherical aggregates can be further used as a potential drug delivery system. Encapsulation of a drug material is possible due to the presence of a hydrophobic bilayer and also the release of the material is gradually possible over time.[143] The other property offered by filomicelles is the increased loading capacity to be used as long-term drug release carrier.[144]

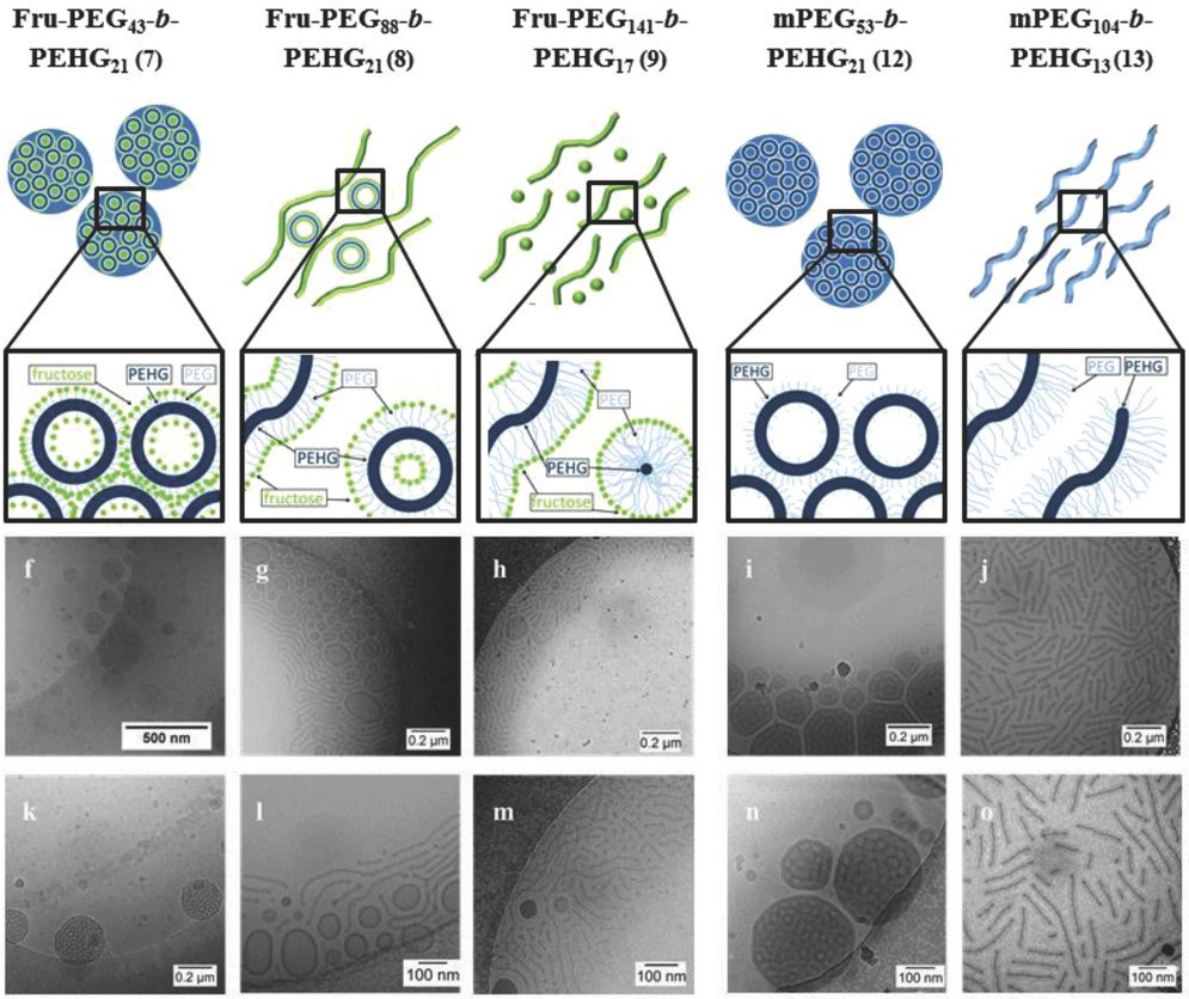

Figure 4 – 11 *Cryo-Tem imaging of the synthesized polymer morphologies in various weight fractions.* ***(Reprinted with permission from Macromolecular Bioscience.[138])***

Furthermore, the encapsulation of a fluorescent dye Nile red was established as a hydrophobic compound in uptake studies. In this case the Nile red served as a model system for other hydrophobic drugs that could be incorporated into the structure. The encapsulation of the fluorescent dye could not be visualized by means of cryo-TEM studies but it facilitated the investigation of such systems by means of fluorescence microscopy. In this case the structure of the polymer aggregates remained unknown but the distribution of the micelles within the cellular environment could be investigated. This represents another critical point which highlights a severe disadvantage of TEM investigations. It will be very difficult to localize polymer nanoparticle drug delivery systems in the cellular framework due to their faint contrast. This further motivates the utilization of the colloidal gold model systems utilized in **Chapter 3**. The drawback of both microscopy techniques, i.e., of fluorescence as well as of TEM, can be addressed by establishing correlative light and electron microscopy (CLEM) methods.[145] This is however a relatively young field and the development of the technique is still in its infancy.

4.4.3. Responsive self-aggregated polymer systems

Responsive polymer systems are of increasing interest due to their possibility to trigger morphological changes of self-assembled nanostructures, which traditional systems do not provide.[146] These changes occur due to the change in the solubility of at least one of the copolymer blocks. There are a variety of polymers which can undergo this solubility changes, e.g., triggered by variation of the temperature or changes of the pH value of the solution.

Morphological changes occurring to a polymer drug carrier system offer appealing possibilities to introduce targeting, precise cell-specificity, low toxicity and ultrasensitivity. The change on the pH value of the solution may cause swelling or shrinking of the polymer system and starts the release of the encapsulated material. This is also a very important property actually in order to utilize the endosomal escape, as described in **Section 3.5**.

Changes on the polymer morphology due to the change of the pH value of the solvent can be visualized also by using cryo-TEM sample preparation techniques and imaging. Yildirim *et al.* synthesized a series of dual pH- and ultrasound responsive statistical copolymers via the reversible addition-fragmentation chain transfer (RAFT) polymerization of 3,4-dihydro-2H-pyran (DHP) protected HEMA 2-((tetrahydro-2H-pyran-2-yl)oxy)ethyl methacrylate (THP-HEMA) and 2-(dimethylamino)ethyl methacrylate (DMAEMA) and characterized p(THP-HEMA)-*b*-p-(DMAEMA) not only at different length compositions but also at different pH values since this polymer system is supposed to show an increase of the volume of the hydrophilic block at acidic pH values and can be further used in drug delivery studies.[147] THP-HEMA (labeled as A) served as a hydrophobic moiety of the polymers since its cyclic acetal functionality can be cleaved under acidic conditions and it was expected that it will interact with the hydrophilic HEMA and result in the disassembly of the corresponding nanoparticles due to the imbalance of the

hydrophilic/lipophilic ratio. On the other hand, DMAEMA (labeled as B) served as a hydrophilic moiety because of its pKa value of ~7.4.

The amphiphilic copolymers of $A_{35}B_{21}$, $A_{35}B_{30}$ and $A_{35}B_{50}$ were prepared by nanoprecipitation and cryo-TEM measurements revealed the self-assembly behavior. Polydisperse vesicles with a size of 20 to 90 nm in diameter were observed. Since their membranes were clearly visible, the thickness was measured to be around 8 ± 2 nm. Larger spherical aggregates with a size of 200 nm were also observed. $A_{35}B_{21}$ was selected to investigate the vesicle formation and drug delivery behavior at different pH values. The $A_{35}B_{21}$ suspension was stored at various pH values for 3 hours. The size of the vesicles was observed to increase with increasing the pH from 7.4 to 8.0 due to the partial deprotonation of the DMAEMA groups. On the other hand, the decrease of the pH resulted in a decrease of the vesicle size. Cryo-TEM measurements of the $A_{35}B_{21}$ suspension at pH 7.4 and 5.0 were performed. Vesicular aggregates with clear membranes were observed for the $A_{35}B_{21}$ suspension at pH 7.4. When the pH was decreased to 5.0, only homogenous vesicles were detected.

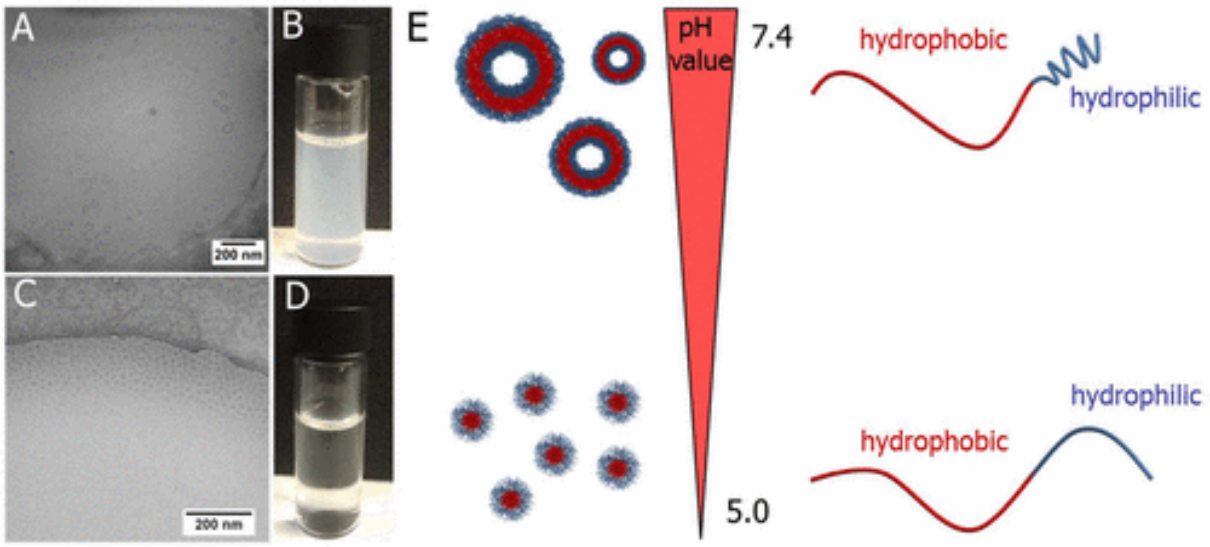

Figure 4 – 12 *Cryo-TEM results of the synthesized polymer morphologies at different pH values. (Reprinted with permission from Biomacromolecules.*[147]*)*

To sum up, the morphological changes of the synthesized pH-responsive polymersome system of p(THP-HEMA)-*b*-p(DMAEMA) was tested under different ratio of the hydrophobic and hydrophilic part and also at different pH values by utilizing cryo-TEM. At the conditions of longer hydrophilic block length, micellar structures were obtained. A morphology transition from vesicles to micelles was also observed when the pH value was changed from 7.4 to 5.0. That was highlighted as a special feature to perform the controlled delivery of hydrophilic drugs. The release occurs because the hydrophilic cargo release is triggered by the loss of aqueous cavities within the vesicles. Additionally, this system was tested to encapsulate a hydrophobic model

drug (Nile Red) into the membrane and also a hydrophilic anticancer drug (DOX·HCl) in the aqueous cavities. The higher release rate under a pH decrease and also increased uptake by cells were verified by other methods. Here, this system proofs that pH-responsive polymersome systems offer great possibilities to load both hydrophobic and hydrophilic molecules and to release them at the endosomal stage.

Cryo-TEM sample preparation allows also to determine the morphological changes of a sample suspensions regarding their LCST behavior. A series of well-defined P*N*iPAm-*b*-PEtOx-*b*-P*N*iPAm triblock copolymers was synthesized by Sahn *et al*. and the morphology transitions at increased temperature were investigated by utilizing cryo-TEM.[148] P*N*iPAm is a well-known polymer exhibiting transitions from hydrophilic to hydrophobic properties at 32 °C. On the other hand, poly(2-ethyl-2-oxazoline) (PEtOx) is a hydrophilic polymer with special properties of biocompatibility and stealth behavior. These two different polymers can be combined into an ABA triblock copolymer and can be used in bioapplications. The synthesis of the triblock copolymers was performed by applying the living cationic ring-opening polymerization (CROP) of EtOx and the subsequent reversible addition-fragmentation chain transfer (RAFT) polymerization of *N*iPAm.

The LCST of the synthesized triblock copolymer was found to be at 28 ˚C. To image the sample aggregation state below and above the LCST, the sample suspension was heated to 50 ˚C and also cooled to 15 ˚C by using the temperature control function of the automatic plunge freezing instrument. For the polymer system at 15 ˚C, only very few loose aggregates were detected. Concentrated phase droplets in a matrix of the phase with lower polymer concentration were observed when the system was heated to 50 ˚C. Round structures with no sharp borders and weak contrast indicated the formation of globuli. The size of these structures was measured as 100 to 200 nm.

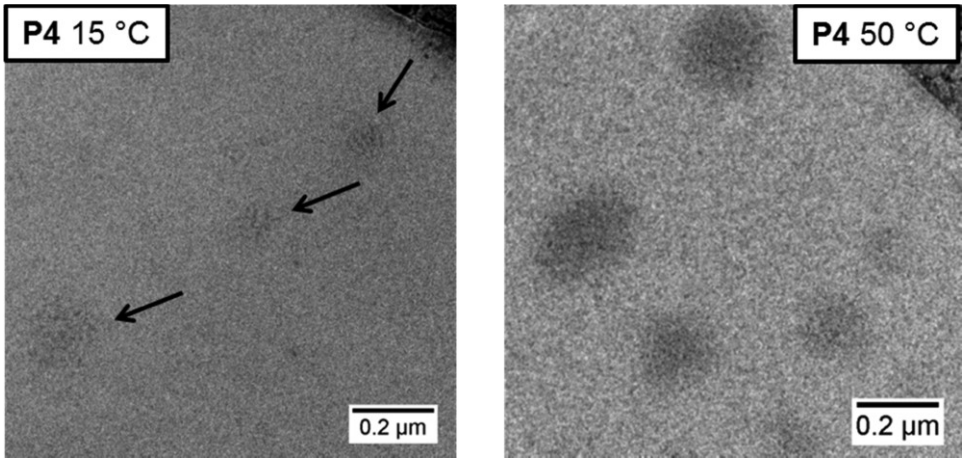

Figure 4 – 13 *Cryo-TEM images of synthesized polymer morphologies at different temperatures. (Reproduced with permission from Macromolecules.[148])*

To sum up, the imaging mode of cryo-TEM which can be regarded as an advanced imaging possibility of TEM represents a very helpful method to visualize soft materials which have low intrinsic contrast. By utilizing cryo-TEM measurements, the morphology of the polymeric structures such as vesicles, micelles and worms can be visualized with high resolution. Even a polymer corona around the polymeric structures can be clearly distinguished and characterized in size. Cryo-TEM is very powerful tool to visualize these structures at their most native-like state. In addition, the effect of external changes such as temperature and pH value on the polymer morphologies can be visualized.

Cryo-TEM was utilized to image the synthesized polymer structures resulting in different morphologies with respect to their weight fraction, pH value and temperature change. It is very obvious that the visualization of polymer morphologies cannot be performed by any other method than cryo-TEM. Meanwhile, the measurement methods by TEM are further improving to observe even more details and also more samples. In particular, the possibility to investigate dynamic systems (i.e., temperature responsive nanostructures) is still one of the missing routines where TEM investigations could provide detailed insights. Currently the utilization of so called sandwich cells or *in-situ* approaches are being developed. Sandwich cells can eliminate the image shift occurring by the beam induced specimen charging. With this method, high resolution images in near atomic structure levels can be obtained.[149] Another option is the *in-situ* measurements by utilizing specially designed holders. By utilization of a microfluidic liquid cell, two liquids can be combined and imaged instantaneously. These developments and improvements will be able to address new investigations in future.

5. Summary

In this thesis, three different concepts for targeted drug delivery have been investigated. These approaches aim on the development of strategies to apply targeted drug delivery in therapeutic applications and can provide information on the mode-of-action of the drug delivery system upon cellular internalization. This requires the investigation of the uptake processes themselves, targets the investigation of intracellular compartments and their integrity, as well as the study of membrane-nanoparticle interactions, and the observation of characteristic changes of the cellular structure after the administration of drug delivery nanoparticles. The studied systems are based on colloidal gold nanoparticles which are functionalized with suitable targeting moieties and their mode of action was primary investigated by means of TEM investigations. As such, the utilization of colloidal gold nanoparticles in these *in-vivo* studies is beneficial as it provides a good contrast in TEM imaging for uptake and metabolism studies, as even individual gold particles can be easily identified within the cells. They are, e.g., much more easily recognizable compared to nanoparticles which are based on polymer materials, even though it has to be mentioned that polymer nanoparticles in general provide a greater versatility in terms of tuning the nanoparticles' properties, such as, size and shape, and can introduce responsive functional subunits (e.g. causing changes of the nanoparticle morphology upon changes of temperature and pH value). The latter is an important feature, which will help to establish concepts for the targeted release of drugs.

Based on these considerations first the functionalization of individual colloidal nanoparticles was tested. For these studies first the functionalization of the gold nanoparticles by grafting of a temperature responsive polymer providing an end-functionalization with four different kinds of sugar moieties was established (**Section 3.3**). The uptake of glucose-, fructose-, mannose- and galactose-functionalized nanoparticles into HEK-293 cells was studied and differences in the uptake rate and intracellular localization of the nanoparticles within the cells were found. This system addresses specifically selective sugar glucose transporters located at the plasma membrane of the cells. These receptors naturally occur with different abundances and can mediate the uptake of different sugar moieties. Furthermore, it could be demonstrated that the utilization of different kinds of sugar moieties have a direct influence on the lower critical solution temperature (LCST) of the nanoparticle systems which evidently will also have a crucial influence of the uptake mechanism of the nanoparticles into cells. The different uptake processes could be discriminated in the TEM studies, by analysis of the localization of the nanoparticles in the cell. They were either found in endosomal structures or were found in the cytosol of the cells. Closer investigations of nanoparticles interacting with the plasma membrane enabled moreover to conclude on the aggregation state of the nanoparticles in the incubation medium.

Additionally, a statistical analysis of a large number of TEM images was performed to compare the uptake rate of four different sugar moieties. It was found that the system functionalized with glucose moieties showed the highest uptake rates.

The second study was conducted with the aim to target a specific organelle. For this purpose, a functionalization procedure for the surface of the colloidal gold nanoparticles with pyruvate was established (**Section 3.4**). Pyruvate is known as an important molecule taking part in the citric acid cycle. As a consequence, the pyruvate functionalization was utilized as a strategy to selectively address the mitochondria of cells, where the citric acid cycle takes place. Studies of HEK-293 incubated for different times with the pyruvate functionalized colloidal gold nanoparticles clearly revealed that the uptake of the nanoparticles stimulated mitophagy. At early stages the damage of the mitochondria could be observed in the TEM micrographs. At later stages, the development of characteristic autophagosomes was found and the defective mitochondria were digested into lysosomes. This system clearly demonstrated the mitochondria specific uptake of the pyruvate functionalized nanoparticles and, moreover, their specific mode of action on the system was studied in detail. The observed mechanisms are promising in terms of developing a suitable strategy to eliminate defective mitochondria out of a cell. This is in particular interesting for diseases which are associated to dysfunction of the mitochondria.

While the first two systems are based on the utilization of surface functionalized colloidal gold nanoparticles the third system investigated in this thesis utilized metal-polymer hybrid nanoparticles (**Section 3.5**, Figure 5 – 1). These consist of a polymer matrix consisting of poly(ethylene imine) (PEI), which is a representative of a polycationic polymer. This system is frequently discussed in literature because of its ability to respond to changes of the pH value. Taking into account that the pH value inside an endosome decreases with the maturation of the endosomes during endocytosis, this system is frequently utilized as a favorable system to establish endosomal escape strategies. The most frequently discussed process which can facilitate this endosomal escape is the proton sponge effect, which postulates a swelling of the nanoparticles as well as of the endosomes, which finally results in a rupture of the endosomal membrane. To overcome the problem of a poor electron contrast in TEM imaging, the system was additionally facilitated with gold nanoparticles, which are randomly distributed inside the polymer matrix of the nanoparticle. This ensures a clear identification of the Au-PEI hybrid nanoparticles in the cells by TEM imaging. The Au-PEI hybrid nanoparticles were localized in endosomal structures and an analysis of their sizes revealed an increased diameter of the PEI matrix after their internalization of the endosome. Additionally, in some occasions, a dramatic increase in the size of the nanoparticles was observed, mainly in cases where they are located close to the endosomal membrane. These specific events were investigated in more detail by utilizing (S)TEM tomography. This method enabled the three-dimensional reconstruction of the structures and allows to closer inspecting the membrane-nanoparticle interaction. The

performed experiments established STEM tomography as a promising method, which enabled also the investigation of thicker slices of up to 300 nm. This is certainly advantageous if the membrane-nanoparticle interactions of larger particles are to be investigated and provides additional advantages to visualize the deformation of membranes. This advanced method contributed to the understanding of the morphological changes which are involved in the postulated proton sponge effect.

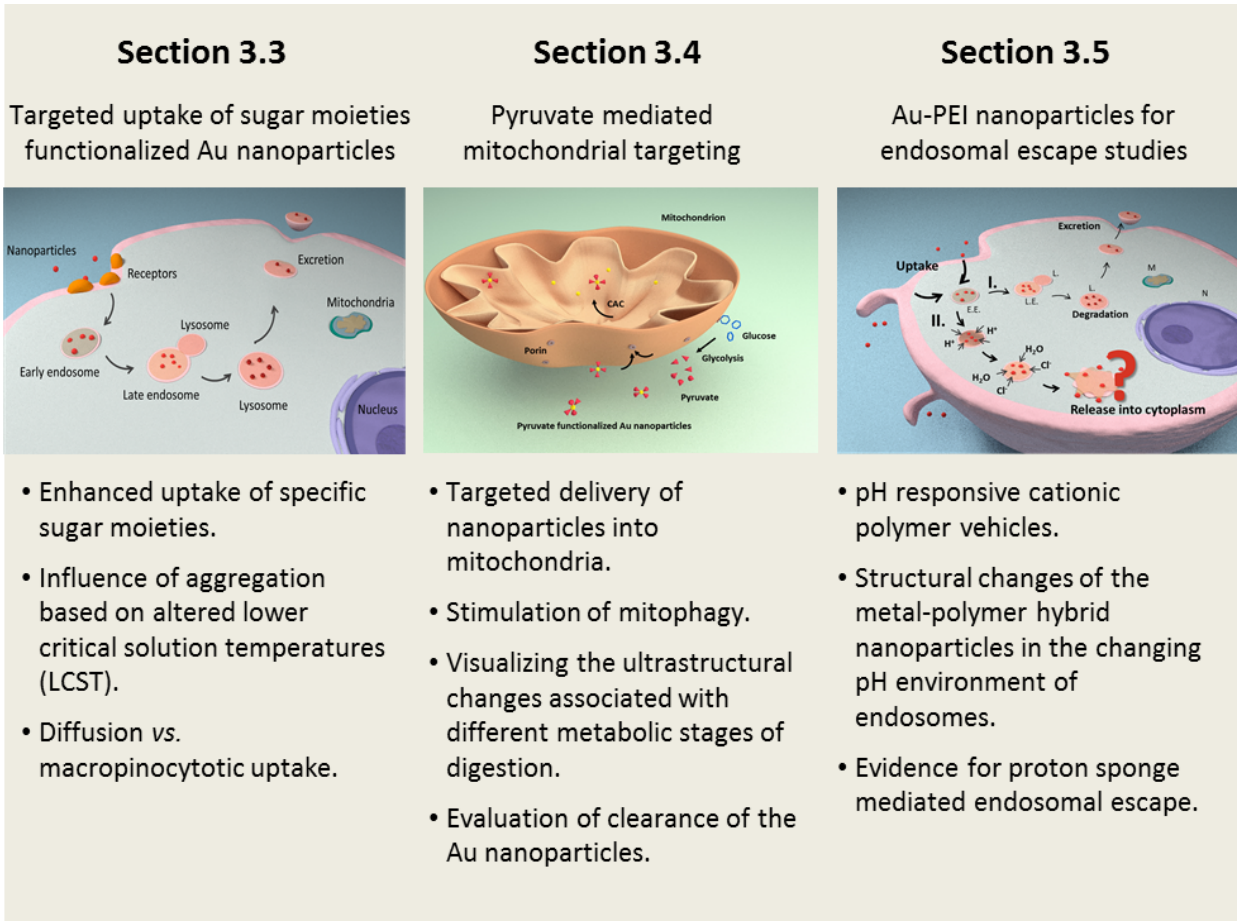

Figure 5 – 1 *The outlook of three main projects studied in this thesis.*

Within this thesis standard as well as advanced TEM imaging methods have been employed and were partially optimized for specific sample requirements. This involves the utilization of advanced measurement techniques as well as adaptations during the preparation of the TEM samples. These studies aimed, e.g., on the investigation of large objects, such as spheroids based on HT-20 cells, which can serve as a model system for tumor tissue. Here image stitching was applied to judge on the cell status in different regions of the spheroid (**Section 4.1**). Another example refers to the visualization of S. aureus incubated into macrophages (**Section 4.2**). Furthermore, EDX analysis was utilized to unambiguously identify CaP particles into monocytes (**Section 4.3**). In this project the CaP nanoparticles were characterized by different

TEM investigations, including cryo-TEM measurements. After their incubation into monocytes, the localization of CaP particles in monocytes was determined by EDX analysis. Cryo-TEM investigations proved to be indispensable also for the characterization of polymer nanoparticles (**Section 4.4**). Such systems represent promising candidates to serve as advanced systems for drug delivery applications. In a number of collaboration projects different block copolymer systems have been investigated in terms of their self-aggregation behavior to determine the morphology of the formed nanoparticles. Of special importance are in this respect nanoparticles which can additionally respond to external triggers. TEM investigations contributed strongly to the understanding of such systems, as morphological changes, triggered by different pH values of the solution or by different temperatures of the solution, can be directly visualized by cryo-TEM investigations.

In this thesis, three main projects and several collaborated projects were studied in order to answer scientific questions in targeted drug delivery systems. The study of uptake of four different sugar moieties functionalized onto Au nanoparticles provided crucial information on the uptake pathway and rate differences, which can potentially later be combined with cancer studies. The study of the pyruvate functionalized Au nanoparticles showed that the targeted delivery into a specific organelle is possible and be utilized into future projects. The utilization of metal-polymer hybrid nanoparticle systems of Au-PEI triggered the endosomal release and the application of advanced imaging technique, tomography would provide detailed three-dimensional information. Additionally, the collaborated projects brought new insights for advanced sample preparation and imaging techniques operated in TEM. All of these experiences gained by this thesis work will enable studying more sophisticated drug systems and improving the success of targeted drug delivery strategies in the future projects.

6. Zusammenfassung

In dieser Arbeit wurden drei verschiedene Konzepte für den zielgerichteten Transport von Wirkstoffpartikelsystemen untersucht. Diese Ansätze sollten zur Entwicklung von Strategien beitragen, die eine Anwendung dieser zielgerichteten Wirkstofftransporter in der Therapie ermöglichen und können zudem zu einem besseren Verständnis ihrer Wirkungsweise nach ihrer Aufnahme in Zellen beitragen. Dieses setzt voraus, dass sowohl die Aufnahmeprozesse als auch die zellulären Strukturen, ihre Integrität, Membran-Nanopartikel-Wechselwirkungen und Veränderungen der zellulären Strukturen nach der Aufnahme der Wirkstoffnanopartikel untersucht werden können. Die verwendeten Systeme basieren auf kolloidalen Goldnanopartikeln, die mit geeigneten Zielgruppen ausgestattet werden können. Dabei dienten insbesondere transmissionselektronenmikroskopische Untersuchungen dazu, ihre Wirkungsweise auf zelluläre Systeme zu studieren. In diesem Zusammenhang bietet die Verwendung von kolloidalen Goldnanopartikeln die Möglichkeit, sogar einzelne Nanopartikel in Zellen zu visualisieren. Damit sind sie, im Gegensatz zu polymerbasierten Nanopartikelsystemen, einfach zu identifizieren, wobei jedoch auch angemerkt werden muss, dass polymerbasierte Nanopartikel generell eine größere Bandbreite von Möglichkeiten bieten, die Eigenschaften der Wirkstofftransportsysteme einzustellen. Dieses bezieht sich vornehmlich auf ihre Größe, ihre Form und die Möglichkeit funktionelle Einheiten einzubauen, die z.B. auf äußere Veränderungen reagieren. Dazu zählen z.B. funktionelle Gruppen, die auf Änderungen der Temperatur oder des pH-Wertes reagieren. Letzteres ist ein wichtiger Aspekt bei der Entwicklung von Konzepten, die eine gesteuerte Wirkstoffabgabe verfolgen.

Ausgehend von diesen Überlegungen wurden zunächst Systeme untersucht, die auf der Funktionalisierung von kolloidalen Goldnanopartikeln basieren. Zu diesem Zweck wurde zunächst die Funktionalisierung der Goldnanopartikel durch Anbindung eines temperatursensitiven Polymers untersucht, das mit vier verschiedenen Zuckern endgruppenfunktionalisiert wurde (**Kapitel 3.3,** Figure 6 – 1). In diesem Fall wurde die Aufnahme von Nanopartikelsystemen mit jeweils einer Glukose-, Fruktose-, Mannose- bzw. einer Galaktosefunktionalisierung in HEK-293 Zellen untersucht. Dabei wurden Unterschiede in der Aufnahmerate und in der intrazellulären Verteilung der Nanopartikel in den Zellen gefunden. Diese Systeme sprechen die in der Plasmamembran der Zelle vorhandenen Glukose-Transportersysteme an. Diese kommen abhängig von der Zellart in unterschiedlicher Häufigkeit vor und können die Aufnahme der verschiedenen zuckerfunktionalisierten Nanopartikel steuern. Darüber hinaus konnte gezeigt werden, dass die Zuckerfunktionalisierung auch einen Einfluss auf das temperaturabhängige Verhalten, insbesondere auf die untere kritische Löslichkeitstemperatur der Polymere haben. Dieses hat offensichtlich weitreichende Konsequenzen für die Zellaufnahme der untersuchten Systeme. Die verschiedenen Aufnahmemechanismen konnten auf der Basis von TEM-Studien und einer Analyse der

Verteilung der Nanopartikel in der Zelle bewertet werden. Sie wurden entweder in endosomalen Strukturen innerhalb der Zelle oder aber im Zytosol der Zelle gefunden. Durch eine gezielte Untersuchung von Nanopartikeln, die mit der äußeren Plasmamembran der Zelle wechselwirken, konnte zudem gezeigt werden, dass eine Aggregation der Nanopartikel im Inkubationsmedium auftritt. Eine statistische Analyse einer Vielzahl von TEM-Bildern erlaubte einen Vergleich der Aufnahmeraten der vier zuckerfunktionalisierten Nanopartikelsysteme. Es konnte herausgefunden werden, dass insbesondere Glukose eine gute Zellaufnahme zeigte.

Das zweite untersuchte System hatte zum Ziel, ein Wirkstofftransportsystem zu entwickeln, das spezielle Zellkompartimente adressiert. Hierzu wurden kolloidale Goldnanopartikel mit Pyruvat funktionalisiert (**Kapitel 3.4**). Pyruvat ist ein wichtiges Molekül, das am Citratzyklus der Zelle beteiligt ist. Dieser findet in den Mitochondrien der Zelle statt. Folglich wurde die Pyruvatfunktionalisierung als Strategie eingesetzt, um mit Nanopartikeln gezielt Mitochondrien zu adressieren. In dieser Studie wurden HEK-293 Zellen für unterschiedliche Inkubationszeiträume citratfunktionalisierten Nanopartikeln ausgesetzt. Nach kurzen Einwirkzeiten konnte eine Schädigung der Mitochondrien mit Hilfe von TEM-Untersuchungen nachgewiesen werden. Nach längeren Einwirkzeiten wurden typische Strukturen in unmittelbarer Nachbarschaft der geschädigten Mitochondrien gefunden, wie z.B. die für Mitophagieprozesse typischen Autophagosomen, bzw. Lysosome, in denen geschädigte Mitochondrien verstoffwechselt werden. Bei diesem System konnte der gezielte Transport der pyruvatfunktionalisierten Nanopartikeln in die Mitochondrien nachgewiesen werden, wobei, als Besonderheit, auch ihr Wirkungsmechanismus näher untersucht werden konnte. Der gefundene Mechanismus ist sehr vielversprechend im Hinblick auf eine mögliche Anwendung als Wirkstoff, um in ihrer Funktion gestörte Mitochondrien aus Zellen zu entfernen. Hier ergeben sich vielversprechende Ansätze für die Therapie von Krankheiten, die auf einer Störung der Mitochondrienfunktion beruhen.

Während die beiden ersten betrachteten Systeme auf der Funktionalisierung der Nanopartikeloberfläche basieren verwendet das dritte in dieser Arbeit untersuchte System Metal-Polymer-Hybridnanopartikel (**Kapitel 3.5**). Diese bestehen aus einer Polymermatrix aus Poly(ethylenimin) (PEI), das ein Vertreter der Gruppe der polykationischen Polymere ist. Dieses Polymer wird in der Literatur häufig verwendet, da es auf Änderungen des pH-Wertes reagiert. Bedenkt man nun, dass sich der pH-Wert beispielsweise auch während des Endozytoseprozesses durch die Reifung der Endosomen in Zellen drastisch ändert, stellt PEI ein vielversprechendes Polymersystem dar, um Wirkstoffstransportysteme herzustellen, die aus den Endosomen ausgeschleust werden können. Ein weitverbreiteter Mechanismus, der dieses Ausschleusen erklärt, ist der Protonen-Schwamm-Effekt. Dieser postuliert die Quellung der Nanopartikel und der Endosomen, die nachfolgend schließlich zum Aufreißen der Endosom-membran führt. Um das Problem der schlechten Sichtbarkeit von Polymeren im Transmissionselektronenmikroskop zu umgehen, beinhaltet das vorgestellte System auch kolloidale Goldnanopartikel, die statistisch

in der Polymermatrix des PEI Nanopartikels verteilt sind. Dies erlaubt die klare Identifikation der Gold-PEI-Hybridnanopartikel auch innerhalb von Zellen mit Hilfe der TEM. Die Gold-PEI-Hybridnanopartikel wurden in Endosomen gefunden, wobei ein Vergleich ihrer Größen innerhalb und außerhalb der Zelle eine klare Zunahme ihres Durchmessers nach der Aufnahme in die Endosomen zeigt. An einigen Stellen der Zellprobe lässt sich eine extreme Zunahme des Partikeldurchmessers beobachten. Dieser tritt vermehrt auf wenn sich die Gold-PEI-Nanopartikel nahe der endosomalen Membran befinden. Diese Probenstellen wurden auch mit Hilfe von (S)TEM-Tomographieaufnahmen weiter untersucht. Die erhaltenen 3D-Rekonstruktionen lieferten weitergehende Informationen über morphologische Veränderungen der Nanopartikel während der Endozytose.

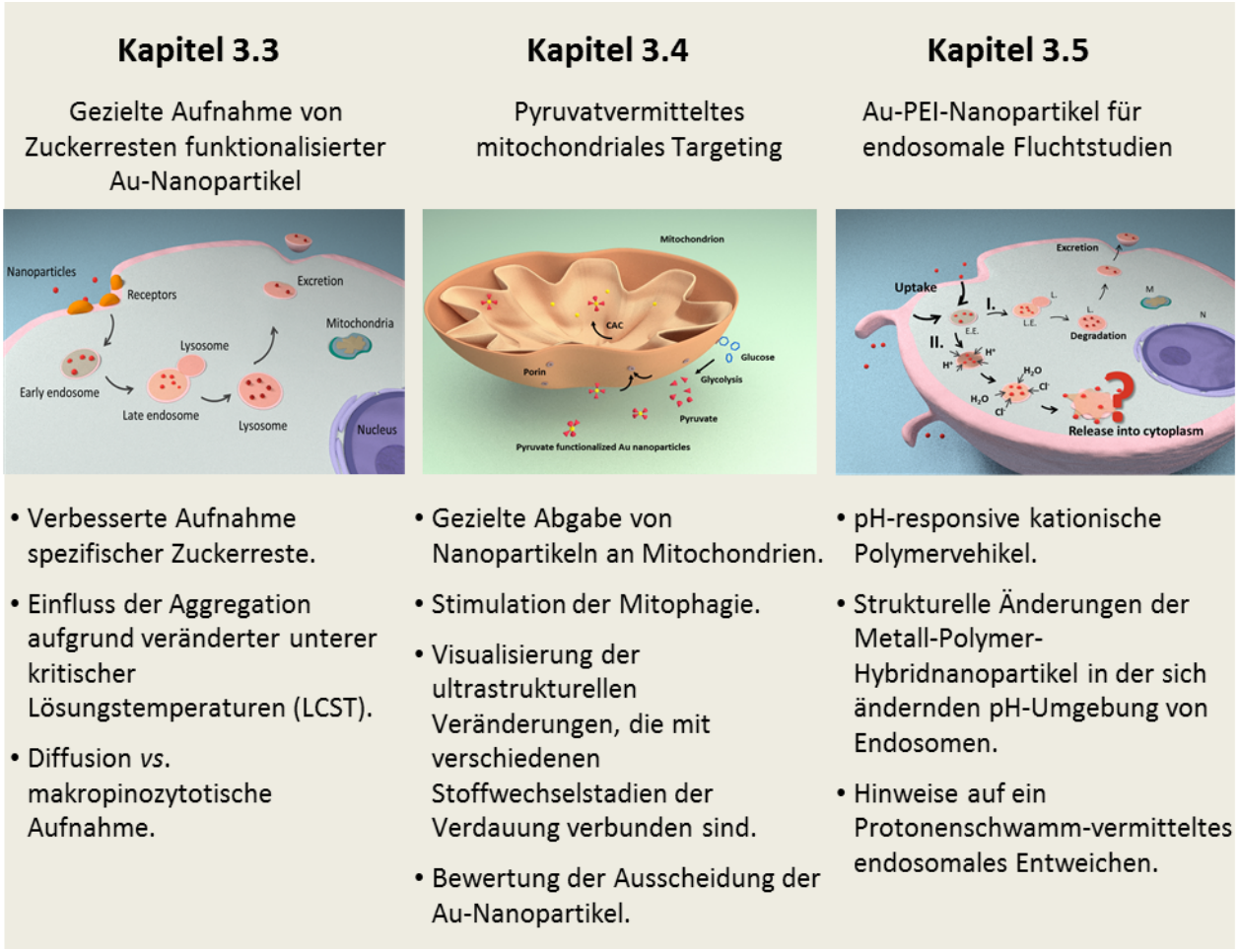

Figure 6 – 1 *Überblick der drei Hauptprojekte, die in dieser Arbeit untersucht wurden.*

In dieser Arbeit wurden sowohl Standard- als auch spezialisierte TEM-Bildgebungsverfahren angewendet. Darüber hinaus wurden die Probenpräparationen an die speziellen Bedürfnisse der einzelnen Proben angepasst. Diese Untersuchungen umfassen beispielsweise die Untersuchung von aus HT-29 Zellen bestehenden Sphäroiden, die als Modelsysteme für Tumorgewebe

verwendet werden. In diesem Fall wurde das s.g. „Image-Stitching“ verwendet, dass es erlaubt den Zellstatus der HT-29 in verschiedenen Bereichen des Sphäroids zu untersuchen (**Kapitel 4.1**). Ein anderes Beispiel ist die Visualisierung von *Staphylococcus aureus* in Makrophagen (**Kapitel 4.2**). Darüber hinaus wurden EDX-Analysen verwendet, um zweifelsfrei CaP Nanopartikel in Monozyten zu identifizieren (**Kapitel 4.3**). In diesem Projekt wurden die CaP Nanopartikel mit verschiedenen TEM Methoden untersucht, unter anderem auch mit cryo-TEM Messmethoden. Nach ihrer Aufnahme in Monozyten konnten die Partikel durch EDX-Untersuchungen eindeutig lokalisiert werden. Die Verwendung cryo-TEM Untersuchungsmethoden hat sich im Rahmen dieser Arbeit als unverzichtbar herausgestellt, insbesondere für die Charakterisierung von Polymernanopartikeln (**Kapitel 4.4**). Derartige Systeme sind vielversprechend für Anwendungen im Bereich der Wirkstofftransportsysteme. In zahlreichen Kollaborationen wurden verschiedene Blockcopolymersysteme hinsichtlich ihrer Selbstorganisationseigenschaften untersucht, um die Morphologie der sich bildenden Nanopartikel zu bestimmen. Von besonderem Interesse sind in diesem Zusammenhang Nanopartikel, die auf Veränderungen der Umgebungsbedingungen reagieren können. TEM-Untersuchungen konnten maßgeblich zum Verständnis derartiger Systeme beitragen, da morphologische Veränderungen, aufgrund veränderter pH-Werte oder der Temperatur, direkt mit Hilfe von cryo-TEM Untersuchungen sichtbar gemacht werde konnten.

In dieser Arbeit wurden drei Hauptprojekte und mehrere Verbundprojekte untersucht, um wissenschaftliche Fragen in gezielten Drug-Delivery-Systemen zu beantworten. Die Untersuchung der Aufnahme von vier verschiedenen Zuckerresten, die auf Au-Nanopartikeln funktionalisiert sind, lieferte wichtige Informationen über den Aufnahmeweg und die Geschwindigkeitsunterschiede, die später mit Krebsstudien kombiniert werden können. Die Untersuchung der Pyruvat-funktionalisierten Au-Nanopartikel zeigte, dass die gezielte Abgabe in eine bestimmte Organelle möglich ist und später in weiteren Projekten verknüpft werden kann. Die Verwendung von Metall-Polymer-Hybridnanopartikelsystemen aus Au-PEI löste die endosomale Freisetzung aus und die Anwendung der fortschrittlichen Bildgebungstechnik Tomographie würde detaillierte dreidimensionale Informationen liefern. Darüber hinaus brachten die Kooperationsprojekte auch neue Erkenntnisse für fortgeschrittene Probenvorbereitungs- und Bildgebungstechniken, die in der TEM betrieben werden. All diese Erfahrungen, die in dieser Arbeit gesammelt wurden, werden dazu beitragen, komplexere Arzneimittelsysteme zu untersuchen und den Erfolg gezielter Strategien zur Arzneimittelabgabe in zukünftigen Projekten zu verbessern.

7. References

[1] P. Ehrlich, *Experimental Researches On Specific Therapeutics*, Hoeber, New York, **1909**.
[2] H. Ringsdorf, *J. Polym. Sci., Polym. Symp.* **1975**, *51*, 135-153.
[3] C. Scholz, J. Kressler, American Chemical Society, Washington, DC, **2013**, p. 363.
[4] I. Ekladious, Y. L. Colson, M. W. Grinstaff, *Nat. Rev. Drug. Discov.* **2018**, *18*, 273-294.
[5] S. Förster, M. Konrad, *J. Mater. Chem.* **2003**, *13*, 2671-2688.
[6] C. I. C. Crucho, M. T. Barros, *Mater. Sci. Eng. C* **2017**, *80*, 771-784.
[7] S. R. Abulateefeh, S. G. Spain, K. J. Thurecht, J. W. Aylott, W. C. Chan, M. C. Garnett, C. Alexander, *Biomater. Sci.* **2013**, *1*, 434-442.
[8] P. Foroozandeh, A. A. Aziz, *Nanoscale Res. Lett.* **2018**, *13*, 339.
[9] L. Treuel, X. Jiang, G. U. Nienhaus, *J. R. Soc., Interface* **2013**, *10*, 20120939-20120939.
[10] S. Xu, B. Z. Olenyuk, C. T. Okamoto, S. F. Hamm-Alvarez, *Adv. Drug. Deliv. Rev.* **2013**, *65*, 121-138.
[11] A. Scheepers, H. G. Joost, A. Schurmann, *JPEN J. Parenter. Enteral. Nutr.* **2004**, *28*, 364-371.
[12] R. B. Hamanaka, N. S. Chandel, *J. Exp. Med.* **2012**, *209*, 211.
[13] S. Zhang, H. Gao, G. Bao, *ACS Nano* **2015**, *9*, 8655-8671.
[14] I. Canton, G. Battaglia, *Chem. Soc. Rev.* **2012**, *41*, 2718-2739.
[15] W. Li, in *Toxicology of Nanomaterials* (Ed.: Z. Z. Yuliang Zhao, Weiyue Feng), Wiley, Weinheim, Germany, **2016**, pp. 211-230.
[16] a)B. Fortuni, T. Inose, M. Ricci, Y. Fujita, I. Van Zundert, A. Masuhara, E. Fron, H. Mizuno, L. Latterini, S. Rocha, H. Uji-i, *Sci. Rep.* **2019**, *9*, 2666; b)A. Gad, J. Kydd, B. Piel, P. Rai, *Int. J. Nanomed. Nanosurg.* **2016**, *2*, 10.16966/12470-13206.16116.
[17] M. Costanzo, F. Carton, A. Marengo, G. Berlier, B. Stella, S. Arpicco, M. Malatesta, *Eur. J. Histochem.* **2016**, *60*, 2640.
[18] B. R. Masters, *History of the Electron Microscope in Cell Biology*, John Wiley & Sons, Ltd, **2009**.
[19] K. R. Porter, A. Claude, E. F. Fullam, *J. Exp. Med.* **1945**, *81*, 233-246.
[20] S. Behzadi, V. Serpooshan, W. Tao, M. A. Hamaly, M. Y. Alkawareek, E. C. Dreaden, D. Brown, A. M. Alkilany, O. C. Farokhzad, M. Mahmoudi, *Chem. Soc. Rev.* **2017**, *46*, 4218-4244.
[21] I. Vhora, S. Patil, P. Bhatt, R. Gandhi, D. Baradia, A. Misra, *Ther. Deliv.* **2014**, *5*, 1007-1024.
[22] F. Moser, G. Hildenbrand, P. Müller, A. Al Saroori, A. Biswas, M. Bach, F. Wenz, C. Cremer, N. Burger, M. R. Veldwijk, M. Hausmann, *Biophys. J.* **2016**, *110*, 947-953.
[23] C. Freese, M. I. Gibson, H.-A. Klok, R. E. Unger, C. J. Kirkpatrick, *Biomacromolecules* **2012**, *13*, 1533-1543.
[24] E. Ruska, *Angew. Chem. Int. Ed.* **1987**, *26*, 595-605.
[25] B. v. Borries, E. Ruska, *Naturwissenschaften* **1939**, *27*, 577-582.
[26] S. K. Sharma, *Handbook of Materials Characterization*, Springer, Cham, Switzerland, **2018**.
[27] L. Marton, *Nature* **1934**, *133*, 911.
[28] M. Winey, J. B. Meehl, E. T. O'Toole, J. Thomas H. Giddings, *Mol. Biol. Cell* **2014**, *25*, 319-323.
[29] H. Fernández-Morán, *J. Biophys. Biochem. Cytol.* **1956**, *2*, 29-30.
[30] G. H. Michler, in *Electron Microscopy of Polymers* (Ed.: H. Pasch), Springer Berlin Heidelberg, **2008**, pp. 199-217.
[31] R. F. Baker, *Nature* **1956**, *178*, 636-637.
[32] S. Brenner, R. W. Horne, *Biochim. Biophys. Acta* **1959**, *34*, 103-110.
[33] S. J. Singer, *Nature* **1959**, *183*, 1523-1524.
[34] J. M. Robinson, T. Takizawa, D. D. Vandré, *J. Histochem. Cytochem.* **2000**, *48*, 487-492.
[35] B. Alberts, A. Johnson, J. Lewis, D. Morgan, M. Raff, K. Roberts, P. Walter, *Molecular Biology of the Cell*, Garland Science, **2015**.

[36] D. G. Robinson, K. Mühlethaler, U. Ehlers, R. Herken, B. Herrmann, F. Mayer, F. W. Schürmann, *Methods of Preparation for Electron Microscopy: An Introduction for the Biomedical Sciences*, Springer Berlin Heidelberg, **2012**.
[37] T. H. Giddings, Jr., E. T. O'Toole, M. Morphew, D. N. Mastronarde, J. R. McIntosh, M. Winey, *Method Cell Biol.* **2001**, *67*, 27-42.
[38] M. J. Dobro, L. A. Melanson, G. J. Jensen, A. W. McDowall, in *Methods in Enzymology, Vol. 481* (Ed.: G. J. Jensen), Academic Press, **2010**, pp. 63-82.
[39] J. Dubochet, A. W. McDowall, *J. Microsc.* **1981**, *124*, 3-4.
[40] Nobel Media AB 2019, **2017**.
[41] J. Frank, J. Zhu, P. Penczek, Y. Li, S. Srivastava, A. Verschoor, M. Radermacher, R. Grassucci, R. K. Lata, R. K. Agrawal, *Nature* **1995**, *376*, 441-444.
[42] R. Henderson, J. M. Baldwin, T. A. Ceska, F. Zemlin, E. Beckmann, K. H. Downing, *J. Mol. Biol.* **1990**, *213*, 899-929.
[43] J. Hutchings, G. Zanetti, *Biochemical Society Transactions* **2018**, BST20170351.
[44] E. Abbe, *Arch. Mikrosk. Anat.* **1873**, *9*, 413-468.
[45] R. A. Serway, C. J. Moses, C. A. Moyer, *Modern Physics*, Cengage Learning, **2004**.
[46] J. Goldstein, D. C. Joy, A. D. Romig, *Principles of Analytical Electron Microscopy*, Springer US, **2013**.
[47] R. Egerton, *Physical Principles of Electron Microscopy: An Introduction to TEM, SEM, and AEM*, Springer US, **2011**.
[48] D. B. Williams, C. B. Carter, in *Transmission Electron Microscopy: A Textbook for Materials Science*, Springer US, Boston, MA, **2009**, pp. 91-114.
[49] E. A. Ellis, L. Cohen-Gould, *Microsc. Microanal.* **2016**, *22*, 2074-2075.
[50] S. J. Pennycook, *Ultramicroscopy* **1989**, *30*, 58-69.
[51] P. Sungur, Master thesis, Friedrich Schiller University Jena (Jena, Germany), **2015**.
[52] A. Loukanov, N. Kamasawa, R. Danev, R. Shigemoto, K. Nagayama, *Ultramicroscopy* **2010**, *110*, 366-374.
[53] S. Utsunomiya, R. C. Ewing, *Environ. Sci. Technol.* **2003**, *37*, 786-791.
[54] J. T. Held, K. I. Hunter, N. Dahod, B. Greenberg, D. Reifsnyder Hickey, W. A. Tisdale, U. Kortshagen, K. A. Mkhoyan, *ACS Appl. Nano Mater.* **2018**, *1*, 989-996.
[55] B. F. McEwen, M. Marko, *J. Histochem. Cytochem.* **2001**, *49*, 553-563.
[56] S. Jonic, C. O. Sorzano, N. Boisset, *J. Microsc.* **2008**, *232*, 562-579.
[57] R. Hovden, P. Ercius, Y. Jiang, D. Wang, Y. Yu, H. D. Abruña, V. Elser, D. A. Muller, *Ultramicroscopy* **2014**, *140*, 26-31.
[58] P. Ercius, O. Alaidi, M. J. Rames, G. Ren, *Adv. Mater.* **2015**, *27*, 5638-5663.
[59] a)S. Hwang, C. W. Han, S. V. Venkatakrishnan, C. A. Bouman, V. Ortalan, *Meas. Sci. Technol.* **2017**, *28*, 045402; b)V. Migunov, H. Ryll, X. Zhuge, M. Simson, L. Strüder, K. J. Batenburg, L. Houben, R. E. Dunin-Borkowski, *Sci. Rep.* **2015**, *5*, 14516.
[60] A. M. Glauert, P. R. Lewis, *Biological Specimen Preparation for Transmission Electron Microscopy*, Princeton University Press, **2014**.
[61] A. Penttila, H. Kalimo, B. F. Trump, *J. Cell Biol.* **1974**, *63*, 197-214.
[62] D. D. Sabatini, K. Bensch, R. J. Barrnett, *J. Cell Biol.* **1963**, *17*, 19.
[63] J. A. Kiernan, *Microscopy Today* **2018**, *8*, 8-13.
[64] J. A. Kiernan, *Histological and Histochemical Methods: Theory and Practice*, 3 ed., Butterworth-Heinemann, Oxford, **1999**.
[65] W. Bernhard, *J. Ultrastruct. Res.* **1969**, *27*, 250-265.

[66] A. M. Glauert, P. R. Lewis, *Biological Specimen Preparation for Transmission Electron Microscopy*, Princeton University Press, **1998**.
[67] A. B. Maunsbach, B. A. Afzelius, in *Biomedical Electron Microscopy: Illustrated Methods and Interpretations*, Academic Press, San Diego, **1999**, pp. 103-124.
[68] J. A. Mascorro, *Novel Choices for Formulating Embedding Media Kits*, SPIE, Monterey, California, United States, **2009**.
[69] a)L. Graham, Orenstein, J. M. , *Nat. Protoc.* **2007**, *2*, 2439-2450; b)E. S. Reynolds, *J. Cell Biol.* **1963**, *17*, 208-212.
[70] S. Hammerschmidt, M. Rohde, in *Streptococcus pneumoniae: Methods and Protocols* (Ed.: F. Iovino), Springer New York, **2019**, pp. 13-33.
[71] E. A. Karpova, R. Gillet, *Trends Biochem. Sci.* **2018**, *43*, 938-950.
[72] N. D. Burrows, R. L. Penn, *Microsc. Microanal.* **2013**, *19*, 1542-1553.
[73] J. Dubochet, M. Adrian, P. Schultz, P. Oudet, *EMBO J.* **1986**, *5*, 519-528.
[74] a)D. Danino, *Curr. Opin. Colloid In.* **2012**, *17*, 316-329; b)J. P. Patterson, Y. Xu, M.-A. Moradi, N. A. J. M. Sommerdijk, H. Friedrich, *Acc. Chem. Res.* **2017**, *50*, 1495-1501.
[75] V. Cabra, M. Samsó, *J. Visualized Exp.* **2015**, 52311-52311.
[76] J. Kuntsche, J. C. Horst, H. Bunjes, *Int. J. Pharm.* **2011**, *417*, 120-137.
[77] Y.-Y. Won, A. K. Brannan, H. T. Davis, F. S. Bates, *J. Phys. Chem. B* **2002**, *106*, 3354-3364.
[78] M. Reifarth, U. S. Schubert, S. Hoeppener, *Adv. Biosyst.* **2018**, *2*, 1700254.
[79] S. Schmidl, C. V. Iancu, J.-Y. Choe, M. Oreb, *Front. Chem.* **2018**, *6*, 183-183.
[80] C. Wang, Y. Wang, Y. Li, B. Bodemann, T. Zhao, X. Ma, G. Huang, Z. Hu, R. J. DeBerardinis, M. A. White, J. Gao, *Nat. Commun.* **2015**, *6*, 8524.
[81] J. Turkevich, P. C. Stevenson, J. Hillier, *Discuss. Faraday Soc.* **1951**, *11*, 55-75.
[82] G. Frens, *Nature Phys. Sci.* **1973**, *241*, 20-22.
[83] L.-H. Fu, J. Yang, J.-F. Zhu, M.-G. Ma, in *Metal Nanoparticles in Pharma* (Eds.: P. D. M. Rai, P. D. R. Shegokar), Springer International Publishing, Cham, **2017**, pp. 155-191.
[84] Y. Chen, Y. Xianyu, X. Jiang, *Acc. Chem. Res.* **2017**, *50*, 310-319.
[85] J. C. Love, L. A. Estroff, J. K. Kriebel, R. G. Nuzzo, G. M. Whitesides, *Chem. Rev.* **2005**, *105*, 1103-1170.
[86] K. C. R. Bahadur, B. Thapa, N. Bhattarai, in *Nanotechnology Reviews, Vol. 3*, **2014**, p. 269.
[87] M. Reifarth, S. Hoeppener, U. S. Schubert, *Adv. Mater.* **2018**, *30*, 1703704.
[88] L. Dykman, N. Khlebtsov, *Chem. Soc. Rev.* **2012**, *41*, 2256-2282.
[89] a)D. M. Stringer, P. Zahradka, C. G. Taylor, *Nutr. Rev.* **2015**, *73*, 140-154; b)R. Augustin, *IUBMB Life* **2010**, *62*, 315-333; c)H. G. Joost, B. Thorens, *Mol. Membr. Biol.* **2001**, *18*, 247-256; d)L.-Q. Chen, L. S. Cheung, L. Feng, W. Tanner, W. B. Frommer, *Annu. Rev. Biochem.* **2015**, *84*, 865-894; e)H. Takanaga, W. B. Frommer, *FASEB J.* **2010**, *24*, 2849-2858; f)L. A. Gallo, E. M. Wright, V. Vallon, *Diab. Vasc. Dis. Res.* **2015**, *12*, 78-89; g)C. Trötschel, A. Poetsch, *J. Proteomics* **2015**, *15*, 915-929; h)G. W. Gould, G. D. Holman, *Biochem. J.* **1993**, *295*, 329-341; i)M. T. Besson, K. Alegría, P. Garrido-Gerter, L. F. Barros, J.-C. Liévens, *PLoS ONE* **2015**, *10*, e0118765; j)I. S. Wood, P. Trayhurn, *Br. J. Nutr.* **2003**, *89*, 3-9; k)M. Mueckler, B. Thorens, *Mol.Aspects Med.* **2013**, *34*, 121-138; l)B. Thorens, M. Mueckler, *Am. J. Physiol. Endocrinol. Metab.* **2010**, *298*, E141-145; m)H. Doege, A. Bocianski, A. Scheepers, H. Axer, J. Eckel, H. G. Joost, A. Schurmann, *Biochem. J.* **2001**, *359*, 443-449.
[90] A. Gandhi, A. Paul, S. O. Sen, K. K. Sen, *Asian J. Pharm. Sci.* **2015**, *10*, 99-107.
[91] C. v. d. Ehe, F. Kretschmer, C. Weber, S. Crotty, S. Stumpf, S. Hoeppener, M. Gottschaldt, U. S. Schubert, in *Controlled Radical Polymerization: Materials, Vol. 1188*, American Chemical Society, **2015**, pp. 221-256.

[92] J. Finsterer, S. Zarrouk Mahjoub, *Seizure - Eur. J. Epilep.* **2012**, *21*, 316-321.
[93] M. P. Murphy, R. C. Hartley, *Nat. Rev. Drug. Discov.* **2018**, *17*, 865.
[94] D. M. Wilson, 3rd, P. J. Brooks, *Environ. Mol. Mutagen.* **2010**, *51*, 349-351.
[95] a)R. Guan, W. Zou, X. Dai, X. Yu, H. Liu, Q. Chen, W. Teng, *J. Biomed. Sci.* **2018**, *25*, 87; b)K. A. Boyle, J. VanWickle, J. Zielonka, G. Cheng, B. Kalyanaraman, M. B. Dwinell, *Cancer Res.* **2018**, *78*, 878.
[96] M. S. Shim, Y. J. Kwon, *Adv. Drug. Deliv. Rev.* **2012**, *64*, 1046-1059.
[97] R. V. Benjaminsen, M. A. Mattebjerg, J. R. Henriksen, S. M. Moghimi, T. L. Andresen, *Mol. Ther.* **2013**, *21*, 149.
[98] L. I. Selby, C. M. Cortez-Jugo, G. K. Such, A. P. R. Johnston, *Wiley Interdiscip. Rev.: Nanomed. Nanobiotechnol.* **2017**, *9*, e1452.
[99] M. S. Shim, X. Wang, R. Ragan, Y. J. Kwon, *Microsc. Res. Tech.* **2010**, *73*, 845-856.
[100] G. Lin, H. Zhang, L. Huang, *Mol. Pharmaceutics* **2015**, *12*, 314-321.
[101] S. K. Samal, M. Dash, S. Van Vlierberghe, D. L. Kaplan, E. Chiellini, C. van Blitterswijk, L. Moroni, P. Dubruel, *Chem. Soc. Rev.* **2012**, *41*, 7147-7194.
[102] a)A. Bolhassani, S. Javanzad, T. Saleh, M. Hashemi, M. R. Aghasadeghi, S. M. Sadat, *Hum. Vacc. Immunother.* **2014**, *10*, 321-332; b)Y. Ding, Z. Jiang, K. Saha, C. S. Kim, S. T. Kim, R. F. Landis, V. M. Rotello, *Mol. Ther.* **2014**, *22*, 1075-1083; c)R. Haag, F. Kratz, *Angew. Chem. Int. Ed.* **2006**, *45*, 1198-1215.
[103] S. Vaidyanathan, B. G. Orr, M. M. Banaszak Holl, *Acc. Chem. Res.* **2016**, *49*, 1486-1493.
[104] J. Nguyen, F. C. Szoka, *Acc. Chem. Res.* **2012**, *45*, 1153.
[105] N. D. Sonawane, F. C. Szoka, A. S. Verkman, *J. Biol. Chem.* **2003**, *278*, 44826.
[106] a)I. Kurtulus, G. Yilmaz, M. Ucuncu, M. Emrullahoglu, C. R. Becer, V. Bulmus, *Polym. Chem.* **2014**, *5*, 1593-1604; b)A. El-Sayed, S. Futaki, H. Harashima, *AAPS J.* **2009**, *11*, 13-22.
[107] E. C. Freeman, L. M. Weiland, W. S. Meng, *J. Biomater. Sci., Polym. Ed.* **2013**, *24*, 398.
[108] A. M. Funhoff, C. F. van Nostrum, G. A. Koning, N. M. E. Schuurmans-Nieuwenbroek, D. J. A. Crommelin, W. E. Hennink, *Biomacromolecules* **2004**, *5*, 32.
[109] a)W. Baumeister, *Curr. Opin. Struct. Biol.* **2002**, *12*, 679-684; b)U. Ziese, C. Kübel, A. J. Verkleij, A. J. Koster, *J. Struct. Biol.* **2002**, *138*, 58-62.
[110] F. Kretschmer, U. Mansfeld, S. Hoeppener, M. D. Hager, U. S. Schubert, *Chem. Commun.* **2014**, *50*, 88-90.
[111] M. Reifarth, E. Preußger, U. S. Schubert, R. Heintzmann, S. Hoeppener, *Part. Part. Syst. Char.* **2017**, *34*, 1700180.
[112] K. M. Tevis, Y. L. Colson, M. W. Grinstaff, *Adv. Biosyst.* **2017**, *1*, 1700083.
[113] G. Lazzari, P. Couvreur, S. Mura, *Polym. Chem.* **2017**, *8*, 4947-4969.
[114] T. A. Wynn, K. M. Vannella, *Immunity* **2016**, *44*, 450-462.
[115] a)R. C. Anderson, R. G. Haverkamp, P.-L. Yu, *FEMS Microbiol. Lett.* **2004**, *240*, 105-110; b)P. Jaggi, S. M. Paule, L. R. Peterson, T. Q. Tan, *Emerg. Infec. Dis.* **2007**, *13*, 311-314.
[116] D. Z. de Back, E. B. Kostova, M. van Kraaij, T. K. van den Berg, R. van Bruggen, *Front. Physiol.* **2014**, *5*, 9-9.
[117] A. Aderem, D. M. Underhill, *Annu. Rev. Immunol.* **1999**, *17*, 593-623.
[118] S. T. Stern, P. P. Adiseshaiah, R. M. Crist, *Part. Fibre Toxicol.* **2012**, *9*, 20.
[119] F. O. Martinez, S. Gordon, *F1000Prime Rep.* **2014**, *6*, 13.
[120] C. D. Mills, *Crit. Rev. Immunol.* **2012**, *32*, 463-488.
[121] O. Werz, J. Gerstmeier, S. Libreros, X. De la Rosa, M. Werner, P. C. Norris, N. Chiang, C. N. Serhan, *Nat. Commun.* **2018**, *9*, 59.
[122] J. C. R. Jones, *Methods Mol. Biol.* **2016**, *1474*, 291-307.

[123] J. Skepper, J. M Powell, *Immunogold Staining of London Resin (LR) White Sections for Transmission Electron Microscopy (TEM)*, Cold Spring Harbor Laboratory Press, **2008**.
[124] W. B. Liechty, D. R. Kryscio, B. V. Slaughter, N. A. Peppas, in *Annu. Rev. Chem. Biomol. Eng., Vol. 1* (Eds.: J. M. Prausnitz, M. F. Doherty, R. A. Segalman), Annual Reviews, Palo Alto, **2010**, pp. 149-173.
[125] H.-J. Yoon, W.-D. Jang, *J. Mater. Chem.* **2010**, *20*, 211-222.
[126] J. R. Joshi, R. P. Patel, *Int. J. Cur. Pharm. Res.* **2012**, *4*, 74-81.
[127] E. A. Simone, T. D. Dziubla, V. R. Muzykantov, *Expert Opin. Drug Deliv.* **2008**, *5*, 1283-1300.
[128] K. Matyjaszewski, *Controlled/Living Radical Polymerization, Vol. 768*, American Chemical Society, **2000**.
[129] J. Rodríguez-Hernández, A. L. Cortajarena, *Design of Polymeric Platforms for Selective Biorecognition*, Springer International Publishing, **2015**.
[130] P. Khalatur, A. R. Khokhlov, *Self-organization of Amphiphilic Polymers, Vol. 59*, **2014**.
[131] V. I. Eliseeva, S. S. Ivanchev, S. I. Kuchanov, A. V. Lebedev, *Emulsion Polymerization and Its Applications in Industry*, Springer US, **2012**.
[132] F. S. Bates, G. H. Fredrickson, **1990**, *41*, 525-557.
[133] J. N. Israelachvili, D. J. Mitchell, B. W. Ninham, *J. Chem. Soc., Faraday Trans. 2* **1976**, *72*, 1525-1568.
[134] S. Fakirov, *Nano-size Polymers: Preparation, Properties, Applications*, Springer International Publishing Switzerland, **2016**.
[135] D. E. Discher, A. Eisenberg, *Science* **2002**, *297*, 967-973.
[136] R. Crawford, B. Dogdas, E. Keough, R. M. Haas, W. Wepukhulu, S. Krotzer, P. A. Burke, L. Sepp-Lorenzino, A. Bagchi, B. J. Howell, *Int. J. Pharm.* **2011**, *403*, 237-244.
[137] P. Bernadó, D. I. Svergun, *Mol. Biosyst.* **2012**, *8*, 151-167.
[138] T. C. Majdanski, D. Pretzel, J. A. Czaplewska, J. Vitz, P. Sungur, S. Höppener, S. Schubert, F. H. Schacher, U. S. Schubert, M. Gottschaldt, *Macromol. Biosci.* **2018**, *18*, 1700396.
[139] a)K. Knop, R. Hoogenboom, D. Fischer, U. S. Schubert, *Angew. Chem. Int. Ed.* **2010**, *49*, 6288-6308; b)N. S. Oltra, P. Nair, D. E. Discher, *Annu. Rev. Chem. Biomol. Eng.* **2014**, *5*, 281-299.
[140] N. Nomura, G. Verdon, H. J. Kang, T. Shimamura, Y. Nomura, Y. Sonoda, S. A. Hussien, A. A. Qureshi, M. Coincon, Y. Sato, H. Abe, Y. Nakada-Nakura, T. Hino, T. Arakawa, O. Kusano-Arai, H. Iwanari, T. Murata, T. Kobayashi, T. Hamakubo, M. Kasahara, S. Iwata, D. Drew, *Nature* **2015**, *526*, 397-401.
[141] A. Godoy, V. Ulloa, F. Rodriguez, K. Reinicke, A. J. Yanez, L. Garcia Mde, R. A. Medina, M. Carrasco, S. Barberis, T. Castro, F. Martinez, X. Koch, J. C. Vera, M. T. Poblete, C. D. Figueroa, B. Peruzzo, F. Perez, F. Nualart, *J. Cell. Physiol.* **2006**, *207*, 614-627.
[142] W. L. Chen, Y. Y. Wang, A. Zhao, L. Xia, G. Xie, M. Su, L. Zhao, J. Liu, C. Qu, R. Wei, C. Rajani, Y. Ni, Z. Cheng, Z. Chen, S. J. Chen, W. Jia, *Cancer Cell* **2016**, *30*, 779-791.
[143] a)S. Rangelov, A. Pispas, *Polymer and Polymer-Hybrid Nanoparticles: From Synthesis to Biomedical Applications*, Taylor & Francis, **2013**; b)S. J. Holder, N. A. J. M. Sommerdijk, *Polym. Chem.* **2011**, *2*, 1018-1028.
[144] N. S. Oltra, P. Nair, D. E. Discher, *Annu. Rev. Chem. Biomol. Eng.* **2014**, *5*, 281-299.
[145] P. de Boer, J. P. Hoogenboom, B. N. G. Giepmans, *Nature Methods* **2015**, *12*, 503.
[146] M.-M. Xu, R.-J. Liu, Q. Yan, *Chinese J. Polym. Sci.* **2018**, *36*, 347-365.
[147] T. Yildirim, A. Traeger, P. Sungur, S. Hoeppener, C. Kellner, I. Yildirim, D. Pretzel, S. Schubert, U. S. Schubert, *Biomacromolecules* **2017**, *18*, 3280-3290.
[148] M. Sahn, T. Yildirim, M. Dirauf, C. Weber, P. Sungur, S. Hoeppener, U. S. Schubert, *Macromolecules* **2016**, *49*, 7257-7267.

[149] N. Gyobu, K. Tani, Y. Hiroaki, A. Kamegawa, K. Mitsuoka, Y. Fujiyoshi, *J. Struct. Biol.* **2004**, *146*, 325-333.

8. Acknowledgements

First of all, I would like to thank Prof. Dr. Ulrich S. Schubert for giving me the opportunity to work in his group as a PhD student for three and half years. During these studies, I was allowed to use various high-end instruments such as TEM available in his group. It was a great opportunity for developing my skills and my future career.

Secondly, I would like to thank PD. Dr. Stephanie Höppener for supervision. It was a great time to be a member of her subgroup during nearly 5 years including my master study.

I thank all the collaborated people: Elisabeth Preußger, Carolin Kellner, Karina Rost, Dr. Alexander Rinkenauer, Dr. Christian von der Ehe, Dr. Michael Pröhl, Dr. Justyna Czaplewska, Dr. Tanja Bus, Tobias Majdanski, Dr. Meike Leiske, Dr. Martin Sahn, Dr. Carlos Guerrero Sanchez, Dr. Ilknur Yildirim, Dr. Turgay Yildirim, Dr. Martin Reifarth, Prof. Dr. Oliver Werz, Dr. Jana Gerstmeier, Prof. Dr. Ulf Wagner and Elisabeth Jäger who provided samples, chemicals, cell cultures and introduction to instruments.

I thank the administrative secretaries Sylvia Braunsdorf and Franca Frister and the safety instructors Dr. Jürgen Vitz and Dr. Uwe Köhn.

I thank Dorit Schmidt from Abbe School of Photonics and Gunda Huskobla from Graduate Academy for giving me advices. I thank Prof. Dr. Holger Gies for his advices at the stage of finalizing my PhD thesis. I thank the Graduate Academy for their services and also providing a short-term scholarship.

In the semester of 2018-2019 I was elected member and board member of the council of PhD students at FSU Jena. I thank our great team for many meetings and events we organized together.

I thank the Hochschulsport Jena for offering such a variety of courses with affordable prices. It was very helpful to reduce the stress after spending long hours in the labs.

In October, 2012 I moved from my lovely and sunny city Izmir to Jena to study a master degree. It turned out now that I will leave this city after 7 years but with 2 degrees! Although there were very tough times related to the homesickness, loneliness and so on (you can insert here a very long list), I believe now (or finally realized and accepted) that I did a good job here. Here is the city where I faced my strength and weakness. I met many good people and collected many good memories which I will always remember. I thank by my whole heart my dearest friends Hatice, Meltem and Aslı. I thank Deniz for his support via long Skype talks. Now it is my turn to get graduated. I thank my Turkish-gang in Jena (Can, Yusuf, Mina, Satvet, Ceren, Aziz, Mustafa and Berkay) for supporting each other here. I thank Ilknur and Turgay for coffee pauses at ZAF. I thank my wisdom-brother Herr Reifarth for his explaining German lifestyle, help to improve my German and our swimming sessions. I thank Emily for her friendship since our master study,

coffee meetings, sharing information on foreigner issues and our great trips to Taiwan and Turkey. I thank Almut and Steffi for their help to improve my German. I thank all the people I met in Jena during these 7 years who were here for long term or short term but shared unforgettable time with me.

I wrote up this thesis at the computer pool of the library because my laptop was under repair for several weeks. I thank Satvet, Emily and Bib-Gençlik for being my library-mates at writing phase. I thank Sarp for proof reading.

I thank my parents and family, who always encourage me to study abroad and stand on my own. I am very happy to have them, although we are kilometers apart for several years.

At last but not least, I thank myself for finding always a way to continue at any circumstances.

9. Publications

T. C. Majdanski, D. Pretzel, J. A. Czaplewska, J. Vitz, **P. Sungur**, S. Höppener, S. Schubert, F. H. Schacher, U. S. Schubert, M. Gottschaldt, *Macromol. Biosci.* **2018**, *18*, 1700396.

M. Pröhl, S. Seupel, **P. Sungur**, S. Höppener, M. Gottschaldt, J. C. Brendel, U. S. Schubert, *Polymer* **2017**, *133*, 205-212.

M. N. Leiske, A.-K. Trützschler, S. Armoneit, **P. Sungur**, S. Hoeppener, M. Lehmann, A. Traeger, U. S. Schubert, *J. Mater. Chem. B* **2017**, *5*, 9102-9113.

I. Yildirim, **P. Sungur**, A. C. Crecelius-Vitz, T. Yildirim, D. Kalden, S. Hoeppener, M. Westerhausen, C. Weber, U. S. Schubert, *Polym. Chem.* **2017**, *8*, 6086-6098.

T. Yildirim, A. Traeger, **P. Sungur**, S. Hoeppener, C. Kellner, I. Yildirim, D. Pretzel, S. Schubert, U. S. Schubert, *Biomacromolecules* **2017**, *18*, 3280-3290.

R. Yañez-Macias, I. Kulai, J. Ulbrich, T. Yildirim, **P. Sungur**, S. Hoeppener, R. Guerrero-Santos, U. S. Schubert, M. Destarac, C. Guerrero-Sanchez, S. Harrisson, *Polym. Chem.* **2017**, *8*, 5023-5032.

M. Sahn, T. Yildirim, M. Dirauf, C. Weber, **P. Sungur**, S. Hoeppener, U. S. Schubert, *Macromolecules* **2016**, *49*, 7257-7267.

10. Selbstständigkeitserklärung

Ich erkläre, dass ich die vorliegende Arbeit selbständig und unter Verwendung der angegebenen Hilfsmittel, persönlichen Mittelungen und Quellen angefertigt habe.

Jena, den 21.06.2019

Unterschrift der Verfasserin/ des Verfassers

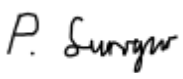

_____

Pelin Sungur